# Mechanisms of Hydrolysis and Thiolysis of *S*-Nitrosoglutathione

Ernesto E. Moran

A Thesis

In

The Department

Of

Chemistry and Biochemistry

Presented in Partial Fulfillment of the Requirements

for the Degree of Doctor of Philosophy at

Concordia University

Montreal, Quebec, Canada

November 2007

*Your file Votre référence*
*ISBN: 978-0-494-37724-6*
*Our file Notre référence*
*ISBN: 978-0-494-37724-6*

**Abstract**

Mechanisms of Hydrolysis and Thiolysis of *S*-Nitrosoglutahione

Ernesto Eugenio Moran, Ph.D.

Hydrolysis of three primary RSNOs, *S*-nitrosocysteine, *S*-nitroso-*N*-acetylated-cysteine, and *S*-nitrosoglutathione and two tertiary RSNOs, *S*-nitrosopenicillamine and *S*-nitroso-*N*-acetylated-penicillamine, was investigated in ~ 4 M $H_2SO_4$ to determine the effects of structure on acid-catalyzed denitrosation. Rate increases of up to 38-fold resulted from dimethyl substitution at the C-SNO carbon. Electron donation from the methyl groups increased the proton affinity of the *NITROSO* sulfur, which was shown by computational methods to be the initial step in the acid-catalyzed hydrolysis. Only minor changes were observed in $k_{obs}$ due to *N*-acetylation, and activation energies of 25.7 ± 1.7 and 23.7 ± 1.3 kcal/mole were measured for *S*-nitroso-*N*-acetylated-cysteine and *S*-nitroso-*N*-acetylated-penicillamine, respectively

Acid-catalyzed GSNO decomposition at pH 2.0 exhibited a sigmoidal decomposition curve typical of autocatalytic processes. Based on strong inhibition on removal of $HNO_2$, $N_2O_3$, or oxygen from the solutions, a chain-reaction mechanism is proposed in which $N_2O_3$ is the chain carrier. Reaction is initiated by $HNO_2$ formation on hydrolysis of the S-NO bond *via* nucleophilic attack at the nitroso *N*, and the overall reaction generates $GSO_3H$, GSOSG, $GSO_2SG$, in addition to $HNO_2$ as decomposition products.

Base-catalyzed GSNO hydrolysis was found to occur mainly *via* nucleophilic attack at the nitroso *N* forming a nitrosated disulfide intermediate that produces GSSG, $GS(NO)S^-$, and a sulfur-free glutathionyl derivative as the GSX products $NO_2^-$ was the main nitrogen product. The percent distribution of the GSX products varied with the $OH^-$ and GSNO concentrations. $N_2O$ was also detected and glutathionyl sulfenic acid GSOH was trapped with dimedone. Thus, base-catalyzed GSNO hydrolysis also proceeded *via* initial $OH^-$ attack at the nitroso sulfur forming nitroxyl (HNO), although this appears to be a minor pathway under our experimental conditions.

*S*-Nitrosoglutathione (GSNO) undergoes denitrosation at neutral pH in the presence of excess glutathione (GSH) even when protected from light and metal-catalyzed decomposition. The major glutathionyl product from these reactions is GSSG, and minor products include $GS(O)NH_2$, GSN(OH)H, and GSOH. Detection of $GS(O)NH_2$ and $N_2O$ suggests that HNO is generated during the reaction. Retardation of GSNO decomposition on addition of dimedone suggests that the mechanism is partially autocatalytic.

The in-source fragmentation of reduced glutathione (GSH), *S*-nitrosoglutathione (GSNO), and oxidized glutathione (GSSG) in a Z-spray ESI source was investigated. The results show that the cone voltage is the major contributor to in-source GSX fragmentation. Cone-voltage-induced fragmentation of the three compounds was pH-dependent, and occurred *via* loss of $H_2O$ and cleavage of the peptide bonds into *b* and *y* ions. Loss of $NH_3$ was observed only for GSH at pH 2.5. Homolytic cleavage of the S-NO bond preceded fragmentation of the glutathionyl moiety, forming a $GS^{\bullet+}$ radical

cation that yields fragment ions unique to GSNO. The results can be used to improve the detection and interpretation of mass spectra of samples containing mixtures of GSX compounds

Direct measurement of underivatized *S*-nitrosoglutathione (GSNO) was achieved by high-performance liquid chromatography (HPLC) using mobile phases at neutral pH and employing UV spectrophotometric (HPLC/UV) and electrospray mass spectrometric (HPLC/ESI-MS) detection. Using UV detection, the method is robust and exhibits good linearity in the range of 0.2–100 μM GSNO with a limit of detection (LOD) of 0.2 μM GSNO. Attempts to improve sensitivity by using ESI-MS detection in an ion trap mass spectrometer resulted in the same LOD and linearity in the range of 0.2–10 μM GSNO.

## Acknowledgements

I would like to thank my thesis supervisors, Dr. Ann English and Dr. Elizabeth Kwong, for their dedication to my training, their guidance, support and patience. I also want to thank them for always pushing me to meet their high scientific standards, which I hope to adhere to as I begin a new stage of my scientific career.

I thank the members of my Research Committee, Dr. Cameron Skinner and Dr. Christopher Wilds, for their help and suggestions, and for guiding my development as a Ph.D. student.

I am grateful to Dr. Sam McClintock for believing in my potential as a scientist, for his friendship, for securing financial support for this project, and for generously giving me access to the research facilities of the Department of Pharmaceutical Research and Development at Merck Frosst Canada.

I want to thank the members of my lab at Concordia for their friendship, help and encouragement. I also thank my coworkers at Merck Frosst Canada whose experience in the area of analytical chemistry was invaluable during my research. Special thanks to Antonio Dilollo, Robert Papp, and Dendi Susanto their support

Lastly I would like to thank my wife and daughters, our parents, and my brothers and sister for their love and patience. Without them, this adventure would not have been possible.

**Table of Contents**

## List of Figures

**List of Schemes**

## List of Tables

**List of Abbreviations**

| | |
|---|---|
| CuZnSOD | copper,zinc-superoxide dismutase |
| CysNO | *S*-nitrosocysteine |
| DM | dimedone; 5,5-dimethyl-1,3cyclohexanedione |
| DTPA | diethylenetriamine-N,N,N′,N″,N‴-pentaacetic acid |
| ESI-MS | electrospray ionization mass spectrometry |
| GAPDH | glyceraldehyde-3-phosphate dehydrogenase |
| GC-MS | gas chromatography mass spectrometry |
| GSH | glutathione; glycine N-(N-L-γ-glutamyl-L-cysteinyl) |
| GSNO | *S*-nitrosoglutathione; glycine N-(N-L-γ-glutamyl-S-nitroso-L-cysteinyl) |
| GSN(OH)H | glutathione N-hydroxysulfenamide |
| GSOH | glutathione disulfide *S*-oxide; glutathione thiosulfinate |
| $GSO_2H$ | glutathione disulfide *S*-dioxide; glutathione thiosulfonate |
| $GS(O)NH_2$ | glutathione sulfinamide |
| GSSG | glutathione disulfide |
| GSX | glutathionyl compound |
| HPLC | high-performance liquid chromatography |
| LOD | limit of detection |

| | |
|---|---|
| LOQ | limit of quantitation |
| MALDI-TOF | matrix-assisted laser desorption ionization time-of-flight |
| $MbFe^{III}$ | metmyoglobin |
| NAC | N-acetyl-cysteine |
| NADPH | nicotinamide adenine dinucleotide phosphate, reduced |
| NAP | N-acetyl-penicillamine |
| NOS | nitric oxide synthase |
| PEN | penicillamine |
| Q-Tof | quadrupole time-of-flight |
| RSNO | *S*-nitrosothiol |
| SNAP | *S*-nitrosopenicillamine |
| RSH | thiol |
| RSOH | sulfenic acid |
| RSSR | disulfide |
| SNAC | *S*-nitroso-N-acetylcysteine |
| SNAP | *S*-nitroso-N-acetylpenicillamine |
| TBAHS | tetrabutylammoniumhydrogen sulfate |

# Chapter 1 - Introduction

## 1.1 Nitric oxide

Nitric oxide (NO) is a relatively stable free radical with the electronic configuration $(\sigma_1)^2(\sigma_1^*)^2(\sigma_2)^2(\pi)^4(\pi^*)^1$. The unpaired electron in the $\pi^*$ orbital makes the molecule reactive towards oxidation to the nitrosonium ion ($NO^+$), reduction to the nitroxyl ion ($NO^-$), reaction with oxygen to yield $NO_2$, and reactions with halogens ($X_2$) to yield XNO (*1*). Nitric oxide is produced *in vivo* through the action of nitric oxide synthases (NOS) that include neuronal NOS, inducible NOS, and endothelial NOS (*2*). All three of these enzymes act by catalyzing the conversion of the amino acid *L*-arginine to citrulline and NO, in an oxidation reaction that requires NADPH and tetrahydrobiopterin as cofactors for NOS (*3*).

### 1.1.1 Physiological effects of nitric oxide

Nitric oxide has been found to regulate a wide variety of physiological functions including smooth muscle relaxation in both the vasculature and gastrointestinal tract. It also contributes to regulation of the respiratory, digestive, and genitourinary systems (*4*). Some of the most investigated roles of nitric oxide are its effects in vascular biology. Studies have shown that nitric oxide can cause vasodilation through a cGMP-dependent mechanism that leads to a fall in intracellular $Ca^{2+}$ flux (*2*). It has also been shown to play a role in platelet adhesion and aggregation, inhibition of vascular smooth cell proliferation, leukocyte addition, and endothelial cell apoptosis (*2*).

Nitroxyl (HNO), the protonated product of the one-electron reduction of NO, is also associated with important pharmacological and toxicological effects. For example,

HNO generated from oxidation of the drug cyanamide (Reaction 1.1) functions as an antialcoholic compound by inhibiting aldehyde dehydrogenase. HNO is a potent vasorelaxant, and may protect ischemic myocardium against reperfusion injury (*5*).

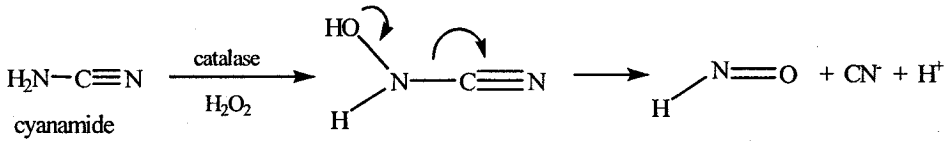


(1.1)

Nitric oxide is a small hydrophobic molecule that can easily pass through certain cell membranes (*6*). But it can diffuse only several cell diameters away from its site of production without being oxidized by endogenous scavengers such as hemoglobin or superoxide ions (*4, 7*). However, it has been proposed that NO can be reversibly incorporated into compounds that transport it from donor to target cells, thus preventing, or diminishing, its inactivation (*4*). *S*-Nitrosothiols (RSNOs) are one class of compounds that have been proposed to act as transporters and reservoirs of NO *in vivo*. In fact, some RSNOs like *S*-nitrosoglutathione (GSNO) (Figure 1.1) and *S*-nitrosocysteine (CysNO) (Figure 1.2) have been detected *in vivo* (*8-10*). Stamler *et al.* have reported that NO circulates in human plasma as *S*-nitrosoalbumin, an *S*-nitrosated form of serum albumin (*11*), suggesting that this RSNO may be a physiological reservoir of NO.

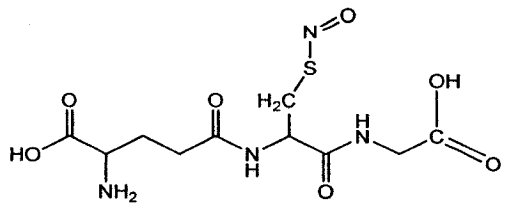

**Figure 1.1. *S*-nitrosoglutathione (GSNO) (*12*)**

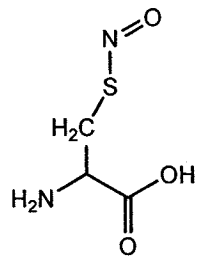

**Figure 1.2. *S*-nitrosocysteine (CysNO) (*12*)**

## 1.2 *S*-Nitrosothiols

RSNOs are derivatives of NO formed on *S*-nitrosation of low-mass thiols or cysteine residues of proteins and peptides (*4*). The simplest procedure for the preparation of RSNOs involves the reaction of the sulfhydryl group with acidified nitrite (Reaction 1.3). At pH < 1.3, the equilibrium lies well to the right of Reaction 1.3, and solutions of *S*-nitrosothiols can be produced in minutes (*3, 13*).

$$NO_2^- + H_3O^+ \rightleftharpoons HNO_2 + H_2O \qquad (1.2)$$

$$RSH + HNO_2 \rightleftharpoons RSNO + H_2O \qquad (1.3)$$

The exact nature of the nitrosating species is a subject of debate. Two mechanisms have been proposed, one involving $H_2NO_2^+$ (Reactions 1.4 and 1.5) and the other involving $NO^+$ as the nitrosating species (Reaction 1.6 and 1.7) (*14*), but no definitive evidence supporting one mechanism over the other has been shown. Reaction of thiols with other reagents such peroxynitrite (Reactions 1.8 to 1.10) can also result in *S*-nitrosation through the formation of $HNO_2$ (*15, 16*) (*17, 18*).

$$HNO_2 + H_3O^+ \rightleftharpoons H_2NO_2^+ + H_2O \quad (1.4)$$

$$H_2NO_2^+ + RSH \rightleftharpoons RSNO + H_3O^+ \quad (1.5)$$

$$HNO_2 + H_3O^+ \rightleftharpoons NO^+ + 2H_2O \quad (1.6)$$

$$NO^+ + RSH \rightleftharpoons RSNO + H^+ \quad (1.7)$$

$$2RSH + ONOO^- \rightleftharpoons RSSR + NO_2^- + H_2O \quad (1.8)$$

$$NO_2^- + H_3O^+ \rightleftharpoons HNO_2 + H_2O \quad (1.9)$$

$$RSH + HNO_2 \rightleftharpoons RSNO + H_2O \quad (1.10)$$

Primary and secondary RSNOs are generally red or pink in color, while tertiary RSNOs are usually green. RSNO formation can be monitored spectrophotometrically in the 330-350 nm ($\varepsilon \sim 10^3$ $M^{-1}$ $cm^{-1}$, $n_o \rightarrow \pi^*$) and 550-600 nm ($\varepsilon \sim 20$ $M^{-1}$ $cm^{-1}$, $n_N \rightarrow \pi^*$) regions. These two absorbance bands have been used to monitor changes in the

concentration of RSNOs caused by decomposition (*15*). RSNOs show significant *S*-N double bond character and can exist in the *cis*- or *trans*-isomers, with primary and secondary RSNOs favoring the *cis*-isomer, while tertiary RSNOs tend to favor the *trans*-isomer (*19, 20*).

Because they exhibit a variety of reactions that can potentially release NO *in vivo*, RSNOs have been studied as useful clinical agents (*4*). They can alter enzyme activity through *S*-nitrosation of enzymes such as clotting factor XII (*21*), or *S*-thiolation of creatine kinase (*22*). RSNOs have also been reported to be involved in signal transduction through protein *S*-nitrosation (*23*), and in the activation and deactivation of the cardiac calcium release channel through *S*-nitrosation and denitrosation, respectively (*24*).

### 1.2.1 Decomposition of S-nitrosothiols

The stability of RSNOs varies widely, with primary and secondary RSNOs showing reported half-lives of seconds to hours, with a few exceptions such as GSNO, and tertiary RSNOs being stable to isolation and long-term storage (*25*). In solution, RSNOs have been shown to undergo decomposition by the action of heat, light, copper catalysis, and the presence of thiolate ions ($RS^-$) (*15*). Thermal and photochemical decomposition reactions are believed to involve the homolytic cleavage of the *S*-N bond to yield the thiol radical, which dimerizes to the disulfide and NO (Reactions 1.10 to 1.13) (*15*):

$$RSNO \rightleftharpoons RS^{\bullet} + NO^{\bullet} \qquad (1.10)$$

$$RS^{\bullet} + RSNO \rightleftharpoons 2RS^{\bullet} + NO^{\bullet} \qquad (1.11)$$

$$RS^{\bullet} + RS^{\bullet} \rightarrow RSSR \qquad (1.13)$$

Copper-catalyzed decomposition occurs as indicated by Reactions 1.14 and 1.15. The true reagent in this mechanism is the $Cu^{I}$ ion, which is generated on reduction of $Cu^{II}$ by the thiolate. The disulfide and NO are produced, and both thiolate and $Cu^{II}$ are regenerated (*15*). Catalysis of RSNO decomposition by other metals including $Zn^{II}$, $Ca^{II}$, $Mg^{II}$, $Ni^{II}$, $Co^{II}$, $Mn^{II}$, $Cr^{III}$, and $Fe^{III}$ has also been studied, but none have shown any reactivity. Weak catalytic activity by $Fe^{II}$ has been reported (*20*).

$$2\,Cu^{II} + 2\,RS^{-} \rightleftharpoons 2Cu^{I} + RSSR \qquad (1.14)$$

$$Cu^{I} + RSNO \rightleftharpoons Cu^{II} + RS^{-} + NO \qquad (1.15)$$

Another important reaction of RSNOs that has been reported is the *trans S*-nitrosation of other thiols (R'SH) present in solution (Reaction 1.16). This reaction has significance *in vivo* because of the high thiol concentration found in cells (*ca.* 5 mM) (*26*) and it represents a mechanism of NO donation by RSNOs.

$$RSNO + R'S^{-} \rightleftharpoons RS^{-} + R'SNO \qquad (1.16)$$

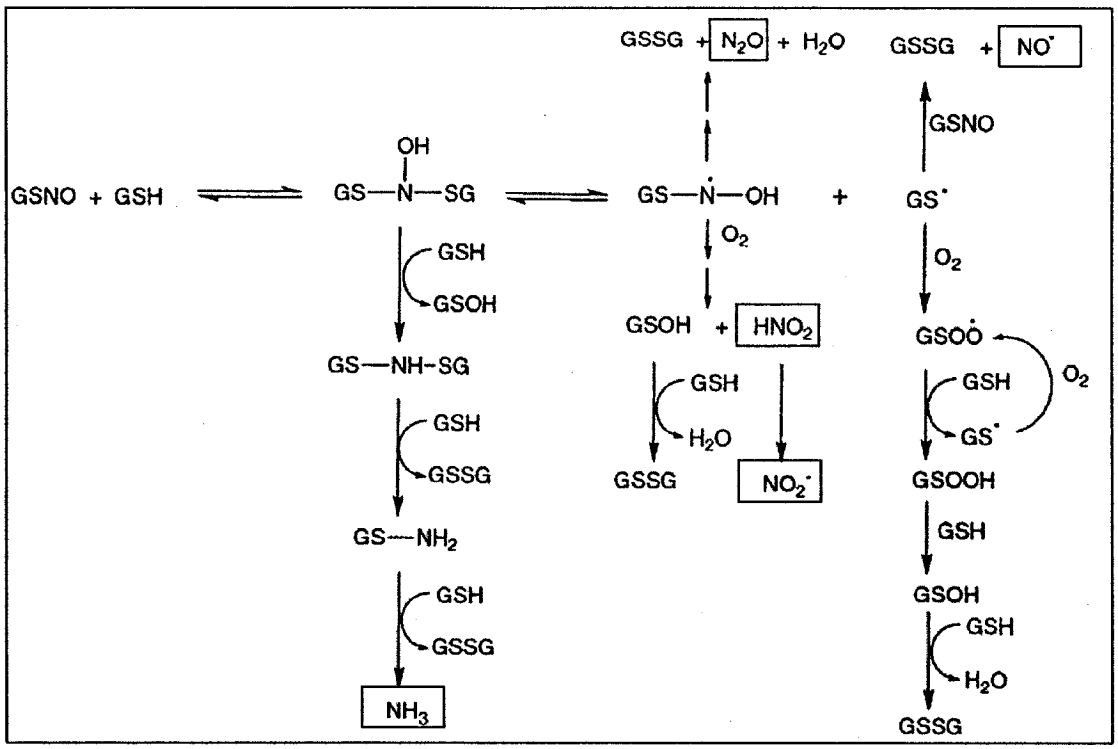


**Scheme 1.1. Reactions of GSNO at high GSH concentration as proposed by Singh *et al.* (27).** The observed and proposed nitrogen-containing compounds derived from the S-NO group of GSNO are enclosed in boxes.

The mechanism is thought to occur *via* nucleophilic attack by the thiolate $R'S^-$ on the nitroso nitrogen, with rates being dependent on the $pK_a$ of the thiol R'SH (*28*). Reaction 1.16 can proceed at physiological pH (*29*), but *trans-S*-nitrosation is not the only reported reaction between RSNOs and other thiols. In the presence of high thiol concentrations, RSNO decomposition (thiolysis) is proposed to occur *via* a *N*-hydroxysulfenamide [RSN(OH)SR] intermediate, with RSSR', $N_2O$, $NH_3$, and $NO_2^-$ being the final products under aerobic conditions. Under anaerobic conditions, NO is evolved from the reaction and the amount of $NH_3$ detected is lower (*27, 30*). Two complex schemes have been proposed for the observed thiolysis reactions between

GSNO and GSH. Scheme 1.1 proposes that excess GSH reacts with the GSN(OH)SG intermediate, while Scheme 1.2 includes the initial generation of HNO via nucleophilic attack of GSH at the sulfur atom of GSNO in addition to reactions *via* the GSN(OH)SG intermediate (*30*). Another report argues that the observed end products of thiolysis are a result of the long incubation times used in the experiments (24–40 h), and that these products are not present immediately after the reaction between the GSNO and G'SH (< 2 min) (*31*).

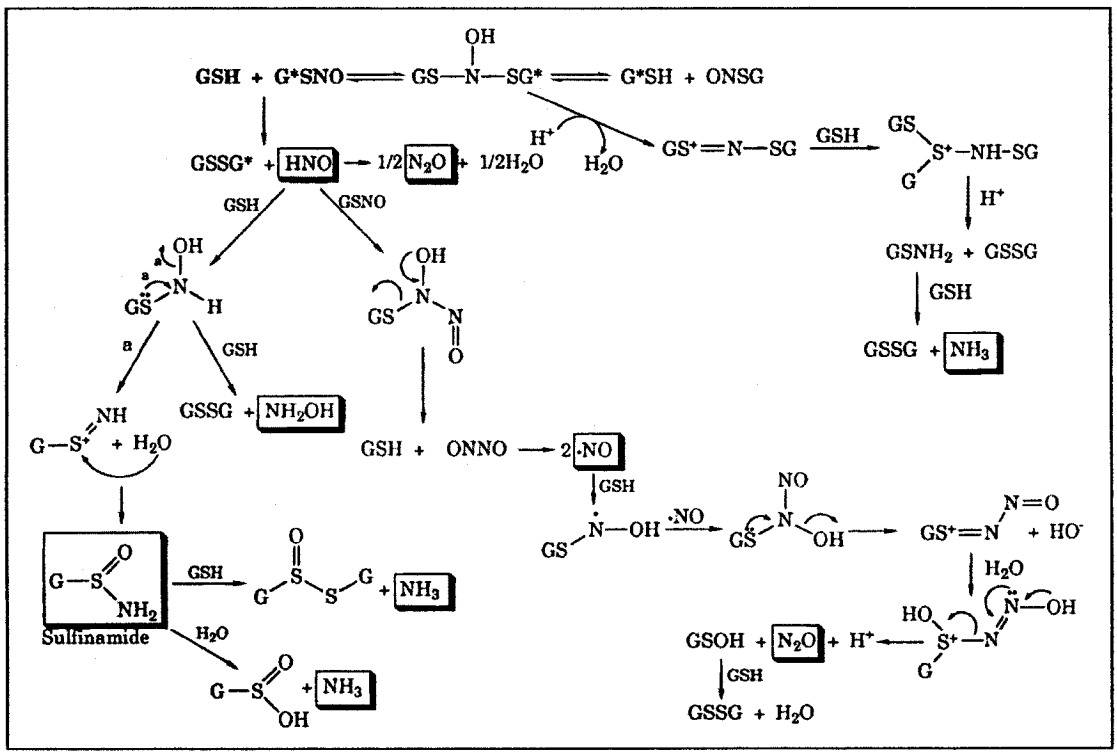


**Scheme 1.2. Reactions of GSNO at high GSH concentration as proposed by Wong *et al.* (*30*).** The observed and proposed nitrogen-containing compounds derived from the S-NO group of GSNO are enclosed in boxes.

The mechanistic details involved in non-reductive heterolytic decomposition of the *S*-NO bond are not completely understood. These reactions are complex with respect to the order of their rate laws and the products of decomposition. In some cases, widely different reaction rates for the decomposition of a given RSNO have been reported (*20*). In most instances, the experimental conditions affect the distribution of the decomposition products. Disulfides (RSSR), disulfide oxides [RS(O)SR, $RS(O_2)SR$], sulfenic acids (RSOH), and sulfonic acids ($RSO_3H$) have been reported as the major products of RSNO decomposition in the absence of excess thiol (*32*). Some authors have shown that if oxygen is strictly excluded, only the disulfide is formed, and that in the presence of $O_2$ decomposition occurs through a chain reaction catalyzed by $N_2O_3$ (*16*). In the presence of excess thiols, complex thiolysis mechanisms have been proposed that involve intermediates such as RSN(OH)SR (*27*), or $RS(O)NH_2$ (*30*) which in turn undergo side reactions that eventually lead to the formation of the final products.

In the mechanism proposed by Singh *et al.* (Scheme 1.1) (*27*), GSH reacts initially with GSNO at the nitroso nitrogen to form a GSH-*N*-hydroxysulfenamide intermediate, GSN(OH)SG, that can react with additional GSH to eventually produce GSSG and $NH_3$. Alternatively, the *N*-hydroxysulfenamide can undergo homolytic cleavage of the S-N bond to yield a GSH-*N*-hydroxy radical and a glutathionyl radical $GS^{\bullet}$. The GSH-*N*-hydroxy radical reacts further to yield GSSG and $NO_2^-$ in the presence of oxygen, or GSSG and $N_2O$ in its absence. The $GS^{\bullet}$ radical can react with GSH and $O_2$ to produce GSSG or with GSNO to produce GSSG and NO. The authors reported detection of GSSG, $NH_3$, $N_2O$, $NO_2^-$, and GSN(OH)SG, but not $GSO_2H$, $GSNH_2$, GSOH, or NO.

In the mechanism proposed by Wong *et al.* (*30*), GSH can react with GSNO at both the *S* or *N* atoms of the *S*-NO bond. Reaction at the nitroso *N* is proposed to form the GSH *N*-hydroxysulfenamide suggested by Singh *et al.* (Scheme 1.1), and this undergoes hydrolysis and additional reactions with GSH to form GSSG and $NH_3$ as the final products. Reaction at the nitroso *S* generates GSSG and HNO, which was detected as $N_2O$. The authors proposed that HNO also reacts with additional GSH to form $NH_2OH$, $NH_3$, GSSG, and a sulfinamide $GS(O)NH_2$. Alternatively, HNO can react with GSNO in a series of reactions that yield GSSG, $N_2O$, and NO. The products identified in the reaction solutions include NO, $N_2O$, $NH_3$, $NO_2^-$, $NH_2OH$, and GSSG. The formation of the sulfinamide $GS(O)NH_2$ was postulated after comparison of its thin-layer chromatographic properties to those of a GS-sulfinamide synthesized separately. The implications of this study are that HNO can be generated in the reaction of GSNO and thiols in high concentrations.

## 1.3 GSNO

*S*-nitrosoglutathione (GSNO) (Figure 1.1) is the *S*-nitroso derivative of glutathione (*L*-γ-glutamyl *L*-cysteinylglycine) (Figure 1.3). The parent thiol, GSH, is a ubiquitous molecule that is produced in all organs, and is the principal nonprotein thiol involved in antioxidant cellular defense (*33*). GSNO is one of the most commonly used sources of NO in the biomedical field (*34*) because of its high potency as a vasodilator (*35*), a muscle relaxer, and an inhibitor of platelet aggregation (*36, 37*). At low concentrations, GSNO has been reported to give protection to the ischemic myocardium (*38*), and in angina pectoris (*39*).

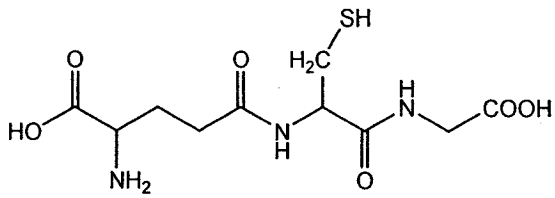


**Figure 1.3. Glutathione (GSH) (*40*)**

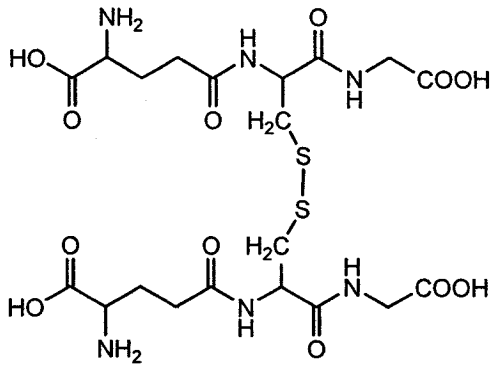


**Figure 1.4. Oxidized glutathione (GSSG) (*41*)**

Exposure of proteins to decomposed GSNO effects glutathiolation (*32, 42*). Li *et al.* (*32*) reported that the major decomposition products of GSNO in aqueous solutions in the dark are glutathione sulfonic acid ($GSO_3H$), glutathione disulfide *S*-oxides [GS(O)SG, $GS(O_2)SG$] and disulfide (GSSG) (Figure 1.4). They found that among these decomposition products, GS(O)SG is the most potent glutathiolating agent for neurogramin RC3 (Ng) and neuromodulin/GAP-43 (Nm). Results from our laboratory (*42*) have shown that recombinant human brain calbindin $D_{28k}$, bovine serum albumin, glyceraldehyde-3-phosphate dehydrogenase (GAPDH), and Cu,Zn-superoxide dismutase (CuZnSOD) can also be glutathiolated in GSNO solutions decomposed at pH ~ 3.5. A

hydrolysis decomposition pathway involving nucleophilic attack at the sulfur atom and yielding GSOH and HNO as intermediates was proposed (37):

$$GSNO + H_2O \rightleftharpoons GSOH + HNO \quad (1.17)$$

$$GSOH + GSNO \rightleftharpoons GS(O)SG + HNO \quad (1.18)$$

$$GSOH + GSOH \rightleftharpoons GS(O)SG + H_2O \quad (1.19)$$

$$2\,GS(O)SG \rightleftharpoons GSO_2SG + GSSG \quad (1.20)$$

$$2HNO \rightarrow N_2O + H_2O \quad (1.21)$$

This mechanism was suggested based on the inhibition of GSNO decomposition by dimedone, which reacts with sulfenic acids (Reaction 1.22) (*43, 44*). Also, metmyoglobin ($MbFe^{III}$), which is a nitroxyl scavenger, was converted to the ferrous nitrosyl form (Reaction 1.23) indicating the formation of HNO. LC-MS was used to identify the GSX products (*42*).

GSOH + 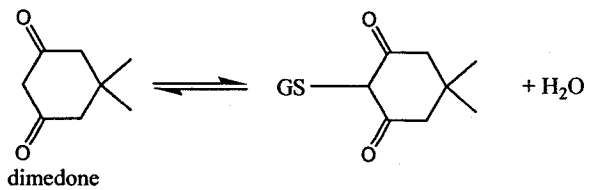 + $H_2O$ (1.22)

dimedone

$$HNO + (MbFe^{III}) \rightleftharpoons MbFe^{II}NO + H^+ \quad (1.23)$$

Hydrolysis of RSNOs has been studied in both acidic and basic solutions. At low pH, the reaction is thought to occur *via* nucleophilic attack by water at the nitroso nitrogen of RSNO, the reverse of *S*-nitrosation (Reaction 1.3) (*45*), and not *via* attack on the sulfur atom (Reaction 1.17). Under basic conditions, hydrolysis has been reported to occur by nucleophilic attack of $OH^-$ also at the nitroso nitrogen. However, the yield of the expected $NO_2^-$ product [$pK_a$ $HNO_2$ = 3.15 at 25°C (*46*)] was only ~50%, which suggests additional reaction at the sulfur atom (*14*).

### 1.3.1 Methods of analysis of GSNO

The decomposition of aqueous solutions of GSNO in the dark has been reported (*12, 41, 47-49*). As in the case of other RSNOs, conflicting reaction rates have been reported that vary as a function of pH, GSNO concentration, and the presence of redox-active metals. The reported decomposition products also vary. Aside from the many different experimental conditions employed, the analytical methodologies used likely contribute to the confusion. Most of the GSNO decomposition studies have used UV-vis spectrophotometry to measure the loss of absorbance at 330-350 nm due to cleavage of the *S*-NO bond (*41, 47-51*), which does not exclude interferences from absorbance of the decomposition products. HPLC coupled with UV-visible detection has also been attempted but, in one case the method used was not able to separate the decomposition products (*52*). A second method made use of long columns and run times of several hours to perform the separation (*32*). GC-MS methods were used to identify the decomposition products, but these analysis have been carried out only after complete GSNO decomposition (*16*), or after long incubation periods of up to 40 h (*27, 30*). Thus, the final products may include those formed from secondary reactions of the initial products.

The need for sensitive and specific analytical methods for the analysis of GSNO and the multitude of GSX products extends to the biomedical settings. Most of the current chromatographic methods involve derivatization to separate and detect GSNO in biological matrices (*53-55*), which can introduce errors and is time-consuming. Some commonly used reversed-phase HPLC methods employ $C_{18}$ analytical columns and mobile phases in the pH range of 2 to 4 (*56-58*). However, it has been shown that GSNO can be formed as an artifact when the analytical matrix is rich in GSH and nitrite, or peroxynitrite (*59, 60*). Currently, there is a lot of debate about the levels of GSNO that have been detected *in vivo*, with some researchers arguing that the high levels detected are due to artifacts of the analytical methodology (*60*).

The formation of GSNO during HPLC analysis can be avoided by performing the analysis in mobile phases at neutral pH. To date only one such method has been reported, and it employs ion-pairing chromatography with UV detection (*60*). The authors suggest that mass spectrometric detection could be used to make the method more sensitive. However, the ion-pairing agent used (tetrabutylammoniumhydrogen sulfate, TBAHS) is not volatile, hence it would likely suppress ionization in the ion source of the mass spectrometer. The analysis of GSNO samples by an in-line LC/MS method using mobile phases at neutral pH has not yet been reported in the literature.

## 1.4 Hypothesis, scope and organization of thesis

*S*-Nitrosothiols are reported to be major pools of nitric oxide *in vivo*, to be involved in *trans-S*-nitrosation reactions, and in the transport of nitric oxide in the body. However, the mechanisms of GSNO decomposition are not completely understood. The hypotheses presented in this thesis are that (i) GSNO decomposition at both low and high

pH, in the dark and in the absence of metal ions and added thiols, is a hydrolytic process initiated by nucleophilic attack occurring mainly at the nitroso nitrogen, (ii) decomposition at low pH occurs *via* a chain mechanism where $N_2O_3$ is the chain carrier, while (iii) at high pH the mechanism includes a nitrosated disulfide intermediate, and (iv) GSNO thiolysis at physiological pH proceeds *via* thiolate attack at both the sulfur and nitrogen atoms of the S-NO bond.

In Chapter 2, the structural dependence of RSNO acid-catalyzed hydrolysis rates was investigated at high acidity. Chapters 3, 4 and 5 describe product analyses using HPLC/UV, HPLC-ESI/MS, and GC/MS in the study of mechanisms of acid- and base-catalyzed hydrolysis and thiolysis of GSNO. In Chapter 6, the effects of instrumental settings on the mass spectra of GSNO were systematically studied. Finally, a chromatographic method to measure GSNO using neutral-pH mobile phases was developed as outlined in Chapter 7.

## 1.5 Contributions of Colleagues

I carried out all the work reported here and prepared the manuscripts. Ann English and Elizabeth Kwong provided intellectual support. Ann English edited the manuscripts.

Robert Papp at Merck Frosst Canada contributed timely suggestions in the development of the HPLC/MS method described in Chapter 7. He also provided instruction and technical support in the operation of the LCQ Deca mass spectrometer.

Alain Tessier at Concordia University provided technical support in the operation of the Q-Tof 2 mass spectrometer.

# Chapter 2 - Rates of *S*-nitrosothiol hydrolysis in concentrated acid

## 2.1 Abstract

The acid-catalyzed hydrolysis of three primary RSNOs, *S*-nitrosocysteine, *S*-nitroso-*N*-acetylated-cysteine, and *S*-nitrosoglutathione and two tertiary RSNOs, *S*-nitrosopenicillamine and *S*-nitroso-*N*-acetylated-penicillamine, was investigated to measure the effects of structure on the denitrosation rates. Substitution of the H atoms on the C-SNO carbon by methyl groups resulted in a 38-fold increase in the $k_{obs}$ for the *N*-acetylated RSNOs and a 12-fold increase for the non-acetylated RSNOs. The increased rates are a result of electron donation from the methyl groups attached to the Cys β-carbon increasing the proton affinity of the nitroso sulfur, which is the initial step in the acid-catalyzed hydrolysis. Only minor changes in $k_{obs}$ due to *N*-acetylation were observed. The activation energy for the process was calculated at 25.7 ± 1.7 kcal/mole for *S*-nitroso-*N*-acetylated-cysteine, and 23.7 ± 1.3 kcal/mole for *S*-nitroso-*N*-acetylated-penicillamine.

## 2.2 Introduction

Nitric oxide is an important molecule in mammalian physiology. NO is synthesized *in vivo* by the action of NO synthases (*3*) and is a key player in biological processes such as vasodilation, inhibition of platelet aggregation, and signalling in the central nervous system (*4*). Similar physiological properties have been attributed to nitroxyl ($NO^-$/HNO), the one-electron reduced form of NO (*61*). *S*-nitrosothiols (RSNOs) are NO-modified thiols that are believed to act as NO transporters *in vivo* and are routinely used as NO donors in the study of NO-related processes (*49*). The mechanisms

of NO donation by RSNOs, however, are not completely understood (*20*). RSNOs are known to decompose by the action of light, heat, and metal-catalyzed reduction to yield NO and the disulfide RSSR (*15*). While not all these mechanisms are relevant *in vivo*, the understanding of such processes is, nonetheless, important in the interpretation of results from studies in which RSNOs are used as NO donors.

Another mechanism of RSNO decomposition is *via* hydrolysis of the *S*-NO bond. Al-kaabi *et al.* investigated the kinetics of decomposition of (±)-2-acetylamino-2-carboxy-1,1-dimethylethanethiol, also known as *S*-nitroso-*N*-acetylated-penicillamine (SNAP, **5**) in the presence and absence of different nucleophiles. They found that, in the absence of nucleophiles, hydrolysis of the *S*-NO bond is strongly acid catalyzed.

Hydrolysis of RSNOs can occur following nucleophilic attack by a water molecule on the *S* or *N* atoms of the *S*-NO bond. Hydrolysis *via* attack at the *N* atom is the reverse of the thiol nitrosation reaction and produces RSH and $HNO_2$ (eq. 2.1). Hydrolysis at the *S* atom would result in the production of RSOH and HNO (eq. 2.2), and was proposed by Tao and English based on strong inhibition of GSNO denitrosation by the sulfenic acid trap, dimedone (*42*).

$$RSNO + H_2O \rightleftharpoons RSH + HNO_2 \qquad (2.1)$$

$$RSNO + H_2O \rightleftharpoons RSOH + HNO \qquad (2.2)$$

*S*-Nitrosoglutathione (GSNO, **3**), which has been detected *in vivo*, is the product of *S*-nitrosation of glutathione, an important antioxidant found in millimolar concentrations in red blood cells (*8-10*). While investigating whether RSNO hydrolysis occurred *via* attack at the sulfur atom (Reaction 1.9), we observed that hydrolysis of

GSNO, a primary RSNO, was much slower than expected based on the published rate for SNAP, a tertiary RSNO. This was contrary to the accepted notion that tertiary RSNOs are more stable than primary RSNOs (*20*).

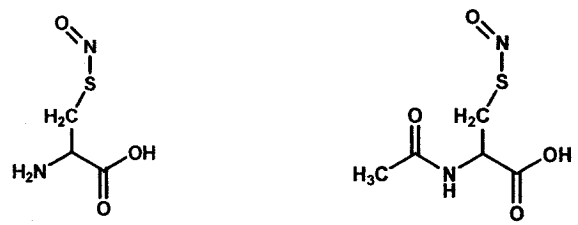

**1**
CysNO



**2**
SNAC

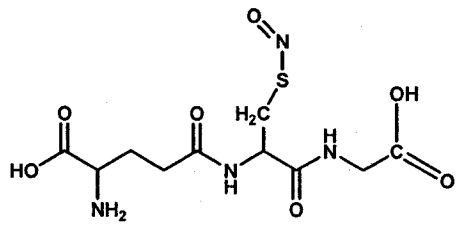

**3**
GSNO

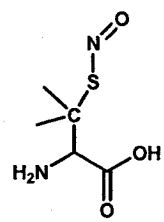

**4**
SPEN

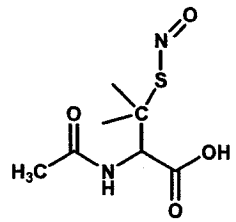

**5**
SNAP

**Figure 2.1. Structural formulas of the *S*-nitrosothiols investigated. 1:** *S*-nitrosocysteine (CysNO), **2:** *S*-nitroso-*N*-acetylated-cysteine (SNAC), **3:** *S*-nitrosoglutathione (GSNO), **4:** *S*-nitrosopenicillamine (SPEN), **5:** *S*-nitroso-*N*-acetylated-penicillamine (SNAP).

The objective of this study was to establish what structural features were responsible for the relatively high hydrolysis rates displayed by SNAP. For example, at low pH SNAP does not contain a charged ammonium group like GSNO, which could influence the steric factors affecting the hydrolysis. Three primary and two tertiary RSNOs, all of them based on cysteine (Figure 2.1), were selected for detailed analysis: *S*-nitrosocysteine (CysNO, **1**), *S*-nitroso-*N*-acetylated-cysteine (SNAC, **2**), GSNO (**3**), *S*-nitrosopenicillamine (SPEN, **4**), and SNAP (**5**). A comparison of the *N*-acetylated and unacetylated derivtives should reveal the role, if any, of the ammonium group. The experiments were conducted in the presence of the $HNO_2$ trap, $NaN_3$ (or $HN_3$ at low pH; $pK_a$ $HN_3$ = 4.72 (*62*)) to drive the reaction in equation 2.1 towards RSNO decomposition. High acidity (~ 4 M $H_2SO_4$) was used to accelerate the hydrolysis so that the rates could be measured in a relatively short period of time (*45*).

## 2.3 Experimental

### 2.3.1 Materials

Diethylenetriaminepentaacetic acid (DTPA) was from Koch-Light Laboratories. All other reagents were purchased from Sigma-Aldrich.

### 2.3.2 Synthesis of RSNO stock solution

Stock RSNO solutions were prepared *in situ* by mixing equal volumes of 20 mM RSH in 125 mM $H_2SO_4$ (aq) with 20 mM $NaNO_2$ in 2 mM DTPA (aq), followed by a 10-min incubation period at room temperature in the dark (*14, 63*). To speed up dissolution, the tertiary thiols were first dissolved in MeOH (50% of the volume of the

final RSH solution), and then diluted with an equal volume of 250 mM $H_2SO_4$ (aq). Fresh stock RSNO solutions were prepared on the same day of the experiment and kept on ice.

### 2.3.3 UV-vis spectrophotometry

The UV-visible spectra were recorded on a HP 8453 UV-vis diode-array spectrophotometer equipped with a thermostatted cell holder (Agilent Technologies), and a 1-mm-pathlength semi-micro cell. To minimize RSNO photodegradation, the spectrophotometer cell holder was covered and the integration time was set to 0.1 s. At this setting each measurement resulted in 0.03% absorbance loss due to photolysis in the beam. Denitrosation was monitored at 335 and 338 nm for the primary and tertiary RSNOs, respectively, after the spectra were background-corrected by subtracting the absorbance in the 800–830-nm region from each sample. A total of 20–30 readings were taken during each experiment, covering 2–3 RSNO half-lives.

### 2.3.4 Reaction conditions

The experiments were conducted in duplicate by mixing 375 μL of 5.0 M $H_2SO_4$ and 75 μL of the $HNO_2$ trap $NaN_3$ (at the desired concentration) in a 700 μL semi-micro quartz cell, equilibrating it at the desired temperature for 5 min in the spectrophotometer cell holder, adding 50 μL of 10 mM stock RSNO, and measuring the UV-vis spectra at the appropriate time intervals. The solutions were protected from light throughout the duration of the experiment.

## 2.4 Results

### 2.4.1 Hydrolysis rate as a function of $HNO_2$ trap concentration

The hydrolysis of RSNOs is a reversible process (Reaction 2.1) that lies largely on the side of RSNO formation (*14*). To measure the rate of RSNO hydrolysis, the reactions were conducted in ~ 4 M $H_2SO_4$ in the presence of the nitrous acid trap, $HN_3$. These reaction conditions were reported to facilitate the acid-catalyzed hydrolysis of SNAP (*45*), and were chosen here to allow us to compare our results to those in the literature. Under these conditions, acid-catalyzed RSNO denitrosation is a pseudo-first order reaction.

The effect of [$HN_3$] on the observed denitrosation rate at 31°C was evaluated to establish the trap concentration at which RSH nitrosation is fully inhibited. Figures 2.2 and 2.3 show the effect of [$HN_3$] on $k_{obs}$ for denitrosation in 3.75 M $H_2SO_4$ of the primary *S*-nitrosothiol, GSNO, and the tertiary *S*-nitrosothiol, SNAP, respectively. In both cases $k_{obs}$ becomes independent of [$HN_3$] at 20 mM, which was the trap concentration used for the rest of this study. The results also reveal that the limiting $k_{obs}$ for SNAP denitrosation at 20 mM $HN_3$ is ~40 times higher than for GSNO. However, since a similar $HN_3$ concentration is required to prevent the back reaction (reverse of eq. 2.1), the rates of *S*-nitrosation by $HNO_2$ must be similar for both thiols.

### 2.4.2 Hydrolysis of primary RSNOs at 31 °C

Hydrolysis rates of three primary RSNOs, CysNO, SNAC, and GSNO, were evaluated to determine if the proximity of the ammonium or carboxylate groups influence hydrolysis.

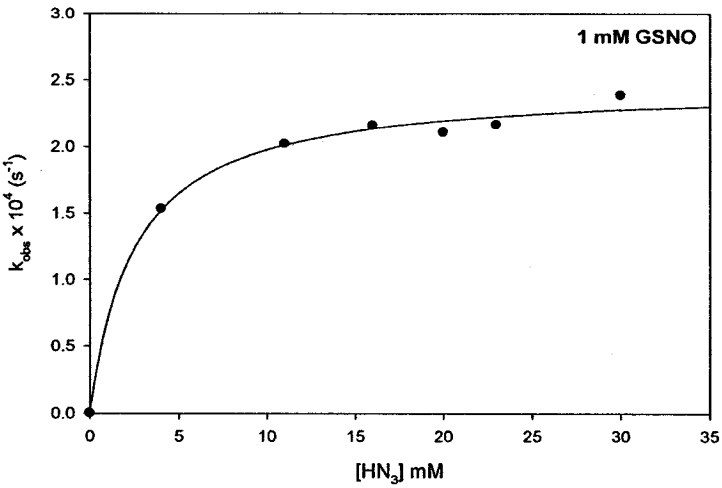


**Figure 2.2. GSNO denitrosation rate constants *vs* [$HN_3$].** The denitrosation of 1 mM GSNO (containing 0.1 mM DTPA, 1 mM NaCl) in 3.75 M $H_2SO_4$ at 31 °C in the dark was monitored at 335 nm over 2 half-lives using a 0.1-s integration time. The $k_{obs}$ values (dark circles) were calculated from plots of ln($Abs_{335}$) *vs* t. The solid line, which shows rate-sturation at high [$HN_3$], was generated by the curve-fitting algorithm in the SigmaPlot® graphing program (*64*).

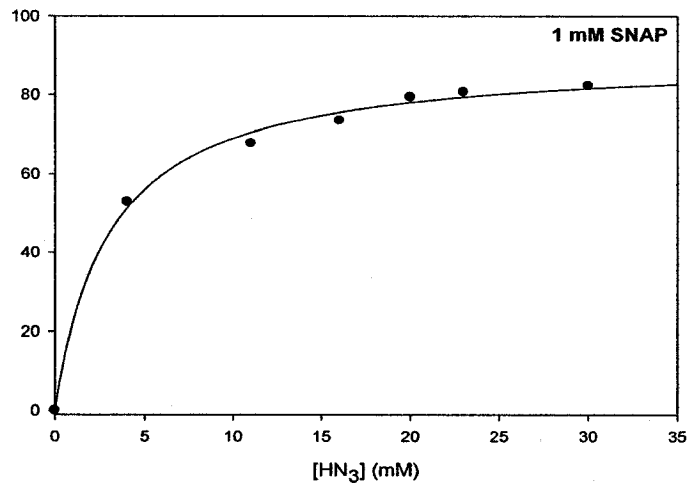


**Figure 2.3. SNAP denitrosation rate *vs* [HN3].** The denitrosation of 1 mM SNAP (containing 0.1 mM DTPA, 1 mM, 2.5% v/v MeOH) in 3.75 M $H_2SO_4$ at 31 °C in the dark was monitored at 338 nm over 3 half-lives using a 0.1-s integration time. The $k_{obs}$ values (dark circles) were calculated from plots of ln($Abs_{338}$) *vs* t. The solid line, which shows rate-sturation at high [$HN_3$], was generated by the curve-fitting algorithm in the SigmaPlot® graphing program (*64*).

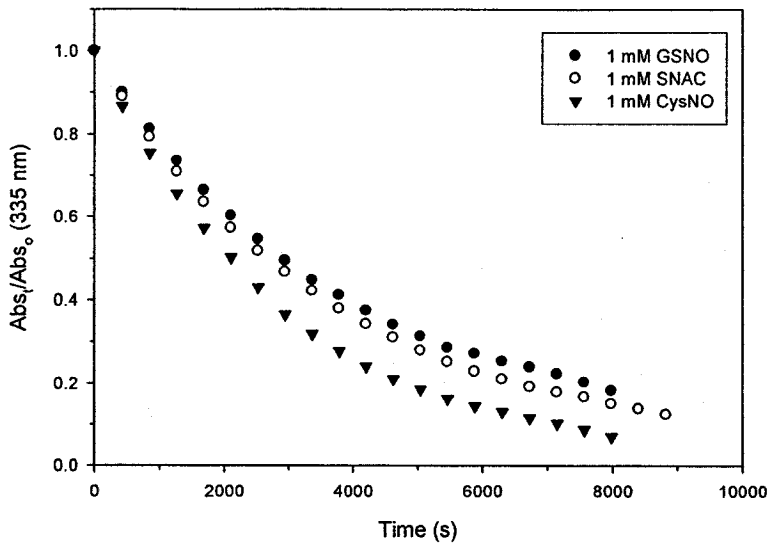


**Figure 2.4. Plots of GSNO, CysNO, and SNAC denitrosation in $H_2SO_4$ in the presence of a $HNO_2$ trap.** The denitrosation of 1 mM RSNO (containing 0.1 mM DTPA, 1 mM NaCl) in 3.75 M $H_2SO_4$ plus 20 mM $HN_3$ ($HNO_2$ trap) at 31 °C in the dark was monitored at 335 nm using 0.1-s integration time .

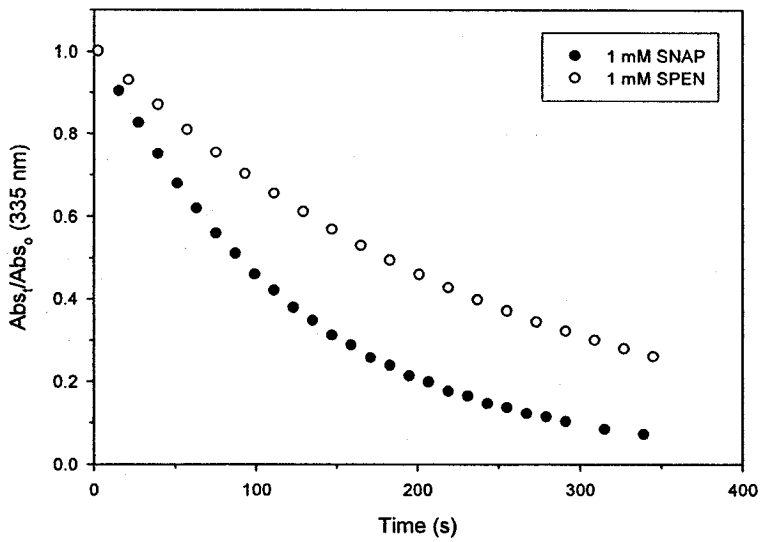


**Figure 2.5. Plots of SNAP and SPEN denitrosation in $H_2SO_4$ in the presence of a $HNO_2$ trap.** The denitrosation of 1 mM RSNO (containing 0.1 mM DTPA, 1 mM NaCl, 2.5% v/v MeOH) in 3.75 M $H_2SO_4$ plus 20 mM $HN_3$ ($HNO_2$ trap) at 31 °C in the dark was monitored at 338 nm using 0.1-s integration time.

The results in Table 2.1 and Figure 2.4 show that there is no significant difference between the denitrosation rates of GSNO and SNAC, and that these rates are only slightly slower than that for CysNO. This indicates that the rate difference between GSNO and SNAP hydrolysis is not primarily due to modifications of the amino or carboxy groups of cysteine, but to the presence of the two methyl groups on the β carbon.

### 2.4.3 Hydrolysis of tertiary RSNOs at 31 °C

To further explore the relationship between hydrolysis rates and structure, the denitrosation of two tertiary RSNOs, SNAP and SPEN, that differ only in *N*-acetylation was monitored at 31 °C. The results (Figure 2.5 and Table 2.1) show that the hydrolysis rate of SNAP, which is *N*-acetylated, is twice that of SPEN. However, *N*-acetylated CysNO (SNAC) exhibits a 1.5-fold slower hydrolysis rate than CysNO indicating that there may be interaction between the *N*-acetyl and methyl groups in SNAP.

### 2.4.4 Temperature dependence

To compare the activation energy for acid-catalyzed hydrolysis of primary and tertiary RSNOs, the SNAC and SNAP hydrolysis rates were measured in the temperature range 18–31 °C. The activation energy ($E_a$) for SNAC hydrolysis is 25.7 ± 1.7 kcal/mole and that for SNAP is 23.7 ± 1.3 kcal/mole (Figure 2.6 and Table 2.1), indicating that $E_a$ for both RSNOs is the same within experimental error. Typical ln(Abs) *vs* t plots used for calculating $k_{obs}$ for the RSNOs at 31 °C are shown in Section 2.7 (Figures A2.1 and A2.2)

## 2.5 Discussion

The acid-catalyzed hydrolysis of SNAP was reported by Al-Kaabi *et al.* (*45*). They investigated the reaction in 0.9–4.4 M $H_2SO_4$ and found that hydrolysis of the *S*-NO

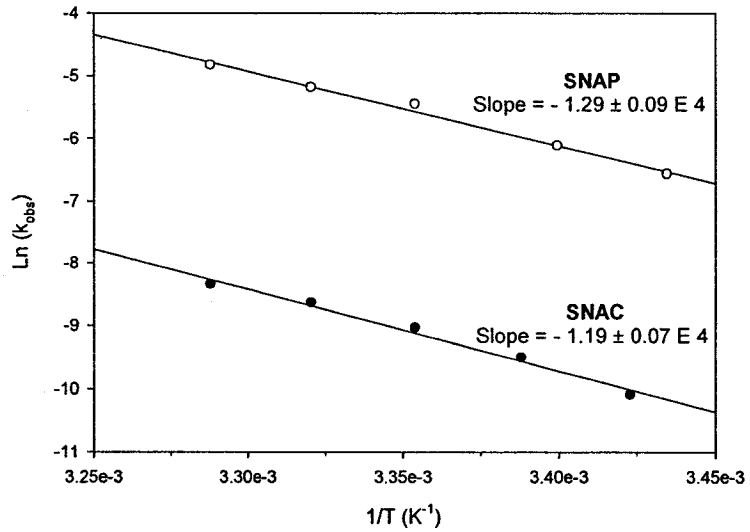


**Figure 2.6. Temperature dependence of $k_{obs}$ for SNAP and SNAC denitrosation.** Closed circles: 1 mM SNAC (containing 0.1 mM DTPA, 1 mM NaCl). Open circles: 1 mM SNAP (containing 0.1 mM DTPA, 1 mM NaCl, 2.5% v/v MeOH) in 3.75 M $H_2SO_4$ + 20 mM $HN_3$. Samples at 18–31 °C, in the dark were monitored using 0.1-s integration time at 335 nm over 2–3 half-lives (SNAC) and at 338 nm over 3 half-lives (SNAP:).The $k_{obs}$ values were calculated from plots of ln(Abs) *vs* t. The linear regression was performed in SigmaPlot® (*64*).

bond is strongly acid-catalyzed, with $k_{obs}$ = 81.7 x $10^{-4}$ $s^{-1}$ in 3.77 M $H_2SO_4$ at 31 °C. They also found that hydrolysis resulted in the formation of the parent thiol, *N*-acetylated-penicillamine (NAP), indicating that the reaction proceeds *via* nucleophilic attack of $H_2O$ at the *N* atom of the *S*-NO bond. In addition, nucleophiles such as $Cl^-$, $Br^-$, and $SCN^-$ were found to accelerate hydrolysis in a concentration-dependent manner (*45*).

The results reported here show that the hydrolysis rates are sensitive to RSNO structure. The five RSNOs studied can be considered cysteine derivatives (Figure 2.1). Within the set of primary RSNOs, SNAC and GSNO differ from CysNO in *N*-acylation of their α-amino groups with an acetyl group and a γ-glutamic acid (γGlu) residue,

respectively. GSNO also differs from CysNO by amidation with a glycine (Gly) residue at its carboxylic group. The tertiary RSNOs, SPEN and SNAP, result from dimethyl substitution at the β-carbon of CysNO and SNAC, respectively (Figure 2.1).

**Table 2.1** Temperature dependence of RSNO denitrosation in 3.75 M $H_2SO_4$ in the dark[a]

| RSNO | Temp (°C) | $k_{obs}$ x $10^4$ ($s^{-1}$)[b] | $E_a$ (kcal/mole)[c] | A ($s^{-1}$)[d] |
|---|---|---|---|---|
| GSNO | 31 | 2.10 ± 0.04 | | |
| CysNO | 31 | 3.23 ± 0.03 | | |
| SNAC | 31 | 2.35 ± 0.03 | 25.7 ± 1.7 | 7.05 x $10^{14}$ |
| | 28 | 1.75 ± 0.01 | | |
| | 25 | 1.18 ± 0.02 | | |
| | 22 | 0.74 ± 0.01 | | |
| | 19 | 0.41 ± 0.01 | | |
| SPEN | 31 | 39.5 ± 0.1 | | |
| SNAP | 31 | 79.4 ± 0.3 | 23.7 ± 1.3 | 7.81 x $10^{14}$ |
| | 28 | 55.8 ± 0.4 | | |
| | 25 | 42.7 ± 0.4 | | |
| | 21 | 22.0 ± 0.1 | | |
| | 18 | 15.0 ± 0.1 | | |

[a] Solutions contained 1 mM RSNO, 1 mM NaCl, 20 mM $HN_3$ and (SNAP and SPEN only) 2.5% v/v MeOH. [b] Calculated from plots of ln(Abs) *vs* t; [c,d] Calculated from the slopes and intercepts of the regression lines of plots of ln($k_{obs}$) *vs* 1/T (Figure 2.6).

The presence of the γGlu and Gly residues in GSNO or the acetyl group in SNAC has little influence on acid hydrolysis since the $k_{obs}$ for GSNO, CysNO, and SNAC (Figure 2.4, Table 2.1) are within 2–4 x $10^{-4}$ $s^{-1}$ at 31 °C. Substituting the β-carbon hydrogens in CysNO by methyl groups results in a 12-fold increase in $k_{obs}$ from 3.23 x

$10^{-4}$ $s^{-1}$ to 39.5 x $10^{-4}$ $s^{-1}$ for SPEN, at 31 °C. A similar substitution in SNAC increased $k_{obs}$ 34-fold from 2.35 x $10^{-4}$ $s^{-1}$ to 79.4 x $10^{-4}$ $s^{-1}$ for SNAP at 31 °C, which is in excellent agreement with that reported by Al-Kaabi *et al.* (81.7 x $10^{-4}$ $s^{-1}$) (*45*).

The increased hydrolysis rate on dimethylation of the β-carbon is attributed to the electron-releasing properties of the methyl group. Recently, it has been proposed in our group that the electronic structure of RSNOs can be expressed as a combination of three resonance structures, including the conventional structure ***S*** plus zwitterionic (***D***) and ionic (***I***) structures (eq. 2.3) (*19*):

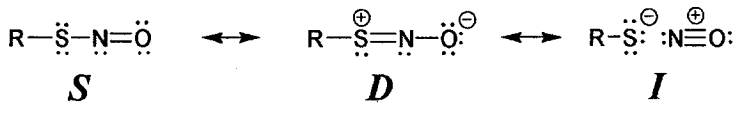


(2.3)

This resonance description can rationalize the structure and reactivity of RSNOs (*19*). We predict that protonation at the nitroso sulfur promotes the ionic resonance structure ***I*** thereby destabilizing the S–N bond and increasing the electrophilicity of the nitrogen. For example, protonated $CH_3SNO$ has ~50% contribution of ***I*** *vs* ~10% in neutral $CH_3SNO$. The predicted proton affinities (PAs) of $CH_3SNO$ indicate that protonation at the *S* atom is thermodynamically favored over protonation at the *O* and *N* (the PAs are 185.4, 181.1 and 181.8 kcal/mol for *S*, *O*, and *N*, respectively). Thus, acid-catalysis of RSNO hydrolysis involves protonation at the *S* atom, which destabilizes the *S*–NO bond, increases the nucleophilicity of the nitroso *N* atom, making it prone to nucleophilic attack by a water molecule. Furthermore, the calculations suggest that the PAs of RSNOs

increase on going from primary to tertiary RSNOs. The calculated PA of $(CH_3)_3CSNO$ is ~8 kcal/mol higher than that of $CH_3SNO$ (193.7 and 185.4 kcal/mol, respectively) (*65*). Thus, the increased hydrolysis rates of tertiary RSNOs can be attributed to the increased proton affinity of their nitroso *S* atom as compared to that in primary RSNOs. In contrast, the two-fold increase in $k_{obs}$ of SNAP *vs* SPEN (Table 2.1) is attributed to the greater electron-withdrawing effect at low pH of the ammonium *vs* *N*-acetyl groups on the α-carbons of SPEN and SNAP, respectively (Figure 2.1)

The observed activation energies for the acid-catalyzed hydrolysis of SNAC and SNAP are the same (Table 2.1), indicating that the reaction proceeds *via* the same transition state for primary and tertiary RSNOs. The values for $E_a$ are 5–8 or 3–6 kcal/mol lower for SNAP and SNAC, respectively, than the previously reported $E_a$ for homolytic dissociation of the *S*-NO bond of the primary RSNOs, $CH_3(CH_2)_5SNO$ (28.9 kcal/mole) and *c*-$C_6H_{11}SNO$ (31.6 kcal/mole) in the temperature range of 60–80 °C in organic solution (*25*). Thus, the $E_a$ values for the reactions studied here probably correspond to the energy needed to heterolytically cleave the $SH^+$-NO bond in aqueous solutions of high acidity.

## 2.6 Conclusions

The results from this study show that rates of acid-catalyzed hydrolysis vary with RSNO structure. Substitution of the hydrogen atoms on the β-carbon of CysNO by methyl groups, which are electron-donating, results in increased proton affinity of the sulfur atom. This accelerates dissociation of the *S*-NO bond since acid-catalyzed hydrolysis requires protonation of the sulfur, as shown computationally. We predict that

electron-withdrawing groups at the β-carbon would lead to a decrease in the rate of acid-catalyzed hydrolysis.

## 2.7 Supplementary Figures to Chapter 2

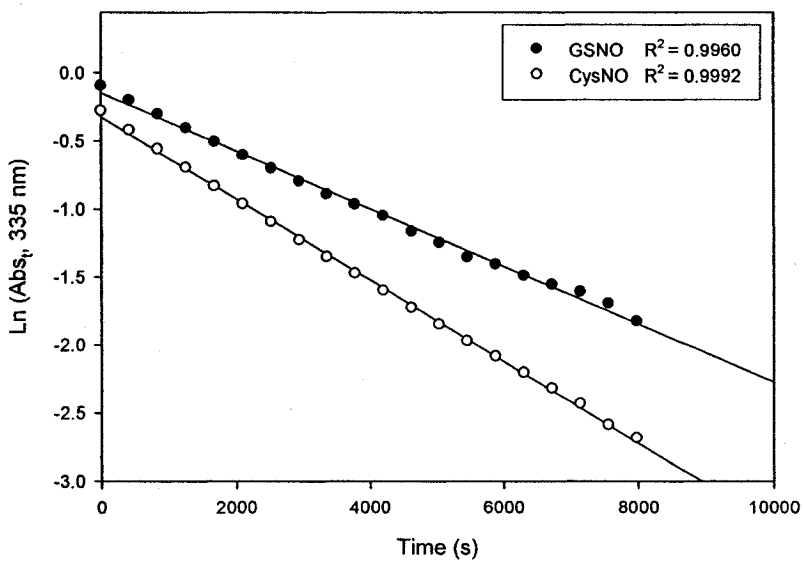


**Figure S2.1. Typical plots of ln(Abs) *vs* t used for calculating $k_{obs}$ for CysNO and GSNO hydrolysis at 31 °C in $H_2SO_4$ in the presence of a $HNO_2$ trap.** The denitrosation of 1 mM RSNO (containing 0.1 mM DTPA, 1 mM NaCl, 2.5% v/v MeOH) in 3.75 M $H_2SO_4$ plus 20 mM $HN_3$ (an $HNO_2$ trap) at 31 °C in the dark was monitored at 335 nm using 0.1-s integration time.

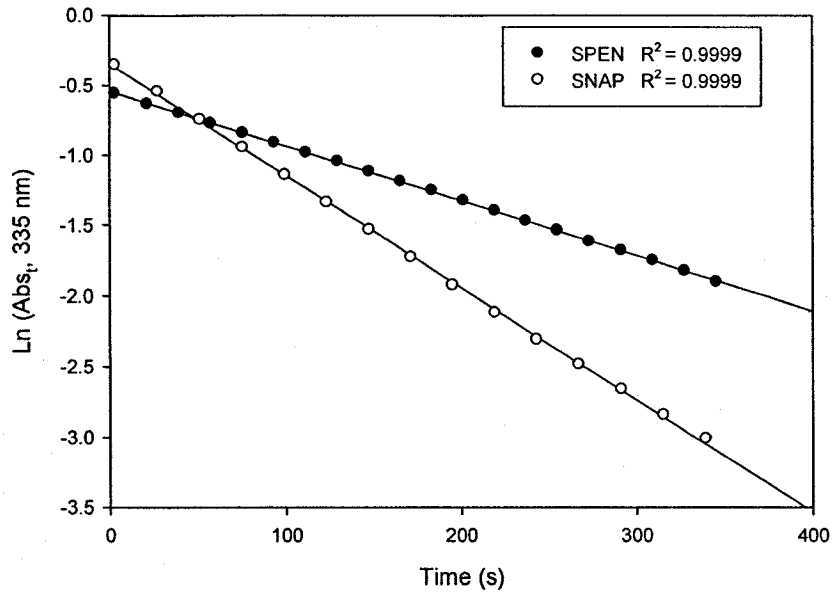


**Figure S2.2. Typical plots of ln(Abs) *vs* t used for calculating $k_{obs}$ for SPEN and SNAP hydrolysis at 31 °C in $H_2SO_4$ in the presence of a $HNO_2$ trap.** The denitrosation of 1 mM RSNO (containing 0.1 mM DTPA, 1 mM NaCl, 2.5% v/v MeOH) in 3.75 M $H_2SO_4$ plus 20 mM $HN_3$ (an $HNO_2$ trap) at 31 °C in the dark was monitored at 338 nm using 0.1-s integration time.

# Chapter 3 - Mechanism of acid-catalyzed GSNO decomposition at pH 2.0

## 3.1 Abstract

The mechanisms of decomposition of GSNO in aqueous solutions at pH 2.0, in the dark and in the presence of metal-ion chelators have been investigated. GSNO decomposition under these conditions exhibits a sigmoidal decomposition curve typical of autocatalytic processes. Based on strong inhibition of the reaction by removal of $HNO_2$, $N_2O_3$, or oxygen from the solutions, a chain reaction mechanism, initiated by the formation of nitrous acid from the hydrolysis of the *S*-NO bond *via* nucleophilic attack at the nitroso *N* atom, is proposed in which $N_2O_3$ is the chain carrier. The overall reaction generates $GSO_3H$, GSOSG, $GSO_2SG$, and $HNO_2$ as decomposition products. These results should be considered in the use of RSNOs as orally administered therapeutic agents.

## 3.2 Introduction

Nitric oxide (NO) is a small, stable, but highly reactive, molecule (*1*). It is produced *in vivo* by the action of NO synthases from the amino acid *L*-arginine (*3*) and is involved in many biological processes such as inhibition of platelet aggregation and adhesion to the vascular walls, smooth muscle relaxation in the vasculature, and neurotransmission in the central and peripheral nervous systems (*4*).

Although free NO can easily pass through certain cell membranes (*6*), it is likely to diffuse only several cell diameters away from its site of synthesis before attenuation of

its bioactivity by the oxidizing action of endogenous scavengers such as hemoglobin and superoxide ions (*4, 7*). As a result, it has been suggested that NO is incorporated into NO-generating species that preserve its bioactivity and serve as NO transporters in blood. One class of compounds proposed to act as NO transporters in the vascular system are *S*-nitrosothiols (RSNOs), which can be formed on the *S*-nitrosation of cysteine-containing proteins and peptides in plasma and in cells (*35, 66*). The participation of RSNOs in NO-related processes is supported by the detection and measurement *in vivo* of RSNOs such as *S*-nitrosoalbumin (*11*), *S*-nitrosoglutathione (GSNO), and *S*-nitrosocysteine (CysNO) (*8-10*), and the findings that RSNOs retain NO-like activity (*10*).

However, the mechanisms by which RSNOs donate NO to its targets are not completely understood (*20*). RSNOs release NO through homolytic cleavage of the *S*-NO bond by the action of light or heat (*15*), but these processes are not likely relevant to the *in vivo* activity of RSNOs (*20*). One accepted mechanism of NO donation that is biologically relevant is *trans S*-nitrosation, in which NO is transferred from RSNO to a second thiol (R'SH) to form a new R'SNO (*26*). RSNO denitrosation *via* hydrolysis of the S-NO bond following nucleophilic attack at either the nitrogen or sulfur atoms would generate nitrite or nitroxyl as the NO products, respectively (eqs. 3.1 and 3. 2) (*14*).

$$RSNO + H_2O \rightleftharpoons RSH + HNO_2 \qquad (3.1)$$

$$RSNO + H_2O \rightleftharpoons RSOH + HNO \qquad (3.2)$$

Nitroxyl ($NO^-$/HNO), the one-electron reduced form of NO, has also been

identified as possessing biological effects similar to those of NO itself, making it another important player in the NO biology (*61*).

Tao and English (*42*) observed that GSNO decomposed in unbuffered aqueous solutions (~ pH 3.5 for 5 mM GSNO) that were stored at room temperature and protected from light. This occurred even in the presence of specific copper chelators, generating GSOSG, $GSO_2SG$, and GSSG as the GSX products. GSNO decomposition, however, was inhibited on the addition of the sulfenic acid trap, dimedone. Based on these observations, they proposed a decomposition mechanism in which hydrolytic denitrosation of GSNO *via* nucleophilic attack at the sulfur atom was the initial step, yielding glutathione sulfenic acid (GSOH) and HNO as reaction intermediates. The proposed mechanism (Reactions 4.5 - 4.9), thus, suggested a route to HNO release by RSNOs *in vivo*, since GSNO hydrolysis could potentially be enzymatically catalyzed.

The goal of this study was to establish if GSNO hydrolysis is indeed initiated by nucleophilic attack at the sulfur atom, thereby generating HNO as a product. A systematic investigation of GSNO decomposition in aqueous solution was conducted by identifying all the decomposition products in the presence of reported sulfenic and nitrous acid traps in acidic buffer at pH 2.0. Since RSNOs could potentially be orally administrated for therapeutic purposes, pH 2.0 was chosen to evaluate their chemical behavior around gastric pH, which is usually 0–4. A new HPLC method for the separation and measurement of GSNO degradates in a relatively short time was developed. This method improves on that used by Li *et al.* (*32*) by shortening the analysis time from 2 h to 30 min, allowing a more detailed observation of GSNO degradate

formation. This new method was evaluated to ensure that the analysis conditions did not contribute to GSNO degradation or reformation.

## 3.3 Experimental

### 3.3.1 Materials

HPLC amber glass vials were purchased from National Scientific (Rockwood, TN), sulfamic acid was obtained from A & C American Chemicals (Quebec, Canada), *p*-cresol was obtained from Acros Organics (Morris Plains, NJ). Phosphoric acid was purchased from Fisher Chemicals (Fairlawn, NJ), dimedone from Lancaster Synthesis (Windham, NH), diethylenetriaminepentaacetic acid (DTPA) from Koch-Light Laboratories (Colnbrook Bucks, England). All other reagents were purchased from Sigma-Aldrich (Milwaukee, WI).

### 3.3.2 Synthesis of GSNO

Stock GSNO solutions were prepared *in situ* by mixing equal volumes of 40 mM GSH in 125 mM HCl and 40 mM aq $NaNO_2$, followed by a 10-min incubation period at room temperature in the dark (*14, 63*). The GSNO concentration was verified spectrophotometrically by measuring the absorption at 335 nm ($\varepsilon$ = 900 $M^{-1}$ $cm^{-1}$) (*67*). Spectra of GSNO solutions were recorded using a HP 8453 UV spectrophotometer (Agilent Technologies) with an integration time of 0.1 s to minimize photodegradation during measurement. A fresh GSNO stock solution was prepared on the same day as the experiments and kept on ice.

### 3.3.3 HPLC/UV and HPLC/MS analysis

The products of GSNO hydrolysis were monitored on a HP 1090 HPLC (Agilent Technologies, Santa Clara, CA) equipped with UV-vis diode-array detector. The gradient method used an Atlantis dC18 analytical column (150x3.0-mm, 5-μm particles, Waters Corp.) thermostated at 35 °C, an injection volume of 6 μL, a flow rate of 1 mL/min, and UV detection at 210 nm. The gradient was as follows: 100% A to 100% B in 20 min followed by an isocratic hold at 100% B for 5 min, and an isocratic hold at 100% A for 5 additional min. Mobile phase A was 50 mM sodium phosphate buffer (pH 3.0), and mobile phase B was 40% acetonitrile + 60% mobile phase A.

Product identification was performed by HPLC/MS. An Agilent 1100 HPLC (Agilent Technologies) equipped with a Spectra System UV6000LP UV detector (Thermo Separation Products, San Jose, CA) was interfaced to a LCQ-Deca ion trap mass spectrometer (ThermoElectron Corporation) equipped with an electrospray ionization source operating in positive mode. The HPLC method used was the same as above except that mobile phase A was 50 mM ammonium formate buffer (pH 3.0) and the eluent flow was split post column to 50 μL/min for introduction to the mass spectrometer. The electrospray voltage was set at 5 kV, the heated capillary was at 200 °C, and the capillary voltage was 35 V.

### 3.3.4 Degradation or formation of GSNO during analysis

The stability of GSNO in each HPLC mobile phase at 35 °C was evaluated to ensure that GSNO degradation did not occur during analysis. A 2-mM GSNO solution prepared in 60% mobile phase A and 40% mobile phase B was stored at 35 °C for up two h. Aliquots of the solution were taken every 30 min and analyzed using the HPLC/UV

method described above. To test for GSNO formation from GSH and $HNO_2$ during HPLC analysis, a solution containing 2 mM GSH and 2 mM $NaNO_2$ in 50 mM sodium phosphate buffer (pH 7.0) was injected onto the HPLC column and analyzed by the HPLC/UV method described in Section 3.3.3.

### 3.3.5 GSNO denitrosation at pH 2.0

A 1 mM GSNO solution in 50 mM phosphate buffer (pH 2.0) was stored in the dark in an amber glass vial at room temperature for 48 h. The UV-vis spectrum of the solution was measured after 0, 17, and 48 h. The pH of the solution was measured each time using an Accumet 50 pH meter with a Ag/AgCl combination electrode (Fisher Scientific, Ontario, Canada).

To monitor GSNO decomposition by HPLC, the 20 mM stock GSNO solution was diluted 10-fold into 50 mM sodium phosphate buffer (pH 2.0), with the required additives (metal chelators, reagent traps, etc.), and injected into the HPLC system. The decomposition was monitored at specific time intervals using the HPLC/UV method described in Section 3.3.3 and identification of the degradation products was performed by HPLC/MS (Section 3.3.3).

### 3.3.6 Effects of metal chelators, product traps, and added GSH or $HNO_2$

Possible metal catalysis of GSNO decomposition was investigated by including the metal chelator DTPA, or the $Cu^{I}$-specific chelator neocuproine (150 μM in both cases) in the GSNO solutions. The formation of GSOH, $HNO_2$, and $N_2O_3$ during degradation was investigated by conducting the experiments in the presence of the 10

mM dimedone, a sulfenic acid trap (*44*), 50 mM sulfamic acid, a $HNO_2$ trap (*68*), or 2 mM *p*-cresol, a $N_2O_3$ trap (*16*).

The effects of added GSH and $HNO_2$ were tested by monitoring the degradation of 2 mM GSNO solutions in 50 mM sodium phosphate buffer (pH 2.0) containing either 0.2 mM GSH, or 0.2 mM $NaNO_2$.

### 3.3.7 GSNO denitrosation under anaerobic conditions

A 2 mM GSNO solution was prepared in Ar-saturated sodium phosphate buffer (pH 2.0) in an amber glass vial and further degassed for 5 min by bubbling with Ar. The vial was tightly capped and placed in a chamber that was continually purged with a flow of Ar. The vial was stored in the chamber at RT and protected from light throughout the experiment. Aliquots of the GSNO solution were removed using a gas-tight syringe at specific time intervals and immediately injected into the HPLC.

### 3.3.8 GSNO denitrosation in 4 M $H_2SO_4$ in the presence of dimedone

A solution of 2 mM GSNO in 4 M $H_2SO_4$ containing 10 mM dimedone was stored in a 2-mL amber glass HPLC target vial at 30 °C for 4 h and protected from light. An aliquot of the solution was diluted 10-fold with 50 mM ammonium formate buffer (pH 3.0) and analyzed by HPLC/UV. As a control reaction, a solution of 2 mM $HNO_2$ and 10 mM dimedone in 4 M $H_2SO_4$ was also analyzed by HPLC/UV and HPLC/ESI-MS.

## 3.4 Results

### 3.4.1 GSNO denitrosation at pH 2.0

Aqueous GSNO solutions have been shown to decompose even when protected from light and metal-catalyzed denitrosation (*32, 42*). Loss of the *S*-NO absorption band at 330–340 nm (*14, 15, 63, 69*) after 0, 17, and 48 h (Figure 3.1A) confirms that 1 mM GSNO decomposition at pH 2.0 involves denitrosation. The pH of the solutions was found to remain constant during the course of the experiments.

### 3.4.2 HPLC analytical method evaluation

GSNO degradation in the HPLC mobile phase at 35 °C was monitored and the results are summarized in Table 3.1. While there is a decrease in the area counts of the GSNO peak, degradation in the mobile phase is < 1% over 120 min. Considering that GSNO was eluted from the HPLC column in < 7 min (Figure 3.1B), its degradation in the mobile phase during the analysis should be < 0.1%, which is within the precision of HPLC analysis of <0.2% RSD.

Since the mobile phase was buffered to pH 3.0, and GSNO is formed from $HNO_2$ and GSH under acidic conditions (Reaction 1.3) (*14, 63*), its generation during HPLC analysis was evaluated. Figure 3.1B shows the chromatograms following injection of 6 μL of a solution containing 2 mM GSH and 2 mM $NaNO_2$ in 50 mM sodium phosphate buffer (pH 7.0) (solid line), and that of a 2 mM GSNO solution in the same buffer (dashed line). No GSNO formation was observed in the chromatogram of the GSH/$NaNO_2$ solution, indicating that no detectable levels of GSNO are formed during the analysis.

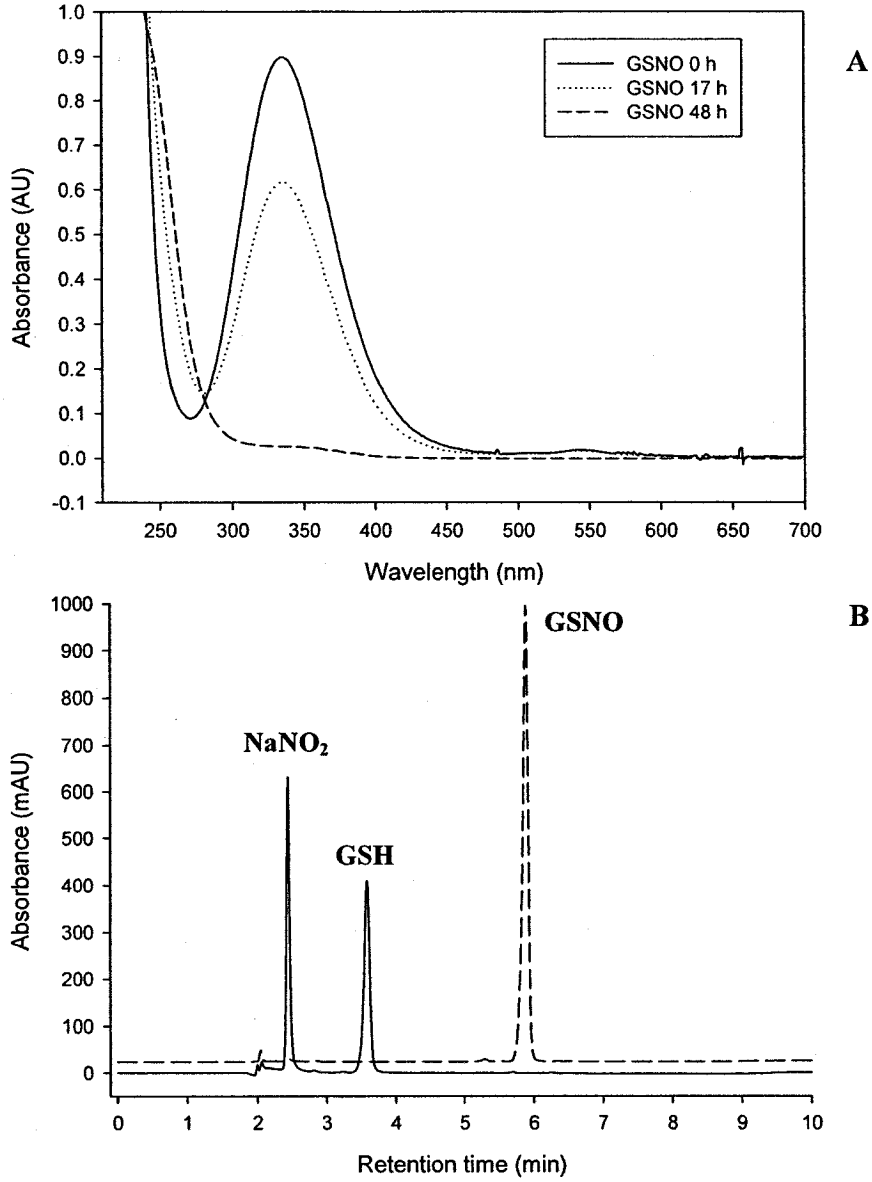


**Figure 3.1. (A) Absorption spectrum of 2 mM GSNO at pH 2.0 *vs* time.** GSNO in 50 mM sodium phosphate buffer (pH 2.0) was stored in an amber glass HPLC vial at room temperature in the dark. Spectra were recorded at 0 h, 17 h, and 48 h in a 0.5-cm pathlength quartz cuvette, integration time 0.1 s. **(B) HPLC chromatograms showing the lack of GSNO formation from GSH and $NaNO_2$ during HPLC analysis. Dashed line**: 2 mM GSNO in 50 mM sodium phosphate buffer (pH 2.0). **Solid line**: 2 mM GSH and 2 mM $NaNO_2$ in 50 mM sodium phosphate buffer (pH 7.0). The HPLC method is described in Section 3.3.3

**Table 3.1.** Stability of GSNO in the HPLC mobile phase at 35 °C [a]

| Time (min) | Peak Area[b] | % change |
|---|---|---|
| 0 | 6906 | 0.0% |
| 30 | 6890 | −0.2% |
| 60 | 6862 | −0.6% |
| 90 | 6851 | −0.8% |
| 120 | 6845 | −0.9% |

[a] 2 mM GSNO stored in 60% mobile phase A (50 mM sodium phosphate buffer, pH 3.0) + 40% acetonitrile. Aliquots of 6 µL were injected and analyzed by HPLC/UV as described in Section 3.3.3. [b] Peak areas at 210 nm.

Figure 3.2A shows a typical chromatogram of decomposed GSNO in sodium phosphate buffer (pH 2.0). The detector was set at 210 nm to increase the likelihood of detecting all degradates. From the corresponding *m/z* ratios obtained by HPLC/ESI-MS analysis (Figure 3.2B), peaks were identified as $GSO_3H$ (Peak 1), two isomers of GSOSG (Peaks 3 and 4), $GSO_2SG$ (Peak 5), GSSG (Peak 6), and GSNO (Peak 7). These GSNO degradates were previously found in unbuffered aqueous solutions (*32, 42*). Peak 2 was identified as $NO_2^-$ by comparing its retention time (2.3 min) and UV spectrum to those of $NaNO_2$ standards. No additional peaks were observed to elute after 15 min.

### 3.4.3 Time course of GSNO decomposition at pH 2.0

The decomposition of 2 mM GSNO solutions in sodium phosphate buffer (pH 2.0) was essentially complete after 50 h. Figure 3.3, which shows the relative GSNO concentration measured by HPLC/UV over that period, reveals only ~ 10% loss of GSNO after 10 h, followed by 75% loss between 10-30 h. Figure 3.4A shows that the consumption of GSNO (peak 7) is accompanied by growth in $GSO_3H$, $NO_2^-$, and the two

GSOSG isomers at similar rates (Peaks 1-4), suggesting that they form in related steps. Formation of $GSO_2SG$ (Peak 5) is seen only after ~ 20 h, indicating that it is a product of a secondary degradation reaction. The chromatograms also reveal that low-intensity Peak 6, identified as GSSG, does not change over 0-50 h, suggesting that the disulfide is not a product of GSNO degradation under these conditions. The intensity of Peak 2 ($NO_2^-$) increases up to approximately the midpoint in the reaction and then begins to decrease, indicating that $NO_2^-$ is consumed in a competing reaction.

**(Next page)**

**Figure 3.2. (A) HPLC/UV and HPLC/MS analysis of GSNO hydrolysis after 26 h at pH 2.0.** A 2-mM GSNO solution in 50 mM sodium phosphate buffer (pH 2.0) was stored in an amber glass HPLC vial at RT for 26 h and protected from light. The sample was analyzed using the HPLC method described in Section 3.3.3. **HPLC peaks: 1**: $GSO_3H$, **2**: $NO_2^-$, **3,4**: GSOSG, **5**: $GSO_2SG$, **6**: GSSG, **7**: GSNO. **(B) ESI mass spectra of the GSNO degradates.** Peak numbers correspond to those in (A). The HPLC/ESI-MS method is described in Section 3.3.3.

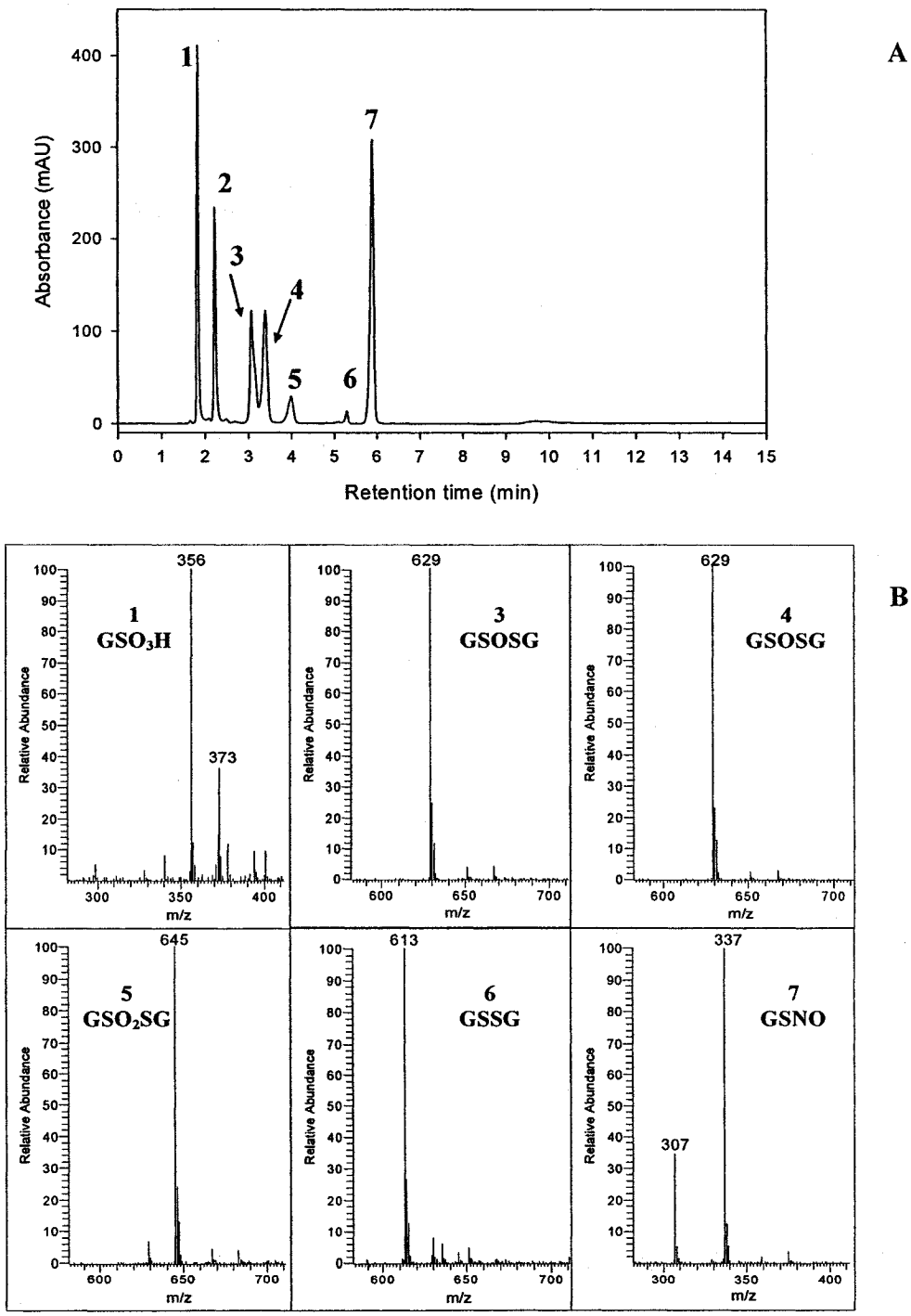
A
B
Absorbance (mAU)
Retention time (min)
1
2
3
4
5
6
7
GSO3H
GSOSG
GSOSG
GSO2SG
GSSG
GSNO
Relative Abundance
m/z
356
373
629
629
645
613
337
307

**Figure 3.2.**

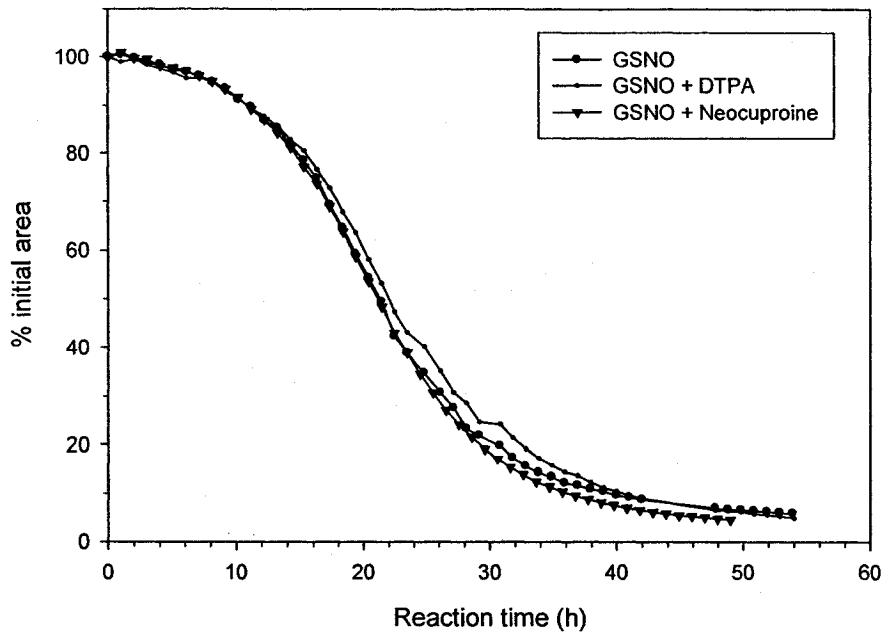


**Figure 3.3. Kinetics of GSNO decomposition in the presence and absence of DTPA and neocuproine.** Solutions containing 2 mM GSNO in 50 mM sodium phosphate buffer (pH 2.0), with 150 μM DTPA or 150 μM neocuproine where indicated, were stored in amber glass HPLC vials at RT and protected from light. The GSNO peak areas in the HPLC chromatograms were measured at 210 nm as described in Section 3.3.3. Extracted from data set shown in Figure 3.4

**(Next page)**

**Figure 3.4. HPLC/UV analysis of GSNO hydrolysis at pH 2.0 in the presence and absence of metal chelators.** **(A)** 2 mM GSNO, **(B)** 2 mM GSNO + 150 μM DTPA, **(C)** 2 mM GSNO + 150 μM neocuproine. Reaction solutions in 50 mM sodium phosphate buffer (pH 2.0) were stored in amber glass HPLC vials at RT for 50 h and protected from light. The HPLC method is described in Section 3.3.3. **Peaks:** **1**: $GSO_3H$, **2**: $NO_2^-$, **3,4**: GSOSG, **5**: $GSO_2SG$, **6**: GSSG, **7**: GSNO.

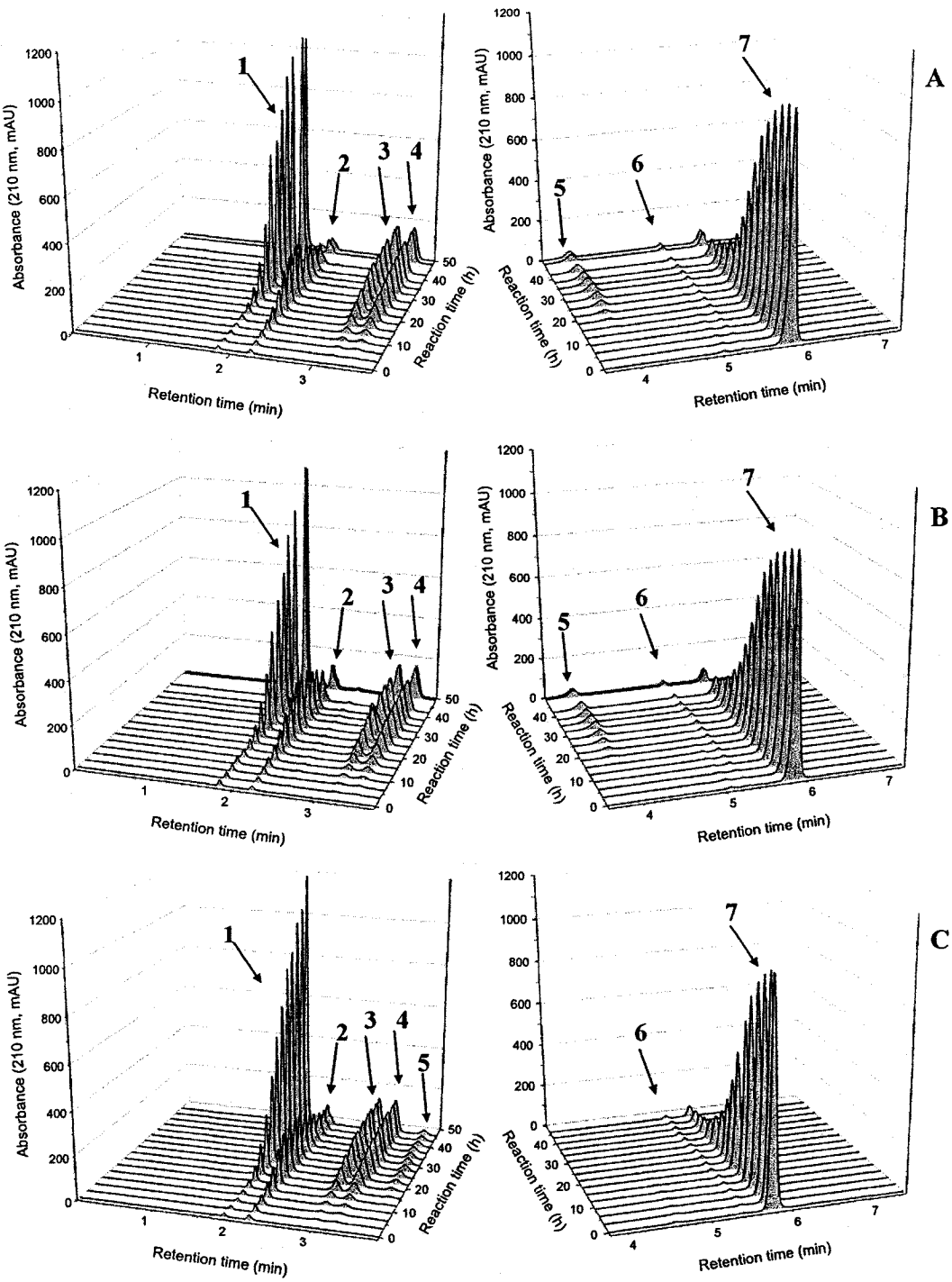
A
B
C
Absorbance (210 nm, mAU)
Retention time (min)
Reaction time (h)
1
2
3
4
5
6
7

**Figure 3.4**

### 3.4.4 Effects of metal chelators

RSNOs are known to undergo reductive denitrosation in the presence of trace copper ions (*20, 41, 70*). However, millimolar aqueous solutions of GSNO have been reported to undergo almost complete denitrosation in ~ 50 h in the dark in the presence of the chelators DTPA and neocuproine, which are specific for $Cu^{II}$ and $Cu^{I}$, respectively. This indicates that a non-copper-catalyzed, non-photolytic decomposition process also takes place (*42*). To investigate if the mechanisms of GSNO decomposition in the dark in the absence and presence of the chelators were similar, GSNO decomposition was monitored in buffered solutions (pH 2.0) containing DTPA or neocuproine. The results confirm the findings of Tao and English (*42*) that denitrosation is complete in ~ 50 h and that it progresses at the same rate in the presence and absence of metal chelators (Figure 3.3). Furthermore, the corresponding chromatograms (Figures 3.4B,C) show that the products of GSNO decomposition are the same in both cases, indicating that the GSNO decomposition occurring over 50 h is not catalyzed by trace copper or by other metals.

### 3.4.5 Effect of dimedone

Tao and English (*42*) observed that GSNO denitrosation was considerably slower in the presence of dimedone, a reagent commonly used as a trap for sulfenic acids (RSOH) (*43, 44*). They suggested that the sulfenic acid GSOH was an intermediate in the reaction and that denitrosation under their experimental conditions proceeded *via* a hydrolytic mechanism that generated GSOH as an intermediate (Reactions 3.5–3.9). Since GSOH formation could be confirmed by the detection of a GS-dimedone adduct (eq. 3.3) (*44*), GSNO decomposition was repeated in the presence of dimedone. The resulting chromatograms (Figure 3.5) confirm that dimedone inhibits the decomposition

of 2 mM GSNO at pH 2.0 since the height of the GSNO peak decreased by < 3% over 50 h. Due to the low consumption of GSNO, no additional peaks were observed in the chromatograms to confirm the formation of a GSOH-dimedone adduct.

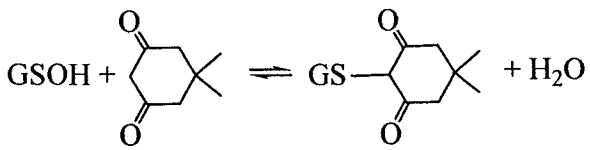


(3.3)

dimedone

GSNO hydrolysis is accelerated at high acidity such as 2-4 M $H_2SO_4$ (Chapter 2) and high temperature (*14, 45*). Thus, to promote dimedone adduct formation, 2 mM GSNO and 5 mM dimedone were incubated in 4 M $H_2SO_4$ for 4 h at 30 °C. Figure 3.6A shows the chromatogram obtained and products were identified as the denitrosated free thiol (GSH) and a compound with the retention time (13.2 min) and UV spectrum of nitrosated dimedone, which forms on adding dimedone to $HNO_2$ (eq. 3.4) (*71*). The formation of nitrosated dimedone in 4 M $H_2SO_4$ was confirmed (Figure 3.6B), and was also observed at pH 2.0 (Figure 3.6B), indicating that the inhibition of GSNO decomposition by dimedone could be due to $HNO_2$ trapping. Since dimedone is both a GSOH and $HNO_2$ trap, it cannot be used to distinguish between these species as intermediates.

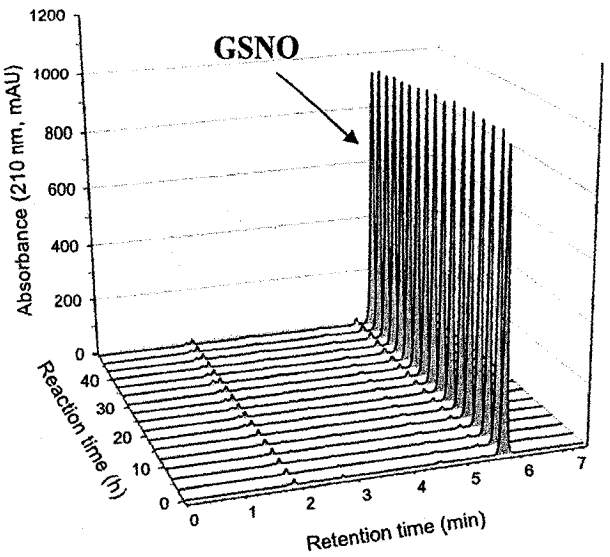


**Figure 3.5. HPLC analysis reveals that dimedone inhibits GSNO decomposition.** A solution of 2 mM GSNO + 10 mM dimedone in 50 mM sodium phosphate buffer (pH 2.0) was stored in a capped amber glass HPLC vial at RT for up to 50 h, protected from light. The HPLC method is described in Section 3.3.3.

Although we did not observe a GS-dimedone adduct in 4 M $H_2SO_4$, it could be below the level of detection. Thus, we examined the effects of added $NaNO_2$ on GSNO decomposition.

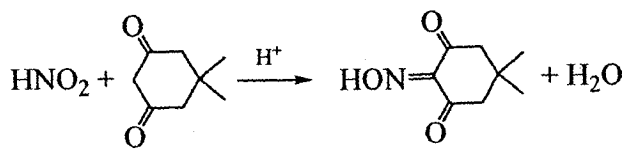


(3.4)

dimedone

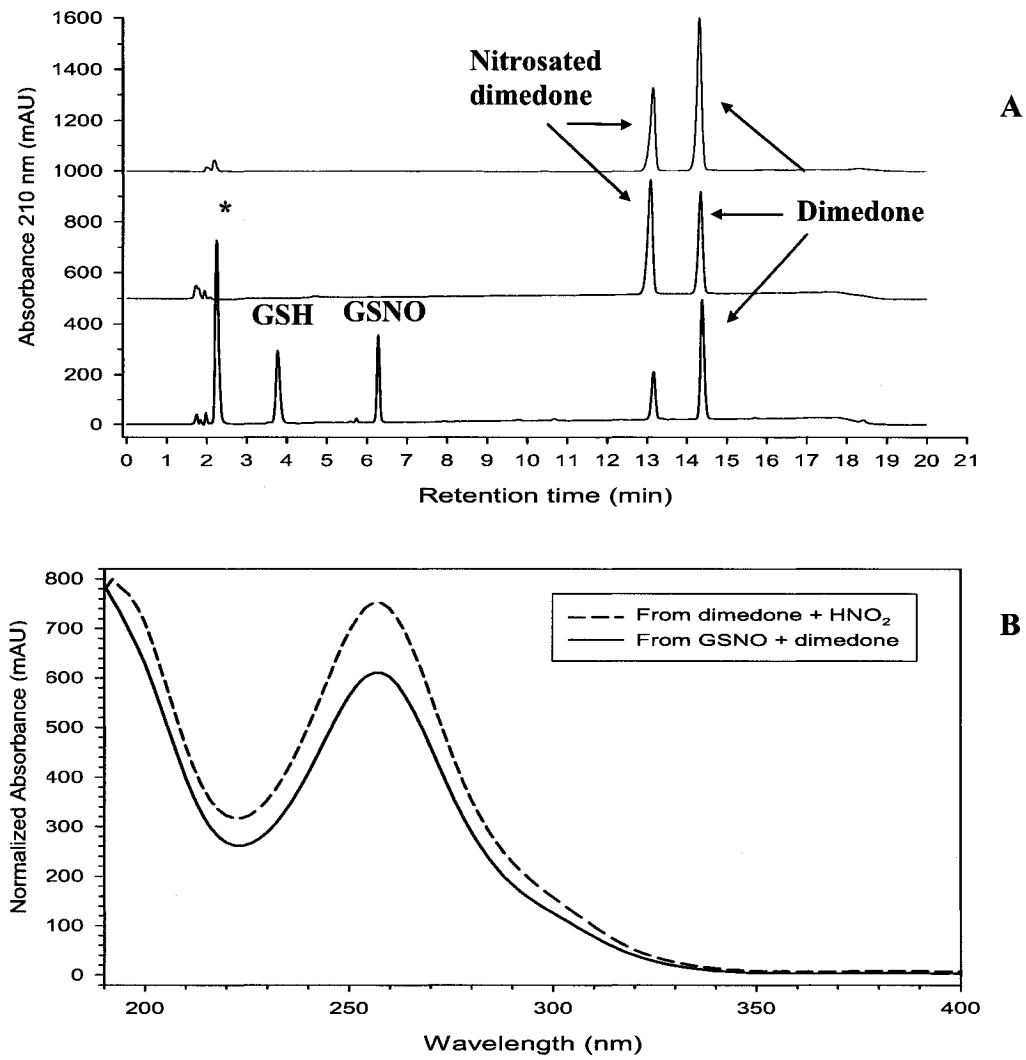


**Figure 3.6 (A) HPLC chromatograms of GSNO plus dimedone. (A) blue line:** 2 mM $NaNO_2$ + 20 mM dimedone in 20 mM sodium phosphate buffer (pH 2.0); **red line:** 2 mM $NaNO_2$ and 10 mM dimedone in 4 M $H_2SO_4$; **black line:** 2 mM GSNO + 10 mM dimedone in 4 M $H_2SO_4$ after storage in an amber glass vial at 30 °C, protected from light, for 4 h. Both samples in $H_2SO_4$ were diluted 10-fold with 50 mM sodium phosphate buffer (pH 3.0) (mobile phase A) prior to HPLC analysis. The HPLC method is described in Section 3.3.3 with an injection volume of 100 µL. **(B) UV-vis spectra of the nitrosated dimedone peak at 13.2 min in the chromatograms in (A); dashed line:** peak from red chromatogram; **solid line:** peak from black chromatogram. The spectra were normalized to 0.8 AU at 190 nm for comparison purposes.

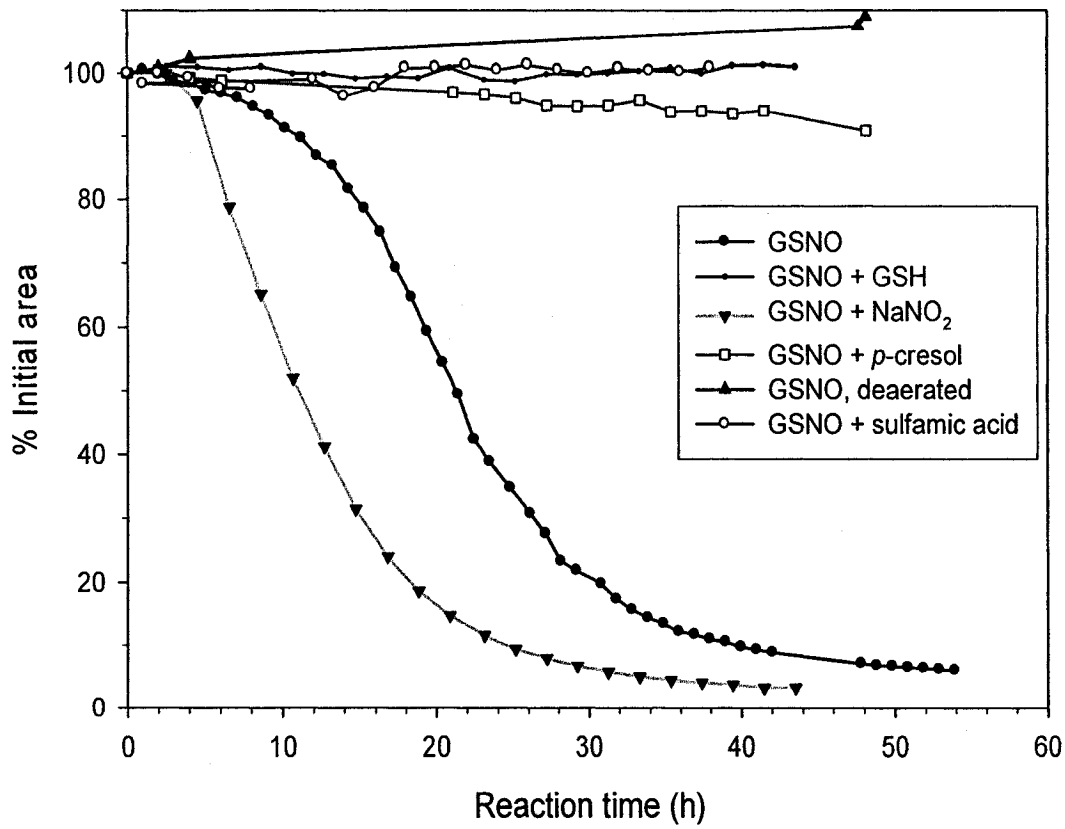


**Figure 3.7. Kinetics of GSNO decomposition in 50 mM sodium phosphate buffer (pH 2.0) in the presence of GSH, $NaNO_2$, *p*-cresol, oxygen, or sulfamic acid.** **(A)** 2 mM GSNO; **(B)** 2 mM GSNO + 0.2 mM GSH; **(C)** 2 mM GSNO + 0.2 mM $NaNO_2$; **(D)** 2 mM GSNO + 2 mM *p*-cresol; **(E)** 2 mM deaerated GSNO; **(F)** 2 mM GSNO + 150 mM sulfamic acid. Samples were stored in amber glass HPLC vials at RT, protected from light. The GSNO peak areas in the HPLC chromatograms were measured at 210 nm. The HPLC method is described in Section 3.3.3.

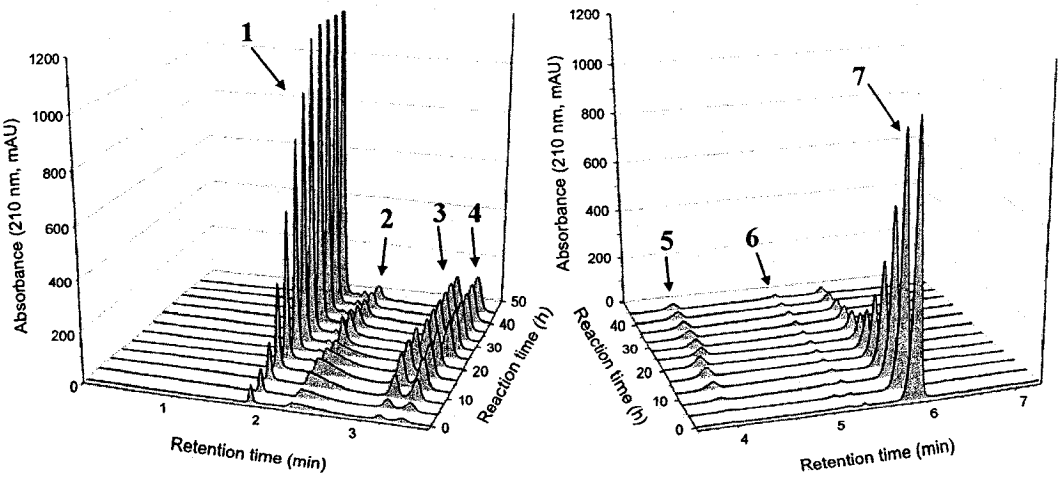


**Figure 3.8. HPLC analysis reveals that added $NaNO_2$ catalyzes GSNO decomposition.** A solution of 2 mM GSNO + 0.2 mM $NaNO_2$ in 50 mM sodium phosphate buffer (pH 2.0) was stored in an amber glass HPLC vial at RT for 44 h, protected from light. The HPLC method is described in Section 3.3.3, and the peaks were identified as **1**: $GSO_3H$, **2**: $NO_2^-$, **3,4**: GSOSG, **5**: $GSO_2SG$, **6**: GSSG, **7**: GSNO.

### 3.4.6 Denitrosation of GSNO in the presence of added $NaNO_2$ and GSH

To probe the role of $HNO_2$ in GSNO decomposition at pH 2.0, denitrosation was monitored following the addition of 0.2 mM $NaNO_2$, which was present as $HNO_2$ at pH 2.0 ($pK_a$ 3.1) (*14*). The induction period was shortened from ~12 to ~3 h, and the GSNO half-life shortened from 21 to ~10 h (Figure 3.7 *vs* 3.3). The chromatograms in Figure 3.8 show that GSNO decomposition starts immediately after mixing the reagents, to generate the same degradate profile observed before (Figure 3.4B). When 50 mM sulfamic acid, a $HNO_2$ trap, (*45*), was added immediately after adding 0.2 mM $NaNO_2$, denitrosation was

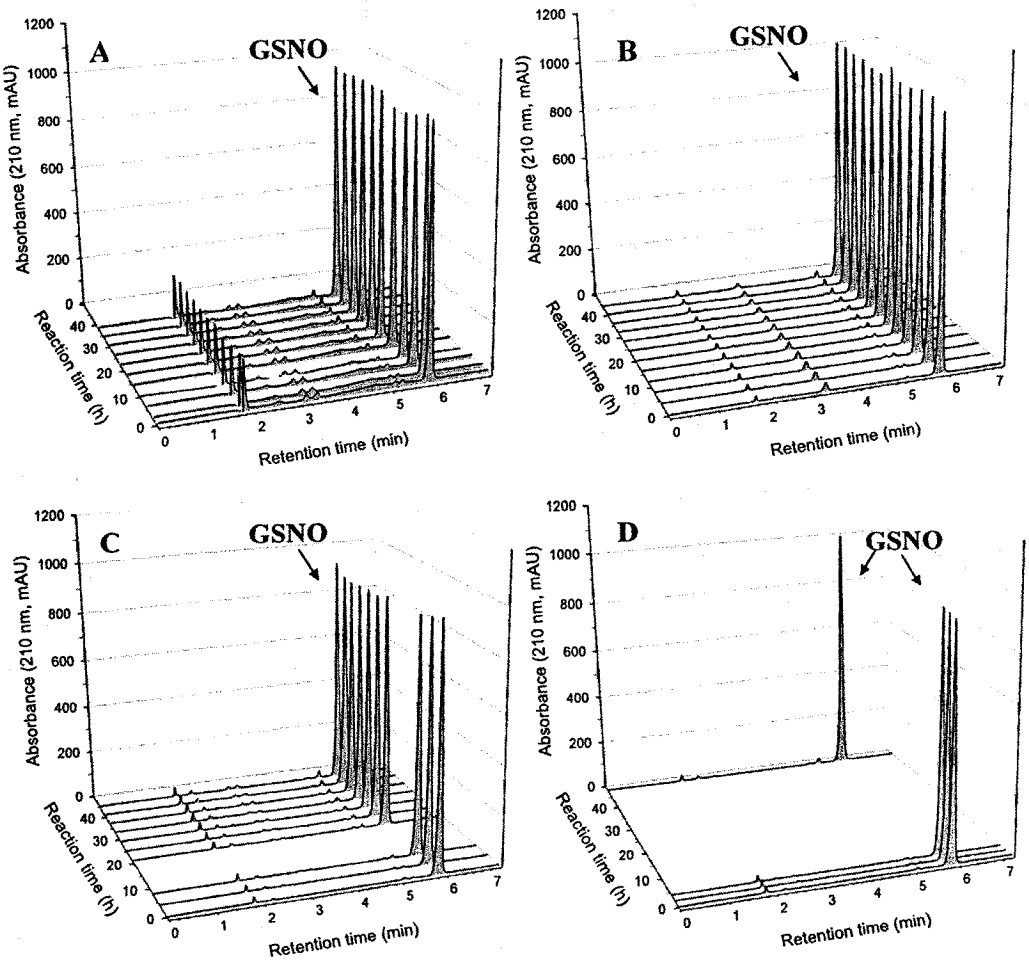


**Figure 3.9. HPLC analysis of GSNO solutions at pH 2.0 containing sulfamic acid, GSH, or *p*-cresol, or under anaerobic conditions.** **(A)** 2 mM GSNO + 50 mM sulfamic acid; **(B)** 2 mM GSNO + 0.2 mM GSH; **(C)** 2 mM GSNO + 2 mM *p*-cresol; **(D)** 2 mM GSNO in Ar-saturated buffer. The HPLC method is described in Section 3.3.3. Samples in 50 mM sodium phosphate buffer (pH 2.0) were stored in capped amber glass HPLC vials at RT, protected from light.

halted for over 42 h (Figure 3.9A), revealing that $HNO_2$ catalyzes GSNO decomposition.

Since $HNO_2$ is formed on GSNO hydrolysis (eq. 3.1), 0.2 mM GSH was added to a 2 mM GSNO solution to force the equilibrium towards GSNO formation. The presence of 0.2 mM GSH, stabilizes 2 mM GSNO at pH 2.0 for over 48 h (Figures 3.7 and 3.9B) suggesting that $HNO_2$ formation on RSNO hydrolysis leads to autocatalysis of GSNO denitrosation.

### 3.4.7 Effects of $N_2O_3$ trapping

Grossi and Montevecchi (*16*) studied the decomposition of several primary and tertiary RSNOs in n-pentane under aerobic and anaerobic conditions. Their results showed that in the absence of $O_2$, RSNOs decompose thermally to yield the disulfide and NO (Reactions 1.10-1.13). However, with $O_2$ present, RSNO decomposition in n-pentane followed an autocatalytic mechanism in which $N_2O_3$, formed in the reaction of $O_2$ and RSNO-derived NO (Scheme 3.2), was the chain carrier:

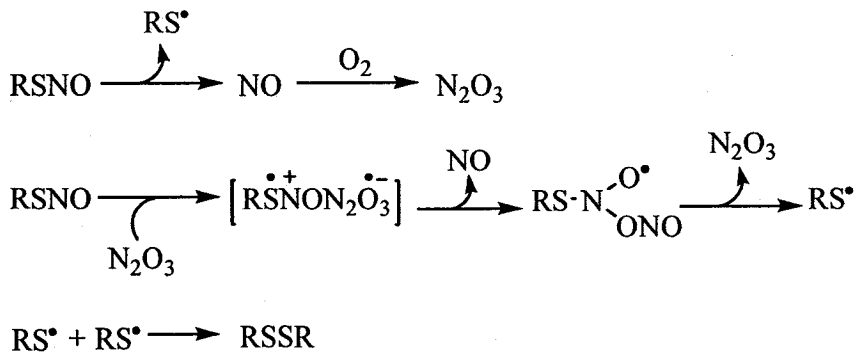


**Scheme 3.1. Autocatalytic chain-reaction mechanism for RSNO decomposition.** This mechanism involving $N_2O_3$ as a chain carrier was proposed by Grossi and Montevecchi (16)

Since $HNO_2$ is known to exist in equilibrium with $N_2O_3$ (Reaction 3.14) (*14*), the participation of $N_2O_3$ was investigated by monitoring GSNO denitrosation in aqueous solution at pH 2 in the presence of the $N_2O_3$ trap, *p*-cresol (*16*). The results show that 2 mM *p*-cresol strongly inhibited the decomposition of 2 mM GSNO in aqueous solution at pH 2 (Figures 3.7, 3.9C), which supports the participation of $N_2O_3$ in the decomposition mechanism.

### 3.4.8 Role of oxygen in GSNO decomposition

HPLC analysis of a 2 mM GSNO solution stored under Ar revealed that no GSNO decomposition occurred in 50 h (Figure 3.9D). This indicates that $O_2$ is required for GSNO consumption consistent with a role for $N_2O_3$ (from $NO_2$ and $O_2$) as proposed by Grossi and Montevecchi (*16*). Table 3.2 summarizes all the products, their retention times and yields in the GSNO decomposition reactions examined here at pH 2.0.

## 3.5 Discussion

The results of this study indicate that decomposition of GSNO in acidic aqueous solution in the dark in the presence or absence of metal chelators is induced by $HNO_2$. We previously proposed (eqs. 3.5 to 3.9) (*42*) that the initial step involved hydrolysis of the S-NO bond *via* nucleophilic attack at the sulfur atom to form glutathione sulfenic acid (GSOH) and nitroxyl (HNO). This conclusion was supported by the inhibition of GSNO decomposition in the presence of dimedone, a sulfenic acid trap (Reaction 3.3), and by the formation of GSOSG and $GSO_2SG$, which are products of GSOH dimerization (*72, 73*).

$$GSNO + H_2O \rightleftharpoons GSOH + HNO \quad (3.5)$$

$$GSOH + GSNO \rightleftharpoons GS(O)SG + HNO \quad (3.6)$$

$$GSOH + GSOH \rightleftharpoons GS(O)SG + H_2O \quad (3.7)$$

$$2\ GS(O)SG \rightleftharpoons GSO_2SG + GSSG \quad (3.8)$$

$$2HNO \rightleftharpoons N_2O + H_2O \quad (3.9)$$

However, attack at the nitroso sulfur is not supported by the present results. No GS-dimedone adduct (Reaction 3.3) was detected when GSNO was allowed to decompose in the presence of dimedone (Figure 3.5). Tao and English (*42*) also observed that dimedone inhibited GSNO decomposition and proposed that it reacted with the GSOH, formed by Reaction 3.5, to give a GS-dimedone thioether (Reaction 3.3) that could regenerate GSNO on further reaction with HNO (Reaction 3.10). However, breakdown of the ether linkage in peptide-dimedone thioethers requires harsh conditions such as in boiling in HCl over 24–48 h (*74*). Thus, GS-dimedone decomposition is not likely to occur at pH 2.0 and room temperature.

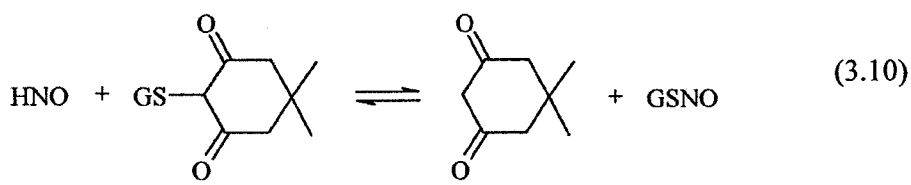


(3.10)

**Table 3.2.** Summary of product yields in acid-catalyzed GSNO hydrolysis [a]

| Reaction[b] | Reaction time (h) | $GSO_3H$ (1.8 min)[d] | Nitrite (2.2 min)[d] | GSOSG (3.1-3.4 min)[d] | $GSO_2SG$ (3.9 min)[d] | GSSG (5.3 min)[d] | GSNO (5.9 min)[d] |
|---|---|---|---|---|---|---|---|
| 2 mM GSNO | 54 | 54 | 5 | 36 | 5 | 1 | 6 |
| 2 mM GSNO + 0.15 mM DTPA | 54 | 59 | 8 | 35 | 4 | 2 | 5 |
| 2 mM GSNO + 0.15 mM neocuproine | 50 | 67 | 11 | 36 | 3 | 4 | 4 |
| 2 mM GSNO + 10 mM dimedone | 51 | - | - | - | - | 2 | 98 |
| 2 mM GSNO + 0.2 mM $NaNO_2$ | 44 | 76 | 9 | 36 | 4 | 1 | 3 |
| 2 mM GSNO + 150 mM sulfamic acid | 38 | - | - | 9 | - | 3 | 92 |
| 2 mM GSNO + 0.2 mM GSH | 44 | - | - | - | - | 3 | 99 |
| 2 mM GSNO +2 mM *p*-cresol | 48 | 2 | 1 | 3 | - | 2 | 91 |
| 2 mM GSNO in Ar-saturated bufffer[c] | 48 | - | - | - | - | 2 | 99 |

[a] Product yields expressed relative to $[GSNO]_0$ based on peak areas measured at 210 nm. Peak areas were not corrected for different molar absorption coefficients of the GSX species at 210 nm. Each value corresponds to a single measurement.

[b] Reactions were carried out in capped amber glass HPLC vials at RT, protected from light.

[c] GSNO was deaerated by purging with Ar for 5 min . The solution was stored under an Ar atmosphere for the duration of the experiment.

[d] Retention time on an Atlantis dC18 (150x3.0-mm, 5-μm particles, Waters) HPLC column at 35 °C. The HPLC method is described in Section 3.3.3. The chromatograms are shown in Figures 3.4, 3.5, 3.8, and 3.9.

GSNO decomposition in air-saturated aqueous solution at pH 2.0 exhibits an induction period, after which the denitrosation rate accelerates (Figure 3.3). This profile is consistent with an autocatalytic chain reaction (*75*) that is initiated by a product formed on hydrolysis of the *S*-NO bond. When 0.2 mM $NaNO_2$ was added to GSNO buffered at pH 2.0, the induction period was significantly shortened, but the same degradate profile was observed as in the absence of added $NaNO_2$. Furthermore, the $HNO_2$ trap, sulfamic acid (eq. 3.11), inhibits GSNO decomposition at pH 2.0 and HPLC analysis revealed that the decomposition products in 4 M $H_2SO_4$ are similar whether the reaction is conducted in the presence of sulfamic acid or dimedone. Thus, dimedone likely inhibits GSNO decomposition by trapping $HNO_2$ and not GSOH as was expected (*43, 44*) and as was assumed in our published mechanism (*76*).

$$HNO_2 + NH_2SO_3^- \rightarrow N_2(g) + HSO_4^- + H_2O \qquad (3.11)$$

Hydrolysis of RSNOs *via* nucleophilic attack at the nitroso *N* atom is the reverse of *S*-nitrosation (eq. 3.1). The equilibrium in this reaction is thought to lie largely on the side of RSNO formation, but it has been reported that small amounts of RSH, and hence $HNO_2$, are present in aqueous RSNO solutions (*13, 14*). Thus, the addition of RSH should force the equilibrium away from $HNO_2$ formation, and further decomposition was halted when 0.2 mM GSH was added to aqueous GSNO solutions (Figure 3.8). This is

consistent with $HNO_2$ release *via* attack at the nitrogen atom being the initial step in GSNO hydrolysis.

Grossi and Montevecchi (*16*) proposed that RSNOs in air-saturated n-pentane solutions decompose *via* an autocatalytic mechanism in which $N_2O_3$ is the chain carrier. Their proposal was supported by inhibition of the decomposition reaction in the presence of *p*-cresol which traps $N_2O_3$ as 2-nitro-*p*-cresol (Reaction 3.12) (*77*). Inclusion of *p*-cresol also inhibits GSNO decomposition in aqueous solutions (Figure 3.9C) which indicates that $N_2O_3$ additionally catalyzes hydrolysis.

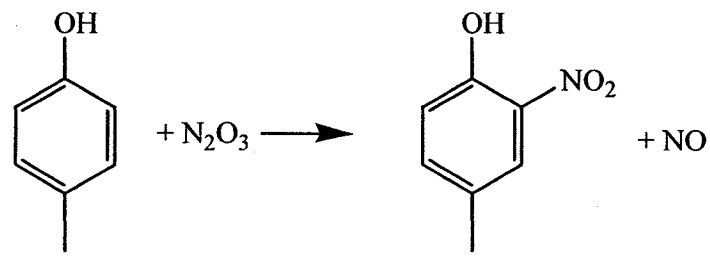


(3.12)

*p*-cresol

$N_2O_3$ could be generated on GSNO hydrolysis since $HNO_2$ is known to exist in equilibrium with $N_2O_3$ (eq. 3.14, $K_{eq} = 3 \times 10^{-3}$) (*14*). $N_2O_3$ could then react with two molecules of GSNO to yield two GSOH and four NO molecules (eq. 3.15). Under aerobic conditions, the resulting NO molecules would react with $O_2$ to yield more $N_2O_3$, thereby propagating the chain (eq. 3.16). This propagation step would not occur in the absence of $O_2$, which would slow down GSNO hydrolysis as observed for anaerobic GSNO solutions (Figure 3.9D). Based on these observations, we revised our previous

mechanisms for GSNO decomposition in aqueous solutions. The following mechanism, taking into consideration the additional analysis carried out here, is proposed:

$$GSNO + H_2O \rightleftharpoons GSH + HNO_2 \quad (3.13)$$

$$2HNO_2 \rightleftharpoons N_2O_3 + H_2O \quad (3.14)$$

$$N_2O_3 + 2GSNO + H_2O \rightarrow 2GSOH + 4NO \quad (3.15)$$

$$4NO + O_2 \rightarrow 2N_2O_3 \quad (3.16)$$

$$2GSOH \rightarrow GS(O)SG + H_2O \quad (3.17)$$

$$2GSOH + O_2 \rightarrow 2GSO_2H \quad (3.18)$$

$$2GSO_2H + O_2 \rightarrow 2GSO_3H \quad (3.19)$$

$$2GSO_2H \rightarrow GSO_2SG + GSO_3H \quad (3.20)$$

All the GSX decomposition products [thiosulfinate (GSOSG), thiosulfonate ($GSO_2SG$), and sulfonic acid ($GSO_3H$)], except GSOH which is unstable (*73*), were identified by LC/MS in this study. This degradate profile agrees with that reported by Li *et al.* (*32*) who investigated the *S*-glutathiolation of proteins by the products of GSNO decomposition in water. In the proposed mechanism (eqs. 3.13-3.20) glutathione sulfenic acid (GSOH) is formed from the reaction of GSNO and $N_2O_3$ (eq. 3.15). Sulfenic acids (RSOHs) are highly unstable and they easily dimerize to yield thiosulfinates (RSOSR) (eq. 3.17). Under oxidizing conditions, GSOH can also be converted to the corresponding

sulfinic ($GSO_2H$) and sulfonic acids ($GSO_3H$) (eqs. 3.18 and 3.19). The sulfinic acid can additionally disproportionate to the thiosulfonate ($GSO_2SG$) and sulfonic acid (eq. 3.20) (*73*).

The disulfide GSSG detected in all chromatograms at a constant level (Figures 3.4, 3.5, 3.8, 3.9) may not be a product of GSNO decomposition but may have been present as an impurity in GSNO, formed during its synthesis (eq. 3.21) (*15*):

$$2GSNO \rightarrow GSSG + 2NO \qquad (3.21)$$

GSSG may also have been present as an impurity in GSH. In their investigations into protein glutathiolation, Li *et al.* (*32*) and Tao and English (*42*) concluded that GSSG was a product of GSNO decomposition. However, the solutions were analyzed only after 24–72 h, while GSSG could have been present in the starting solutions.

Zhao *et al.* (*78*) have recently reported the results of computational analysis of MeSNO decomposition in the gas phase and experimental n-hexyl-*S*NO decomposition in acetonitrile, and concluded that the chain carrier for RSNO decomposition is the nitrosonium ion, $NO^+$ (Scheme 3.2). In their proposed mechanism, reaction of $NO^+$ with RSNO yields a dinitroso cation [$RS(NO)NO^+$] that reacts with a second RSNO molecule. This will lead to the formation of RSSR and NO through a catalytic cycle involving a cationic nitrosated disulfide intermediate $RS(NO^+)SR$ that transfers $NO^+$ to another RSNO equivalent and restarts the cycle. $N_2O_3$ can also effect nitrosation *via* $NO^+$ (*14*),

and in their computational analysis, Zhao *et al.* (*78*) suggest that reaction of RSNO with $N_2O_3$ is likely to produce the [RS(NO)NO$^+$] intermediate in Scheme 3.2.

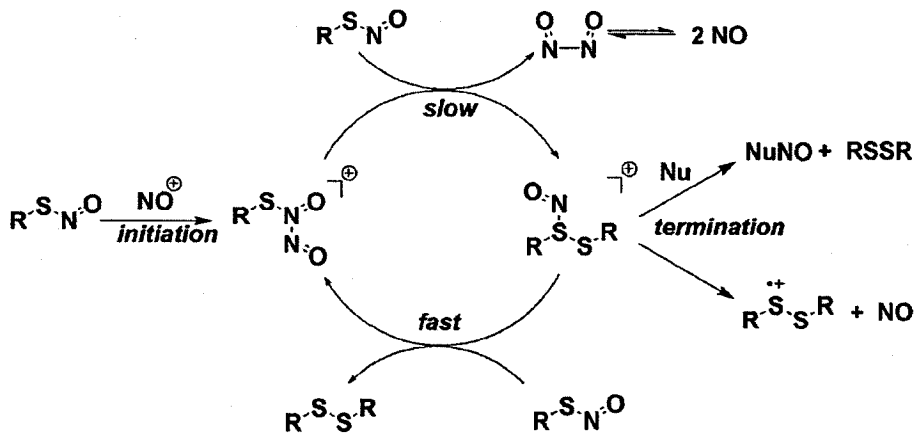


**Scheme 3.2. Decomposition cycle for NO$^+$-catalyzed decomposition of RSNO.** This mechanism, proposed by Zhao *et al. (78)*, does not include reactions with $O_2$.

However, disulfide formation as predicted by Scheme 3.2 is not supported by our data since the levels of GSSG do not increase as the reaction proceeded. It could be argued that GSSG is being formed and consumed at the same rate but additional reactions involving GSSG consumption are not obvious based on the mechanisms given in eq. 3.5–3.9 or eq. 3.13–3.20.

## 3.6 Conclusions

Decomposition of GSNO in aqueous solutions at pH 2.0 is catalyzed by trace $HNO_2$. This occurs *via* an oxygen-dependent, autocatalytic process with $N_2O_3$ as the chain carrier, as suggested by Grossi and Montevecchi (*16*) in their study of RSNOs in organic solvents. The initial step is nucleophilic attack by $H_2O$ at the nitroso nitrogen to generate GSH and $HNO_2$. This is the reverse of thiol *S*-nitrosation by $HNO_2$ (Reaction 1.3), and thus can be prevented by addition of GSH which shifts the hydrolysis equilibrium towards GSNO formation.

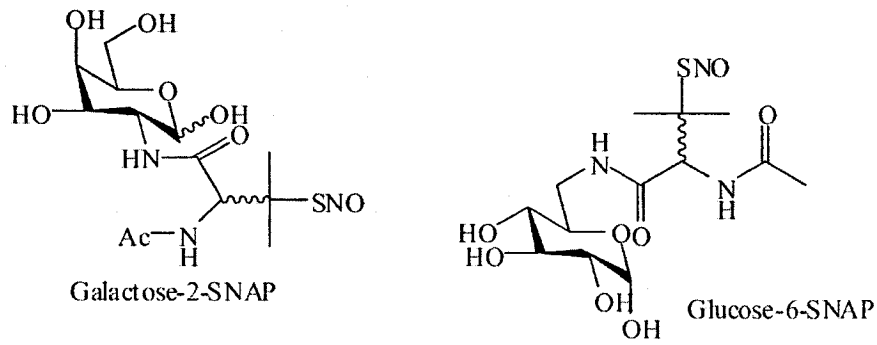


**Scheme 3.3. Examples of sugar-SNAP compounds (*4*).**

The findings from this study should be taken into consideration when working with acidic solutions of GSNO since they contain trace amounts of $HNO_2$ (*13*). Therefore, the presence of small amounts of the GSNO decomposition products, such as the potent glutathiolating agent GSOSG, is likely. These findings have implications for therapeutic uses of RSNOs as NO donors. Several novel compounds such as *S*-nitrosated dipeptides and sugar-SNAP compounds (Scheme 3.3) have shown improved

pharmacological properties as NO donating agents as compared to SNAP itself (*4*). Also, *S*-nitrosated versions of existing orally-administered non-steroidal anti-inflammatory drugs (NSAID) such as *diclofenac* have been developed as bifunctional compounds to minimize undesirable side effects that include gastrointestinal bleeding (*4, 79*). Orally administered RSNOs could undergo decomposition under the acidic conditions of the stomach (pH 1–2) in the presence of high $HNO_2$ levels from the dietary intake of nitrite-rich foods. Decomposition of RSNOs during their residence time in the stomach, which would vary depending on the dosage form used, could result in diminished potency and in unwanted side effects from the degradation products.

# Chapter 4 - Decomposition of *S*-nitrosoglutathione in alkaline solution

## 4.1 Abstract

The decomposition of *S*-nitrosoglutathione (GSNO) in 10 mM and 20 mM aqueous NaOH was investigated. Base-catalyzed hydrolysis occurred mainly *via* nucleophilic attack at the nitroso nitrogen forming a nitrosated disulfide intermediate that produces GSSG, $GS(NO)S^-$, and a sulfur-free glutathionyl derivative as the GSX products, and nitrite as the main nitroso nitrogen product. The percent distribution of the GSX products was dependent on the initial $OH^-$ and GSNO concentrations and changed when the NaOH concentration was doubled. $N_2O$ was detected and a glutathionyl sulfenic acid adduct was trapped with dimedone. Thus, base-catalyzed GSNO hydrolysis also proceeded *via* initial $OH^-$ attack at the nitroso sulfur forming nitroxyl (HNO), although only to a minor extent under our experimental conditions.

## 4.2 Introduction

In the past 15 years there has been increased interest in the chemistry of *S*-nitrosothiols (RSNOs) or thionitrites. This is due to the postulates that nitric oxide exists in mammalian plasma in the form of *S*-nitrosoalbumin and that RSNOs act as storage forms of the biologically important NO molecule (*11*). Studies have focused on the effects of RSNOs on vasodilation, as well as their interaction with proteins and enzymes (*80-84*). Generally, RSNOs have been found to exhibit similar physiological properties to NO itself. But the mechanisms by which RSNOs transfer NO to its physiological targets are not well understood (*4, 20-24*).

RSNOs can rapidly generate NO by the action of heat or light *via* the homolytic cleavage of the *S*-NO bond (eqs. 4.1 and 4.2), or by copper-catalyzed, reductive cleavage (eqs. 4.3 and 4.4) (*15*):

$$RSNO \rightleftharpoons RS^{\bullet} + NO^{\bullet} \quad (4.1)$$

$$RS^{\bullet} + RSNO \rightleftharpoons RSSR + NO^{\bullet} \quad (4.2)$$

$$2\,Cu^{II} + 2\,RS^{-} \rightleftharpoons 2Cu^{I} + RSSR \quad (4.3)$$

$$Cu^{I} + RSNO \rightleftharpoons Cu^{II} + RS^{-} + NO \quad (4.4)$$

RSNOs also undergo slow denitrosaton *via* hydrolysis (Chapters 2 and 3) (*14*). In a study of the reactivity of nitrogen nucleophiles including piperidine, pyrrolidine, propylamine, hydrazine, and ammonia towards RSNOs, Munro and Williams (*34*) indicated that hydrolytic RSNO denitrosation can be base-catalyzed. The final nitrogen-containing product was $NO_2^-$ from nucleophilic attack by $OH^-$ on the nitrogen of the *S*-NO bond:

$$2RSNO + 2OH^{-} \rightarrow RSSR + 2NO_2^{-} + 2H^{+} \quad (4.5)$$

Since only 50% of the expected $NO_2^-$ was detected, the authors proposed that nucleophilic attack by $OH^-$ at the sulfur atom (eq. 4.6) was also taking place:

$$RSNO + OH^- \rightarrow RSOH + NO^- \quad (4.6)$$

$$NO^- + H^+ \rightleftharpoons HNO \quad (4.7)$$

The possibility that HNO ($pK_a = 11.4$ (*85*)) may be generated from base-catalyzed RSNO hydrolysis has important implications in biology because HNO has been shown to have some similar and some opposing pharmacological effects as NO. However, HNO formation from base-catalyzed RSNO decomposition has not been conclusively demonstrated. We report here the findings from our investigation into the decomposition of *S*-nitrosoglutathione (GSNO) in 10 mM, 20 mM and 200 mM aqueous NaOH. A goal of this study was to determine whether the products formed were consistent with HNO formation due to attack at sulfur atom of the *S*-NO bond.

## 4.3 Experimental

### 4.3.1 Materials

HPLC amber glass target vials were purchased from National Scientific (Rockwood, TN). Dimedone was purchased from Lancaster Synthesis (Windham, NH), diethylenetriaminepentaacetic acid (DTPA) from Koch-Light Laboratories (Colnbrook Bucks, England). Nitrous oxide ($N_2O$, 99% pure) was obtained from BOC Canada (St Laurent, Quebec). All other reagents were purchased from Sigma-Aldrich.

### 4.3.2 Synthesis of GSNO stock solution

Stock GSNO solutions were prepared as described in Section 3.3.2. The pH of the GSNO solutions was adjusted to pH 7 with NaOH, and the concentration verified as

described in Section 3.3.2. A fresh GSNO stock solution was prepared on the same day as the experiment and kept on ice.

### 4.3.3 UV-vis spectrophotometry

Spectra of GSNO solutions were obtained as described in Section 3.3.2

### 4.3.4 HPLC/UV and HPLC/MS analysis

The products of GSNO hydrolysis were monitored by HPLC as described in Section 3.3.3. Product identification was by HPLC/MS as described in Section 3.3.3. The injection volume was adjusted to compensate for the different GSNO concentrations used.

### 4.3.5 GSNO denitrosation in NaOH solutions in the presence and absence of dimedone

A solution of 8 mM GSNO in 200 mM aqueous NaOH containing 0.1 mM DTPA was stored in the dark in a quartz cuvette at room temperature. The UV-vis spectrum of the solution was measured every 5 min over 50 min. To monitor GSNO decomposition by HPLC, a GSNO stock solution was diluted to achieve the desired GSNO concentration in 10 mM or 20 mM NaOH containing 0.1 mM DTPA. The decomposition was conducted at RT in the dark and monitored at specific time intervals using the HPLC method described in Section 3.3.3. Identification of the degradation products was performed by HPLC/MS (Section 3.3.3). A solution of 0.8 mM GSNO and 5 mM dimedone in 20 mM NaOH containing 0.1 mm DTPA was monitored in the same manner.

### 4.3.6 Measurement of $N_2O$ by headspace gas chromatography/mass spectrometry (GC/MS)

Nitrous oxide formation due to base-catalyzed GSNO decomposition at RT (~23 °C) in the dark was monitored by analyzing the headspace above 5-mL reaction solutions in 10-mL sealed glass vials. Aliquots (1 mL) of the headspace was injected into a headspace GC/MS system consisting of a 6890N gas chromatograph equipped with a 7694 headspace sampler and interfaced to a 5973 mass selective detector (Agilent Technologies, Santa Clara, CA). Chromatographic separation was achieved with a HP-Plot Q column (30-m x 0.53-mm, 40-μm film thickness; J&W Scientific, Folsom, CA) at 30°C using the method of Accorsi *et al.* (*86*). The detector was operated in positive-ion SIM mode. Calibration standards were prepared by injecting different volumes of $N_2O$ gas with an airtight syringe into 10-mL sealed glass vials containing 5 mL of water. All vials were allowed to equilibrate at 41 °C for 2 h prior to analysis.

## 4.4 Results

### 4.4.1 GSNO decomposition in 200 mM, 20 mM, and 10 mM NaOH

The decomposition of 8 mM GSNO in 200 mM NaOH at RT in the dark was monitored by UV-vis spectrophotometry. The resulting spectra (Figure 4.1) show the disappearance of the *S*-NO absorption band ($\lambda_{max}$ = 335 nm) indicating that denitrosation occurred rapidly in 200 mM NaOH. The spectra also show the evolution of a new visible band centered around 410 nm as well as red-shifting of the UV band of GSNO. No isosbestic points are observed, indicating the conversion of GSNO to more than one species. A visual examination of the reaction vials at the end of the experiments revealed

that the solutions had changed from a reddish-pink color, typical of primary RSNOs, to a yellow-orange color. This was stable for at least 12 h in 200 mM NaOH at RT in sealed vials, but disappeared slowly over 16 h when in unsealed vials. The yellow-orange color was lost on acidification with HCl, and upon heating to 41 °C.

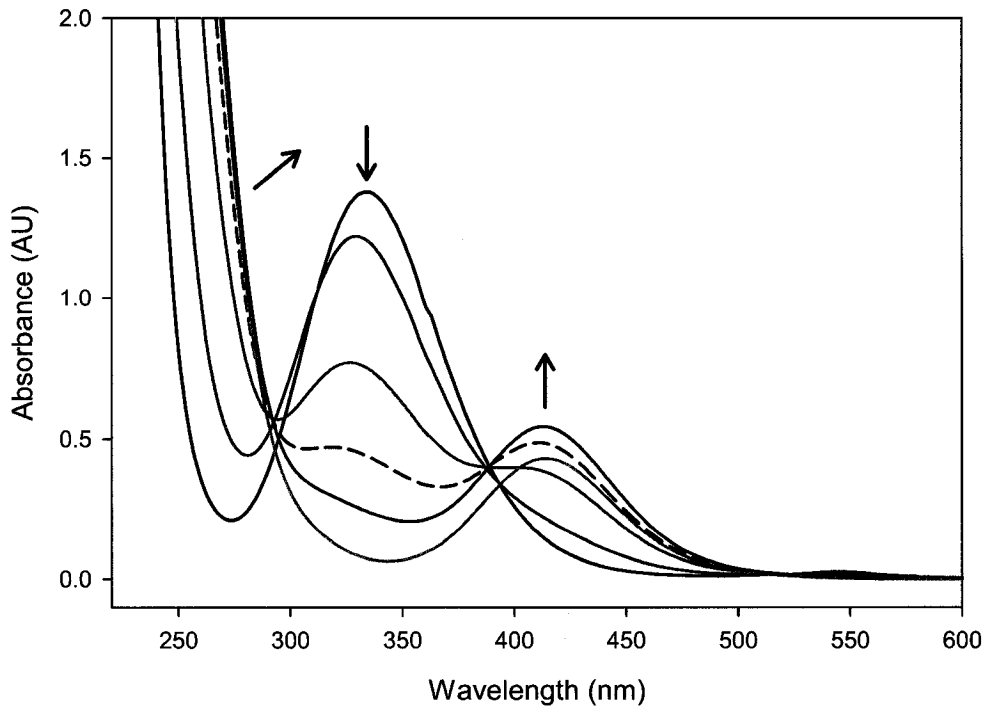


**Figure 4.1. UV-vis spectra of 8 mM GSNO in 200 mM NaOH (aq) containing 0.1 mM DTPA.** Spectra were recorded at RT over 50 min in an unsealed 0.2-cm pathlength quartz cuvette, integration time 0.1 s. The spectra at 0 min **(black)**, 10 min **(red)**, 20 min **(green)**, 30 min **(dashed black)**, 40 min **(blue)**, 55 min **(dark yellow)**.

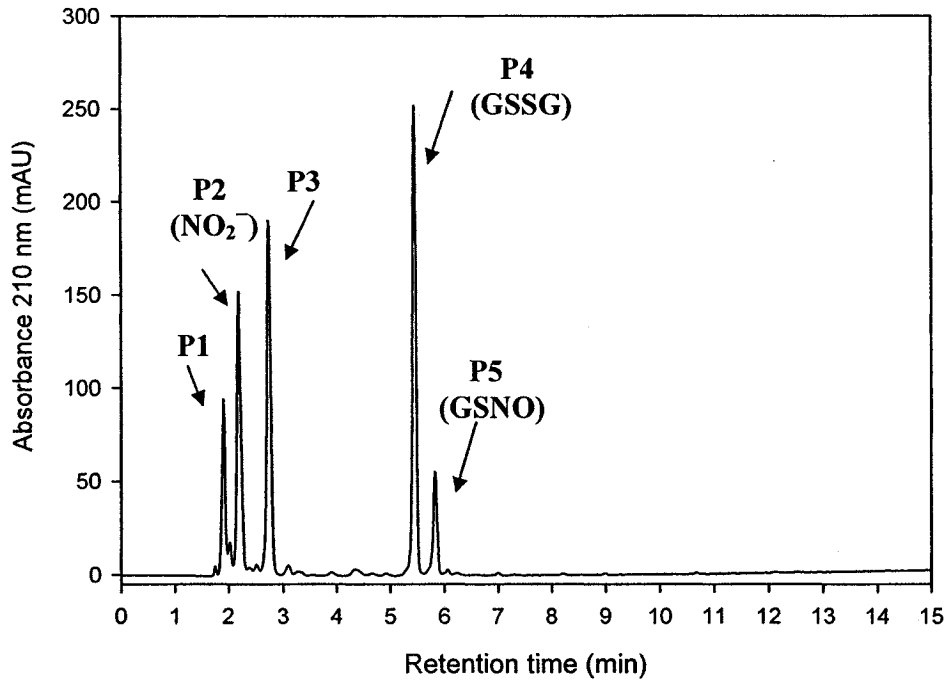


**Figure 4.2. HPLC analysis of GSNO degradates on base hydrolysis in 20 mM NaOH.** A solution of 1.6 mM GSNO in 20 mM NaOH (containing 0.1 mM DTPA) was stored in a capped amber glass HPLC vial at RT for 4 h, protected from light. The HPLC chromatogram was recorded as described in Section 4.3.4. $NO_2^-$ was present in P2 (see Section 3.4.2) and the mass spectra of P1, and P3–P5 are shown in Figure 4.3.

The HPLC/UV chromatogram of decomposed GSNO in 20 mM NaOH shown in Figure 4.2 revealed the formation of 4 major degradates, peaks 1–4. The identity of peak 4 was established by its ESI-MS spectra (Figure 4.3) as GSSG, and peak 5 as the reactant, GSNO. Peak 2 was identified as $NO_2^-$ since it exhibits the same retention time and UV spectrum as $NaNO_2$ standards. The ESI-MS spectra of P1 and P3 show base peaks at *m/z* 340 and 274, respectively, and their fragmentation patterns reveal that they contain a glutathionyl moiety, and correspond to products originating from a nitrosated

disulfide as discussed in Section 4.5. There were no chromatographic peaks that could be identified as GSH.

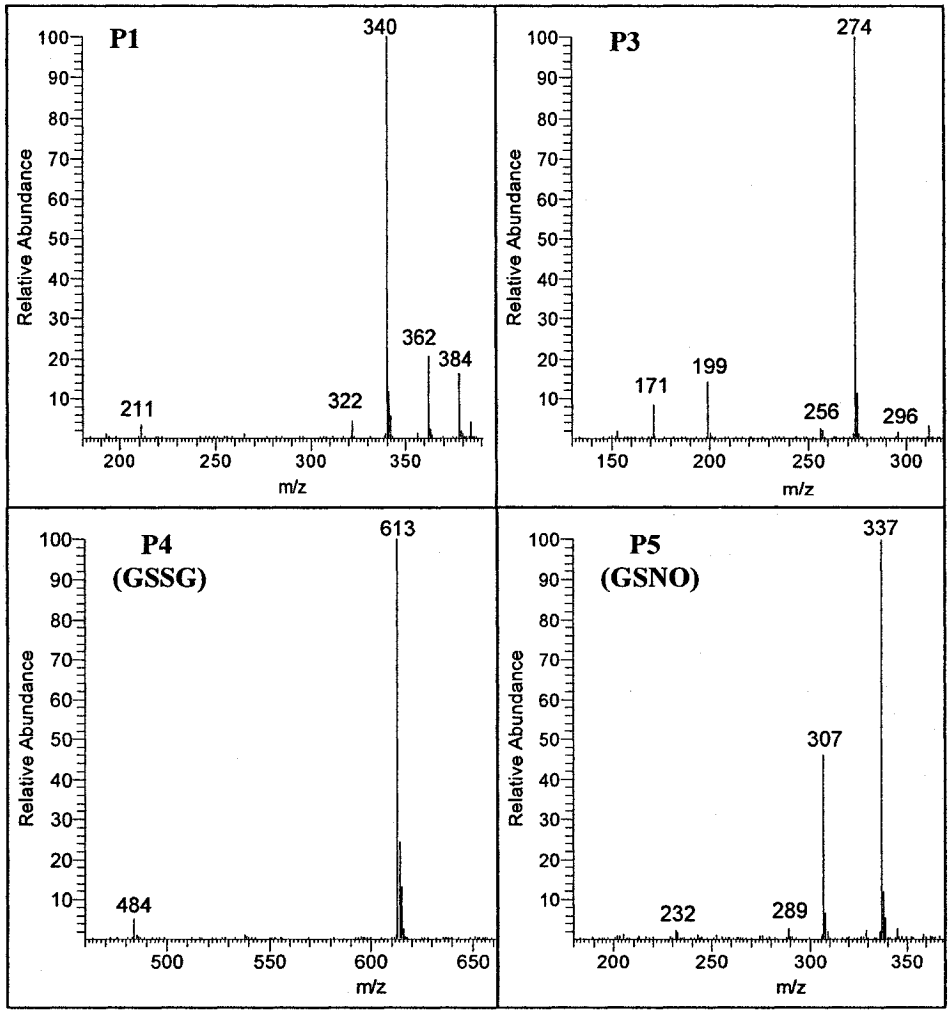


**Figure 4.3. ESI mass spectra of degradates formed on GSNO hydrolysis in 20 mM NaOH.** The sample was analyzed by HPLC, and the labels (P1, P3, P4, P5) correspond to the HPLC peaks in Figure 4.2. The HPLC/ESI-MS method is described in Section 4.3.4.

### 4.4.2 Time course of GSNO decomposition

The time course of 0.4-6.4 mM GSNO decomposition in 10 and 20 mM NaOH was monitored by HPLC/UV at 210 nm to determine the kinetics of GSNO disappearance at different reactant concentrations. The GSNO concentration was varied between 0.4–6.4 mM because preliminary experiments indicated that the degradate distribution was dependent on [GSNO]. The HPLC/UV chromatograms for these experiments are presented in Figures 4.4 and 4.4. The disappearance of GSNO (P5) and formation of four major degradates (P1-P4) on hydrolysis can be seen. Figures 4.4 and 4.5 also show that the concentration of the degradates does not change once GSNO is depleted, suggesting that the observed products result from reaction of GSNO with either NaOH or an intermediate product.

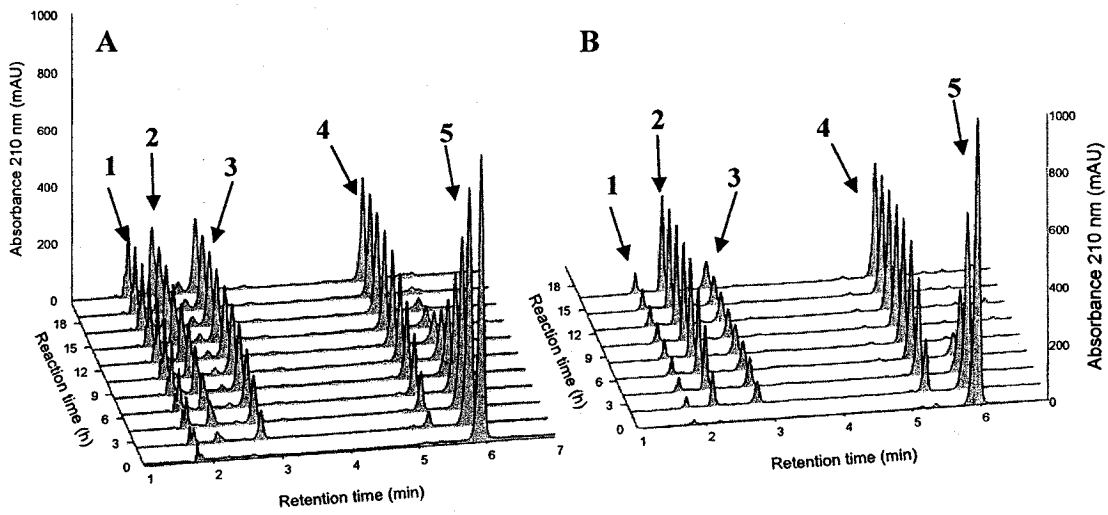


**Figure 4.4. HPLC analysis of GSNO hydrolysis in 10 mM NaOH. (A)** 0.4 mM GSNO and **(B)** 1.6 mM GSNO. Samples in 10 mM NaOH (containing 0.1 mM DTPA) were stored in capped amber glass HPLC vials at RT for up to 20 h, protected from light, the HPLC analysis was carried out as described in Section 4.3.4, and the peak assignments are: **1** Peak 1, **2** $NO_2^-$, **3** Peak 3, **4** GSSG, **5** GSNO (Figure 4.3).

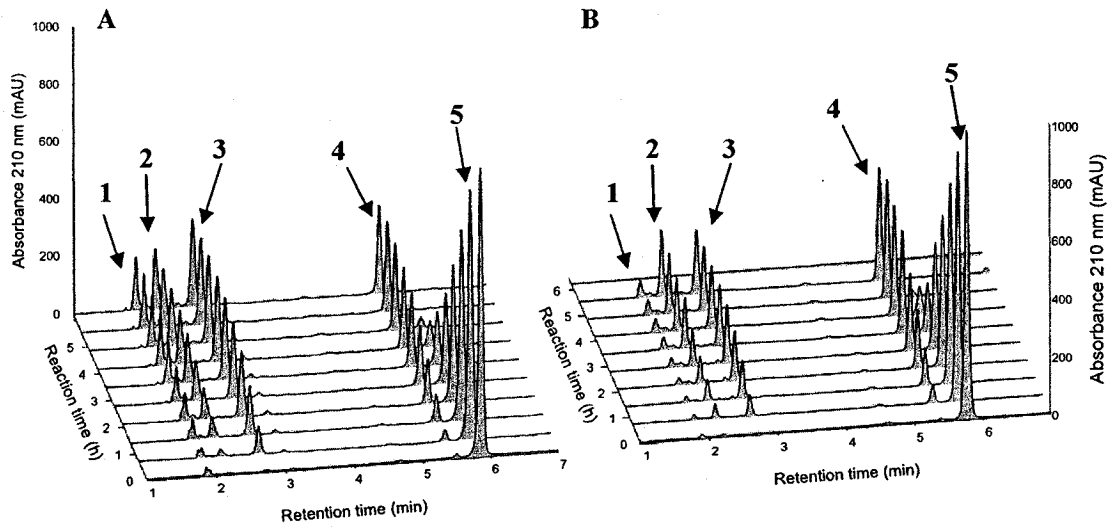


**Figure 4.5. HPLC analysis of GSNO hydrolysis in 20 mM NaOH. (A)** 0.8 mM GSNO and **(B)** 3.2 mM GSNO. The experimental conditions are given in the legend to Figure 4.4. The peak assignments are: **1** Peak 1, **2** $NO_2^-$, **3** Peak 3, **4** GSSG, **5** GSNO (Figure 4.3).

The quantitative results from the HPLC/UV experiments are summarized in Table 4.1. Since the only standards available for quantitation purposes were GSSG and $NaNO_2$, the results in Table 4.1 include quantitative amounts of GSSG and $NO_2^-$ and relative amounts of Peak 1 and Peak 3 expressed as a percentage of the initial GSNO based on the corresponding peak areas. Previously, Munro and Williams (*34*) reported that only 50% of the expected amounts of $NO_2^-$ were present on base-catalyzed GSNO decomposition, assuming stoichiometric conversion of GSNO to GSSG and $NO_2^-$. The results in Table 1 show that the GSSG yield varied from 87% at a $[OH^-]_o/[GSNO]_o$ ratio of 20:6.4, and decreased to 53% when the $[OH^-]_o/[GSNO]_o$ ratio was 20:0.8. The relative concentrations of P1 and P3 show an inverse correlation to that of GSSG, and the sum

[GSSG] + [P1] + [P3] equals 104±8% of $[GSNO]_o$. This suggests that P1 and P3 together account for any GSX not converted to GSSG. A reason for the deviation from 100% is that both P1 and P3 likely have molar absorptivities at 210 nm that differ from that of GSSG. The $NO_2^-$ yield exhibits a similar dependence on $[OH^-]_o/[GSNO]_o$ as GSSG in 20 mM NaOH, but a constant yield (68±1%) in 10 mM NaOH.

**Table 4.1.** Product yields in base-catalyzed GSNO hydrolysis[a]

| $[GSNO]_o$ mM | $[OH^-]_o$[b] mM | Reaction time[c] (h) | GSSG yield[d] (%) | $NO_2^-$ yield[d] (%) | $N_2O$ yield (%) | P1 yield[e] (%) | P3 yield[e] (%) |
|---|---|---|---|---|---|---|---|
| 0.4 | 10 | 18 | 68 | 69 | - | 17 | 24 |
| 0.8 | 10 | 15 | 67 | 69 | - | 14 | 21 |
| 1.6 | 10 | 15 | 72 | 68 | - | 10 | 14 |
| 3.2 | 10 | 14 | 75 | 67 | 7.0 | 6 | 10 |
| | | | | | | | |
| 0.8 | 20 | 6 | 53 | 51 | 4.5 | 17 | 30 |
| 0.8 + dimedone | 20 | 5 | 83 | 62 | - | 10 | 14 |
| 1.6 | 20 | 6 | 70 | 65 | - | 11 | 23 |
| 3.2 | 20 | 6 | 83 | 73 | - | 7 | 24 |
| 6.4 | 20 | 6 | 87 | 71 | - | 6 | 20 |

[a] All yields are expressed relative to $[GSNO]_o$, n = 1.

[b] Hydrolysis was carried out in 10 and 20 mM NaOH in capped amber glass HPLC vials at RT and the products were analyzed by HPLC as described in Section 4.3.4.

[c] Time when GSNO was no longer detected at 210 nm.

[d] Calculated by comparison to the injection of standards.

[e] Expressed relative to $[GSNO]_o$ based on peak areas measured at 210 nm. Peak areas were not corrected for the different molar absorption coefficients of GSNO, P1, and P3 at 210 nm.

Table 4.1 also includes the results from the determination of $N_2O$ by headspace GC/MS analysis performed for 3.2 mM GSNO in 10 mM NaOH and 0.8 mM GSNO in 20 mM NaOH. $N_2O$ is formed as a result of HNO dimerization (eq. 1.13) and is considered here to be a marker of HNO formed during hydrolysis. The results, expressed as percent $[GSNO]_o$, reveal that only 4.5% and 7.0% of the nitroso nitrogen of GSNO was detected as HNO in 10 and 20 mM NaOH, respectively. Thus, only a small fraction of GSNO hydrolysis likely results from $OH^-$ attack at the sulfur atom.

In the presence of dimedone (Figure 4.6), new peaks are seen at longer retention times (10–14 min). Based on the *m/z* values observed in the mass spectra of P6-P9 (Figure 4.7), these peaks likely correspond to the dimedone adduct of GSOH (*m/z* 446, P6)

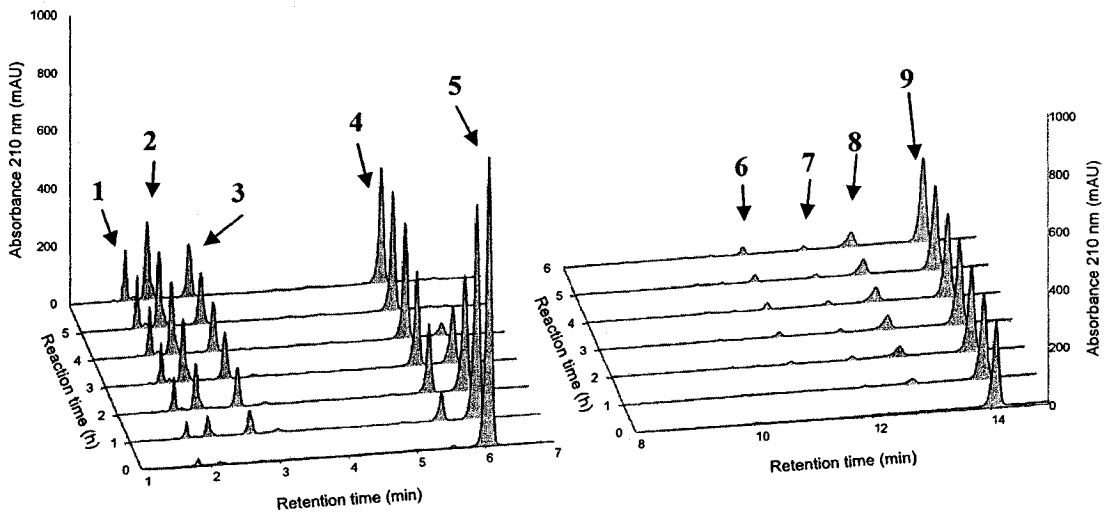


**Figure 4.6. HPLC analysis of GSNO hydrolysis in 20 mM NaOH in the presence of dimedone.** A solution of 0.8 mM GSNO + 5 mM dimedone in 20 mM NaOH (containing 0.1 mM DTPA) was stored in a capped amber glass HPLC vial at RT for up to 8 h, protected from light. The HPLC analysis was carried out as described in Section 4.3.4. and the assignments are **1** Peak 1, **2** $NO_2^-$, **3** Peak 3, **4** GSSG, **5** GSNO, **6** GS-dimedone, **7** GSS-dimedone, **8** nitrosated dimedone, **9** dimedone.

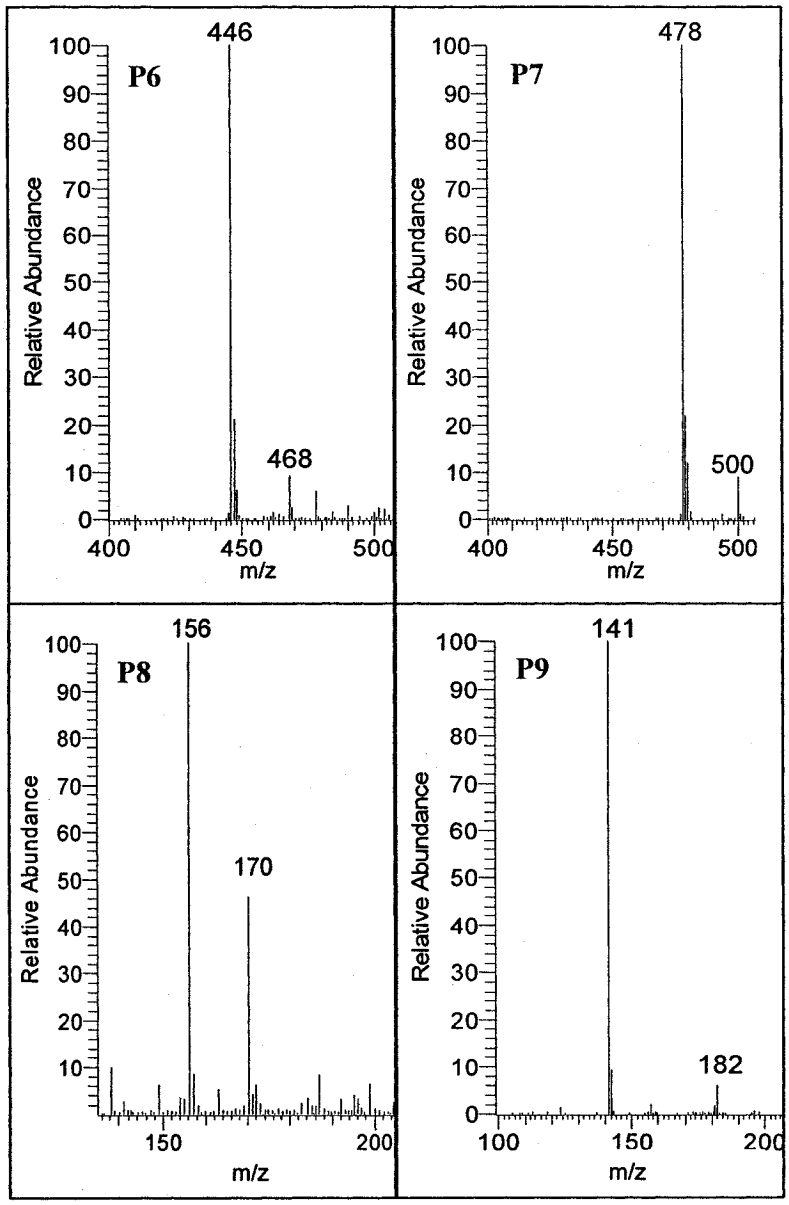


**Figure 4.7. ESI mass spectra of GSNO degradates formed on base hydrolysis in 20 mM NaOH in the presence of dimedone.** The labels (P6, P7, P8, P9) correspond to the HPLC peaks in Figure 4.6. The HPLC/ESI-MS method is described in Section 4.3.4.

that results from $OH^-$ attack on the *NITROSO* sulfur (eq. 4.6), a dimedone adduct with GSSH (*m/z* 478, P7), nitrosated dimedone (*m/z* 170, P8), and unreacted dimedone (*m/z* 141, P9). The trapping of intermediates with dimedone leads to significantly higher GSSG and lower P3 yields than in its absence (Figure 4.6 *vs* 4.5A; Table 6.1).

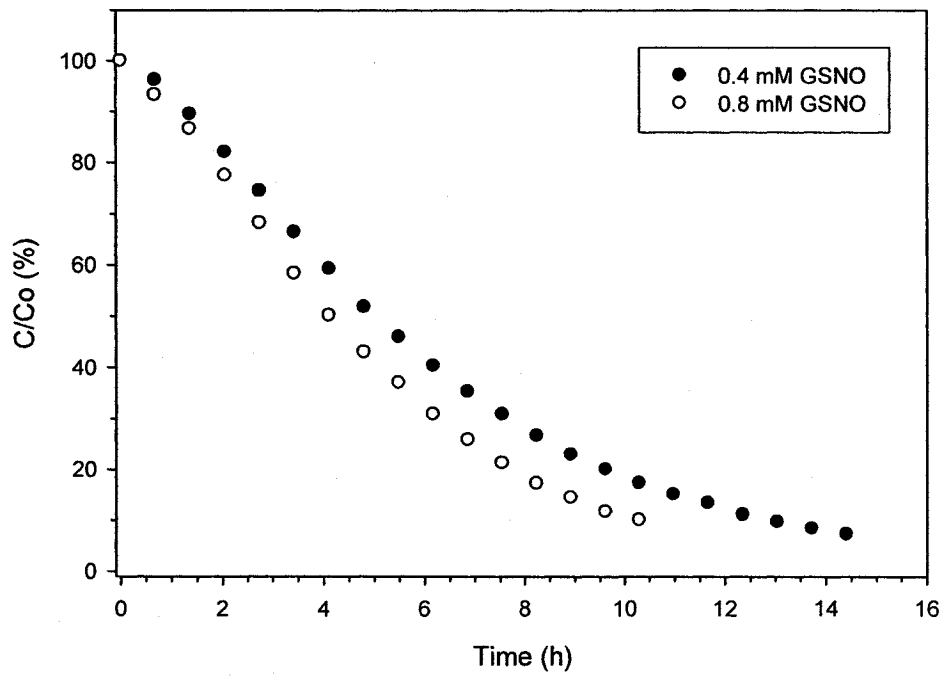


**Figure 4.8. Kinetics of GSNO decomposition in 10 mM NaOH (aq). Closed circles:** 0.4 mM GSNO. **Open circles:** 0.8 mM GSNO. Samples in 10 mM NaOH (containing 0.1 mM DTPA) were stored in capped amber glass HPLC vials at RT, protected from light. The GSNO peak areas in the HPLC chromatograms were measured at 210 nm, and the HPLC method is described in Section 4.3.4. n=1 for each kinetic run.

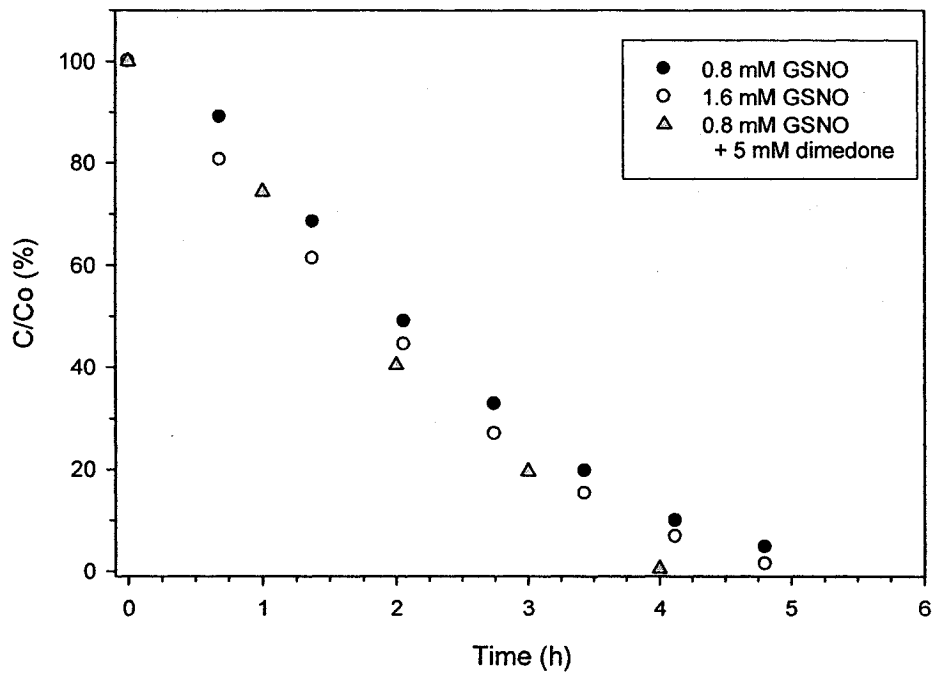


**Figure 4.9. Kinetics of GSNO decomposition in 20 mM NaOH (aq). Closed circles:** 0.8 mM GSNO. **Open circles:** 1.6 mM GSNO. **Gray triangles:** 0.8 mM GSNO + 5 mM dimedone. Samples in 20 mM NaOH (containing 0.1 mM DTPA) were stored in capped amber glass HPLC vials at RT, protected from light. The GSNO peak areas in the HPLC chromatograms were measured at 210 nm, and the HPLC method is described in Section 4.3.4. n=1 for each kinetic run.

The published rate law for RSNO base hydrolysis (*14*) is:

$$\text{Rate} = k[\text{RSNO}][\text{OH}^-] \qquad (4.7)$$

The data in Figures 4.8 and 4.9 reveal that, as expected, the GSNO decomposition rate is largely independent of [GSNO] under pseudo-first-order conditions, [$OH^-$]>>[GSNO]. The rate also doubles when the NaOH concentration is increased from 10 mM to 20 mM.

However, the plots of GSNO decomposition in 10 mM NaOH exhibit a short incubation period, suggesting the existence of a competing autocatalytic decomposition pathway not predicted by eq. 4.7. The incubation period is less apparent in 20 mM NaOH (Figure 4.8 *vs* 4.9), and the addition of dimedone to the solution did not result in significant changes in the reaction kinetics (Figure 4.9) although the product profile was altered considerably (Table 4.1)

## 4.5 Discussion

In their study of the reactivity of SPEN with different nucleophiles, Munro and Williams observed only a 50% yield of $NO_2^-$ on base-catalyzed SPEN hydrolysis (*34*). They proposed a secondary reaction such as nucleophilic attack by $OH^-$ on the sulfur atom of SPEN with the release of $NO^-$ (eq. 4.6) to account for the low $NO_2^-$ yield. The results from this study show that the GSSG and $NO_2^-$ yields in the alkaline decomposition of GSNO increase with $[GSNO]_0$ in 20 mM NaOH, but not in 10 mM NaOH (Table 4.1). The GSSG and $NO_2^-$ yields approached 50% only for 0.8 mM GSNO hydrolysis in 20 mM NaOH and increased to 65–70% at 1.6 mM GSNO (Table 4.1). Munro and Williams (*34*) studied hydrolysis of 1 mM SPEN in 60–200 mM NaOH in the absence of other nucleophiles.

Our results also show that $N_2O$ is formed as result of base-catalyzed hydrolysis of GSNO (Table 4.1). This suggests that $OH^-$ performs nucleophilic attack on the sulfur as well as the nitrogen atom of the *S*-NO bond. Since the $N_2O$ yield is only ~ 4.5% (Table 5.1), attack at the sulfur is likely a minor reaction in GSNO alkaline decomposition even when the GSSG and $NO_2^-$ yields are only ~50%.

The changes in the UV-vis spectra and solution color observed in our experiments are similar to those reported by Munro and Williams (*87*) in the reactions of 1 mM GSNO, SPEN, or CysNO with 1 mM $Na_2S$ in aqueous solutions at pH ~11 in that the disappearance of the *S*-NO UV absorption band at 330–350 nm was accompanied by the appearance of a band at 410 nm, and that the final solutions were orange-yellow in color. Based on similar observations in previous studies of the reactions of NO with $Na_2S$, NaSH, and $Na_2S_2$ (*87-89*), the authors concluded that RSNO reacts with $HS^-$ to form a nitroso disulfide ($ONSS^-$) either through a $HSNO/ONS^-$ intermediate that further reacts with $HS^-$ (eqs. 4.8 and 4.9), or through a $HSS^-$ intermediate that acts as a nucleophile (eq. 4.10 ). The proposed reactions reported in (*87*) are:

$$RSNO + HS^- \rightarrow RSH + HSNO/ONS^- \quad (4.8)$$

$$HSNO/ONS^- + HS^- \rightarrow ONSS^- \quad (4.9)$$

$$RSNO + HSS^- \rightarrow RSH + ONSS^- \quad (4.10)$$

The UV-vis spectra in Figure 4.1 are almost identical to those reported (*87*) for 1 mM GSNO with 1 mM $HS^-$ ($H_2S$ $pK_{a1}$ = 7.04, $pK_{a2}$ = 11.96 (*90*)) in water at pH ~ 9.8. Thus, the reaction of GSNO with $OH^-$ may lead to the formation of degradates containing a nitrosated disulfide $GS(NO)SG^-$ species as the major competing decomposition pathway. However, the mechanism probably differs from that proposed by Munro and Williams since the GSH buildup predicted by eqs. 4.8 and 4.10 was not detected in our experiments.

Based on the products we detected (Table 4.1), the mechanism we propose for GSNO hydrolysis is given by eqs. 4.11–4.15. Nucleophilic attack by $OH^-$ on the GSNO nitroso nitrogen produces $GS^-$ and $NO_2^-$ (eq. 4.11), $GS^-$ dimerizes and is oxidized by $O_2$ to form GSSG and $H_2O_2$ (eq. 4.12):

$$GSNO + 2OH^- \rightarrow GS^- + NO_2^- + H_2O \quad (4.11)$$

$$2GS^- + O_2 + 2H_2O \rightarrow GSSG + H_2O_2 + 2OH^- \quad (4.12)$$

$$GS^- + G'SNO \rightarrow GS(NO)SG'^- \quad (4.13)$$

$$GS(NO)SG'^- \rightarrow GS(NO)S^- + G \quad (4.14)$$

In addition, $GS^-$ can attack a second GSNO molecule at the sulfur atom to generate a nitrosated disulfide $GS(NO)SG'^-$ (eq. 4.13). Interestingly, computational studies of $CH_3SNO$ decomposition have led to the proposal of nitrosated disulfides as possible RSNO decomposition intermediates that form RSSR and nitrogen products (*78*). $RS(NO)SR^-$ are also proposed intermediates in *trans-S*-nitrosation reactions (*91*). Cleavage of the S-G′ bond of $GS(NO)S\text{-}G'^-$ would yield $GS(NO)S^-$ and a sulfur-free

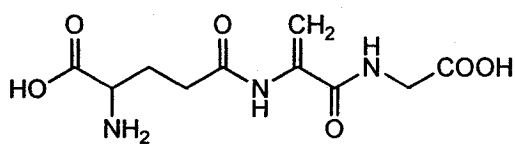


**Figure 4.10. Proposed structure for the sulfur-free glutathionyl derivative.** This derivative is formed in Reaction 4.14.

glutathionyl derivative (G in eq. 4.14). The structure proposed for G (Figure 4.10) is consistent with the observation of a $(M+H)^+$ ion at *m/z* 274 for P3 in Figure 4.3.

The yellow-orange color of the solutions is attributed to $GS(NO)S^-$. The color disappears by the action of heat, acidification, or simply over time, presumably due to denitrosation to yield $GSS^-$. Rao and Gorin *(92)* observed the formation of $CysSS^-$ in the reaction of cystine with $HS^-$, and CysSSH was formed on acidification with "strong hydrochloric acid". Based on its *m/z* (274, Figure 4.3), P3 is assigned to the sulfur-free molecule in Figure 4.10, while P1 is probably GSSH (*m/z* 340) resulting from the denitrosation and protonation of $GS(NO)S^-$. No peaks corresponding to $GS(NO)S^-$ or GS(NO)SH (predicted *m/z* 370) were observed, presumably due to $GS(NO)S^-$ denitrosation and protonation in the acidic HPLC mobile phase (pH 3.0).

The mechanism defined by Reactions 4.11–4.14 would account for the products detected in our experiments and for the inverse correlation of [GSSG] yields with those of [P1] and [P3] (Table 4.1). Since formation of P1 and P3 require excess $OH^-$, it is conceivable that $OH^-$ catalyzes the cleavage of the $GS(NO)SG'^-$. The higher NaOH concentrations used by Munro and Williams (*34*) would result in P1 and P3 yields similar to those observed for 0.8 mM GSNO in 20 mM NaOH where the $NO_2^-$ yield approaches 50%.

A goal of this study was to investigate whether base-catalyzed GSNO hydrolysis resulted in the formation of HNO on $OH^-$ attack at the nitroso sulfur. The detection of $N_2O$ in the headspace of the solutions and the formation of dimedone adducts of GSOH are evidence for this GSNO decomposition pathway occurring under our experimental

conditions. However, the results show that only a small portion (<10%) of the decomposition occurs *via* $OH^-$ attack at the *NITROSO* sulfur.

## 4.6 Conclusions

GSNO decomposition in alkaline solutions is mainly the result of nucleophilic attack by $OH^-$ at the nitroso nitrogen to produce GSSG and $NO_2^-$. When $OH^-$ is in large excess, a second decomposition pathway is observed that eventually produces GSSH and a sulfur-free glutathionyl derivative. The detection of these products suggests the initial formation of a nitrosated disulfide intermediate $(GS(NO)SG)^-$, which yields the observed decomposition products.

GSNO decomposition *via* nucleophilic attack by $OH^-$ at the *NITROSO* sulfur occurs only to a minor extent under our conditions. The reaction produces HNO as evidenced by the formation of GSOH and $N_2O$. This observation has implications in biology since it could provide a route for the biosynthesis of HNO *in vivo* catalyzed by hydrolytic enzymes.

# Chapter 5 - Thiolysis of GSNO at pH 7.4

## 5.1 Abstract

*S*-Nitrosoglutathione (GSNO) undergoes denitrosation in the presence of excess glutathione (GSH) when protected from light and metal-catalyzed decomposition. Product analysis of reactions between 1 mM GSNO and 1, 5, and 10 mM GSH shows that GSSG is the major glutathionyl product and $GS(O)NH_2$, GSN(OH)H, and GSOH, are minor products. These degradates result from direct GSH reaction with GSNO, and not from slow secondary reactions as previously argued. Retardation of GSNO decomposition on trapping GSOH with dimedone suggests that the mechanism is partially autocatalytic. Detection of $GS(O)NH_2$ and $N_2O$ suggests that HNO is generated during thiolysis.

## 5.2 Introduction

The mechanisms of NO transfer from RSNOs to physiological thiol targets is a topic of much current interest (*42, 76, 82, 83, 93-96*). *S*-Nitrosothiols exhibit similar physiological effects as NO itself (*35-39, 97*), and have been proposed to act in the storage and transport of endogenously generated NO (*8-11*). It is currently believed that RSNOs effect their NO-like biological actions by *trans-S*-nitrosating low-molecular-mass (LMM) thiols and cysteinyl groups of proteins and enzymes, thereby altering their function. For example, *trans-S*-nitrosation by GSNO results in *S*-nitrosation of hemoglobin at its Cys$\beta$93 residues (*98-100*), which confers vasodilator properties on the protein (*11*).

However, studies on RSNO decomposition in the presence of excess free thiol have shown that *trans-S*-nitrosation is not the only reaction channel. For example, GSNO decomposition in the presence of high GSH concentrations produces mainly the disulfide, GSSG, and ammonia as end products (*30, 52*) (Schemes 1.1 and 1.2). Such GSNO decomposition pathways are relevant in the context of the intracellular environment where GSH concentrations are high (*101*).

Singh *et al.* (*27*) studied the reactions between 1 mM GSNO with 1–10 mM GSH. They proposed a set of pathways originating from initial attack of GSH on the nitroso nitrogen of GSNO, forming GS-N(OH)-SG as an intermediate that led to the detection of GSSG, $NH_3$, $N_2O$, NO, and $NO_2^-$ (Scheme 1.1) after 40 h. Wong *et al.* (*30*) also studied the GSNO/GSH system and, in addition to the products identified by Singh *et al.*, proposed a second set of reaction pathways that included attack by GSH on the GSNO sulfur. Based on the detection of $NH_2OH$ and a product postulated to be the sulfinamide, $GS(O)NH_2$, attack on sulfur was assumed to generate the biologically important nitroxyl (HNO) (Scheme 1.2). The end products from this study were detected after long incubation times of 24–40 h, which prompted Tsikas *et al.* to suggest that the products resulted from secondary reactions (*31*).

The purpose of the present study was to investigate the prompt reactions of GSNO in the presence of high GSH concentrations at neutral pH. The growth of the GSX products was monitored continuously by HPLC and electrospray mass spectrometry (ESI-MS). The results are consistent with the published reaction pathways, including attack on the GSNO sulfur (Scheme 1.2).

## 5.3 Experimental

### 5.3.1 Materials

HPLC amber glass target vials were purchased from National Scientific, dimedone (DM) from Lancaster Synthesis, diethylenetriaminepentaacetic acid (DTPA) from Koch-Light Laboratories. All other reagents were purchased from Sigma-Aldrich. Stock GSNO solutions were prepared as described in Section 3.3.2, adjusted to pH 7.4 with NaOH, and the concentrations verified (Section 3.3.2). A fresh GSNO stock solution was prepared on the same day as the experiment and kept on ice.

### 5.3.2 UV-vis spectrophotometry and HPLC/UV and HPLC/MS analysis

Spectra of GSNO solutions were obtained as described in Section 3.3.2 to verify GSNO concentrations. The products of GSNO thiolysis were monitored by HPLC/UV as described in Section 3.3.3. Product identification was by HPLC/MS as described in Section 3.3.3. The injection volume was adjusted to compensate for the different GSNO concentrations used.

### 5.3.3 GSNO Thiolysis by GSH at pH 7.4

GSNO thiolysis by GSH was monitored by HPLC by adding GSNO stock solution into 50 mM sodium phosphate buffer (pH 7.4) containing GSH at the desired concentrations. All reaction solutions contained 0.1 mM DTPA to prevent copper-catalyzed decomposition. The reaction was monitored at specific time intervals using the HPLC method described in Section 5.3.2 and the reactions were conducted at 23 °C in the dark. Identification of the reaction products was performed by HPLC/MS (Section 5.3.2).

### 5.3.4 Headspace GC/ESI-MS analysis

The headspace above a solution of 1 mM GSNO plus 10 mM GSH was analyzed for $N_2O$ using the experimental conditions described in Section 4.3.6

## 5.4 Results

### 5.4.1 Products of GSNO thiolysis by GSH

The decomposition of 1 mM GSNO in the presence of 1, 5, or 10 mM GSH at pH 7.4 was investigated using HPLC/UV-vis to monitor the disappearance of GSNO and appearance of the thiolysis products. A typical chromatogram of the products (Figure 5.1), shows overlapping peaks at the solvent front with retention times of 1.7–1.9 min as well as three major chromatographic peaks identified by LC/ESI-MS (Figure 5.2) as the starting reactants, GSH and GSNO, and GSSG. The identity of all the components in the overlapping peaks could not be established because the solvent front contains buffer salts and other polar components that complicate the ESI mass spectra. However, the shoulder with a retention time of ~ 1.9 min was identified by LC/ESI-MS as glutathione sulfinamide, $GS(O)NH_2$ (Figure 5.2A), which can arise from the reaction of GSH and HNO (*102, 103*). No other major degradation products were observed in the chromatograms.

The time course of 1 mM GSNO thiolysis (Figure 5.3) reveals that the reaction occurs rapidly as reported (*26-28, 30, 104*). Most of the GSNO is consumed in < 8 h and the intensity of the product peaks remained unchanged over 24 h. No new degradates appeared in the chromatograms (data not shown) indicating that the observed products result from direct reactions of GSNO with GSH or other unstable intermediates, and not

from slow secondary degradate decomposition reactions as suggested by Tsikas *et al.* (*31*). The chromatograms in Figure 5.3 also reveal that the major GSX product is GSSG (peak 3).

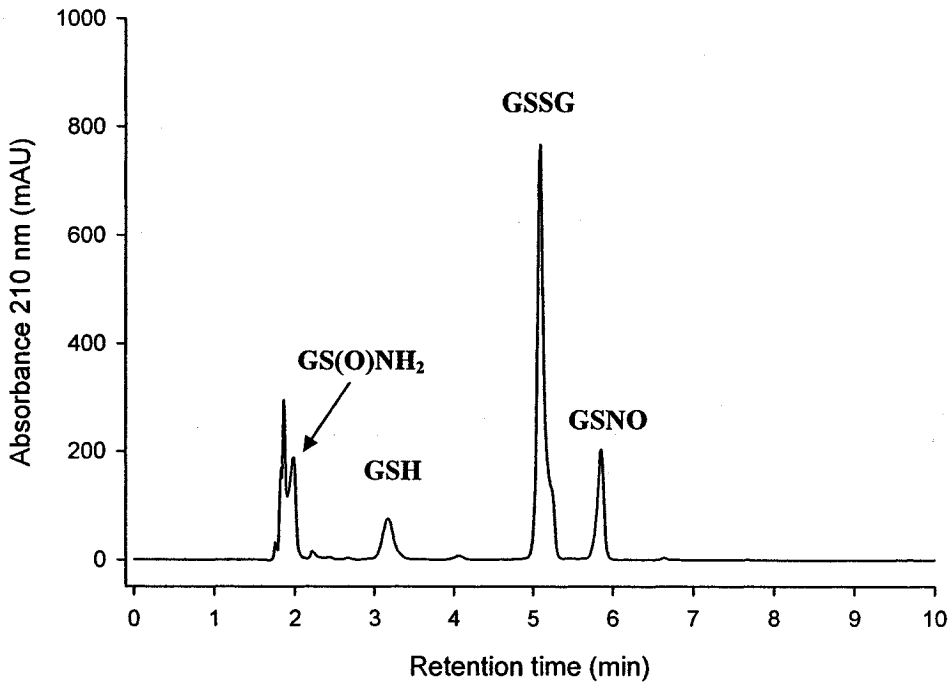


**Figure 5.1. HPLC chromatogram of the GSNO thiolysis products formed after 8 h at pH 7.4.** A solution containing 1 mM GSNO and 1 mM GSH in 50 mM sodium phosphate buffer (pH 7.4) (containing 0.1 mM DTPA) was stored in a capped amber glass HPLC vial at RT for 8 h protected from light. Compounds were identified by HPLC/ESI-MS and the mass spectra are shown in Figure 5.2. The HPLC method is described in Section 5.3.3.

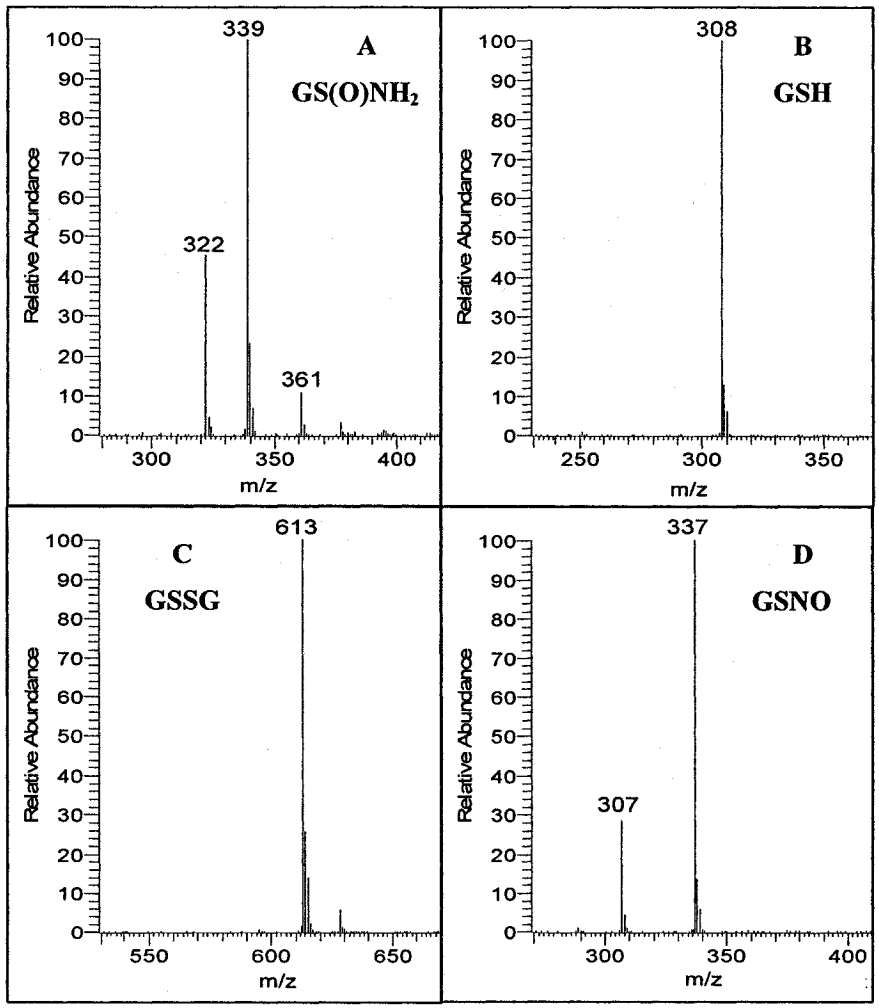


**Figure 5.2. ESI mass spectra of the GSNO thiolysis products formed after 8 h at pH 7.4.** The experimental details are given in the legend of Figure 5.1 and the HPLC/ESI-MS method is described in Section 5.3.3.

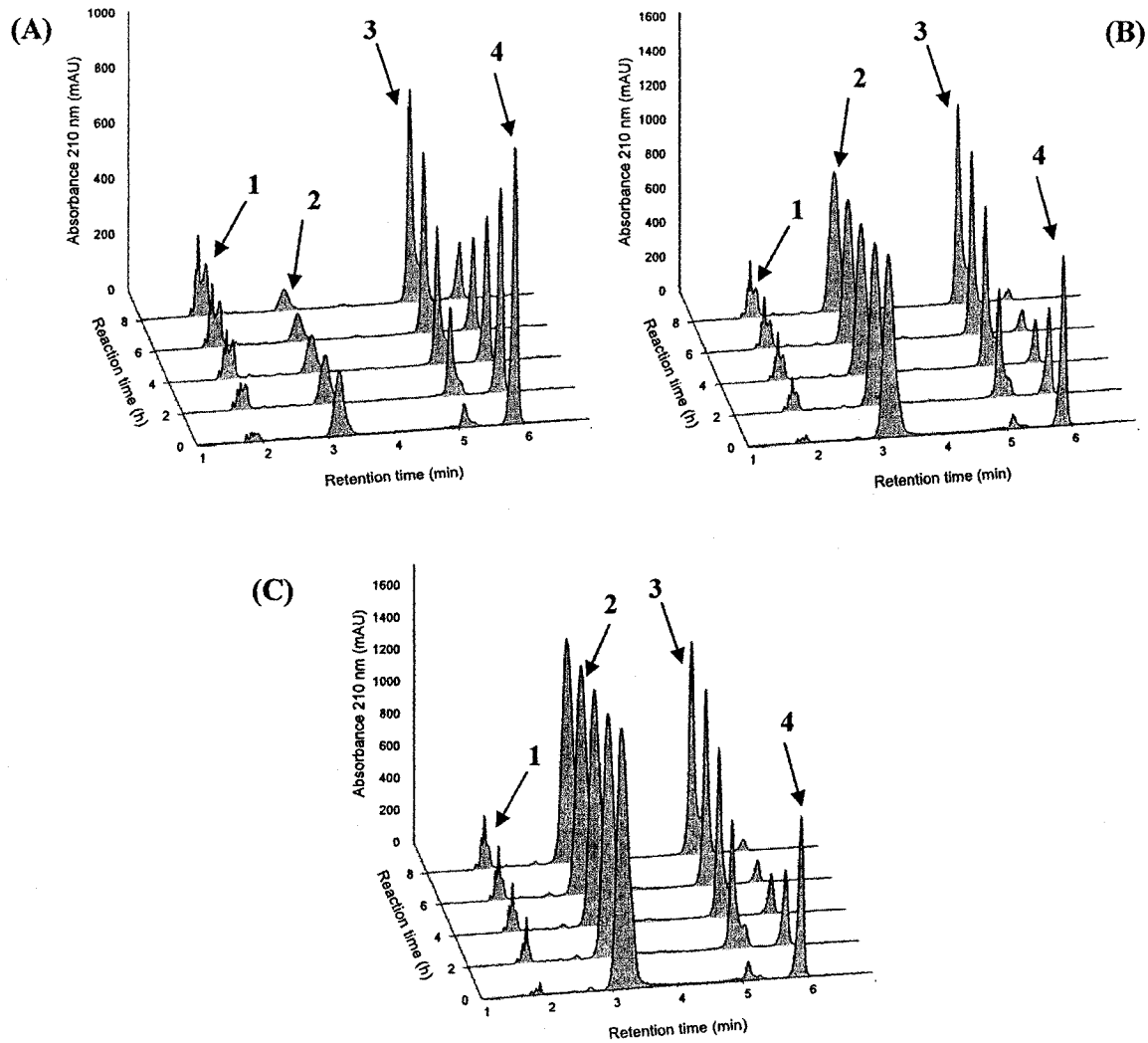


**Figure 5.3. HPLC analysis of GSNO thiolysis at pH 7.4.** Solutions of 1 mM GSNO plus **(A)** 1 mM GSH **(B)** 5 mM GSH and **(C)** 10 mM GSH in 50 mM sodium phosphate buffer (pH 7.4) (containing 0.1 mM DTPA) were stored in a capped amber glass HPLC vial at RT for 8 h and protected from light. The HPLC chromatograms were recorded as described in Section 5.3.3 and the peaks assignments are: **1** $GS(OH)NH_2$, **2** GSH, **3** GSSG, and **4** GSNO.

The rate of GSNO thiolysis by 5 mM GSH is significantly slower in the presence of 5 mM dimedone (Figure 5.4) with 23% of the initial GSNO still remaining after 18 h. In addition to the product peaks 1–4 observed in Figure 5.3, new peaks with retention times of 8–15 min originate from the trapping of unstable intermediates by dimedone (DM), which is known to trap sulfenic acids (eq 4.3). Based on their mass spectra (Figure 5.6), P5 and P6 were assigned to two conformers of GSNH-DM (*m/z* 461) and P7 to GS-DM (*m/z* 446) arising from the reactions of dimedone with GSN(OH)H and GSOH, respectively. These species are proposed intermediates in the GSNO thiolysis pathways (Schemes 1.1 and 1.2) that lead to the formation of GSSG and $NH_3$. P8 at *m/z* 141 corresponds to unreacted dimedone.

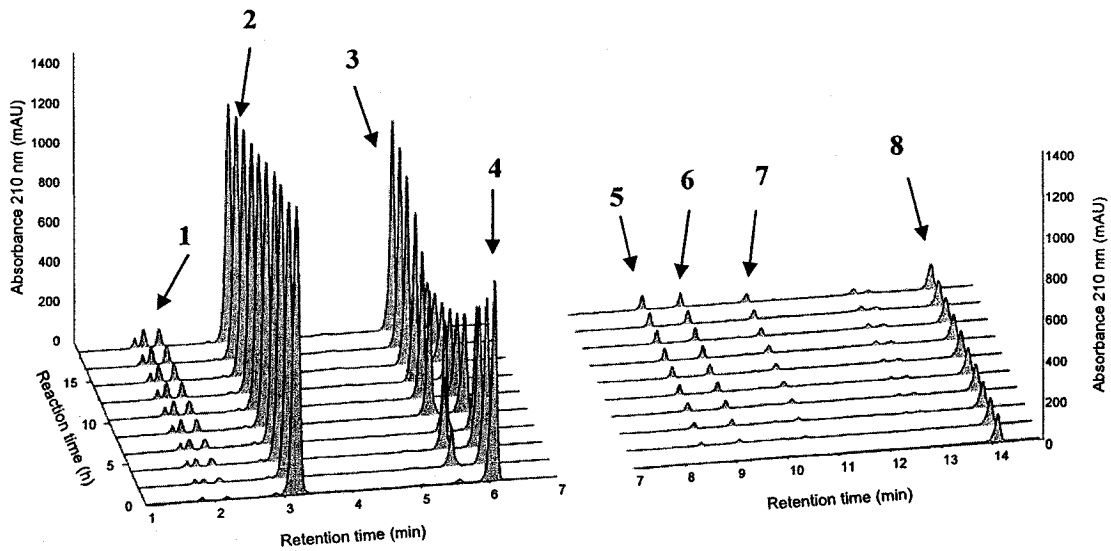


**Figure 5.4. HPLC analysis of GSNO thiolysis in the presence of dimedone at pH 7.4.** A solution of 1 mM GSNO + 5 mM GSH + 5 mM dimedone in 50 mM sodium phosphate buffer (pH 7.4) (containing 0.1 mM DTPA) was stored in a capped amber glass HPLC vial at RT for 18 h protected from light. The HPLC chromatograms were recorded as described in Section 5.3.3, and the peak assignments are: **1** $GS(OH)NH_2$, **2** GSH, **3** GSSG, **4** GSNO, **5,6** GS(NH)-dimedone, **7** GS-dimedone, **8** dimedone.

Figure 5.5 summarizes the kinetics of GSNO decomposition in the presence of different GSH concentrations and dimedone. The data reveal that the rate increased dramatically when 1 mM GSH was added but 1 mM GSNO decayed at similar rates in solutions containing 1–10 mM GSH, which is not consistent with the proposed simple rate law (eq. 5.1). The addition of dimedone caused a 4-fold decrease in the rate of thiolysis by 5 mM GSH which is also inconsistent with eq. 5.1.

$$v = k[RSNO][RSH] \qquad (5.1)$$

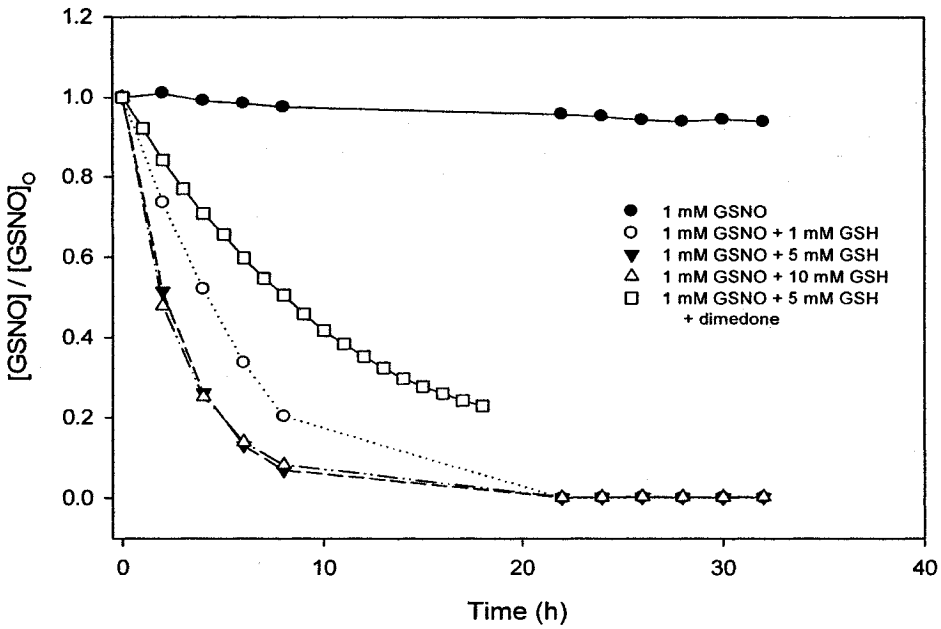


**Figure 5.5. Kinetics of GSNO decomposition in the presence of GSH and dimedone.** Solutions of 1 mM GSNO + GSH and dimedone at the concentrations indicated in 50 mM sodium phosphate buffer (pH 7.4) (containing 0.1 mM DTPA) were stored in capped amber glass HPLC vials at RT and protected from light. The HPLC method as described in Section 5.3.3. The lines do not represent mathematical fits of the data but were drawn for clarity.

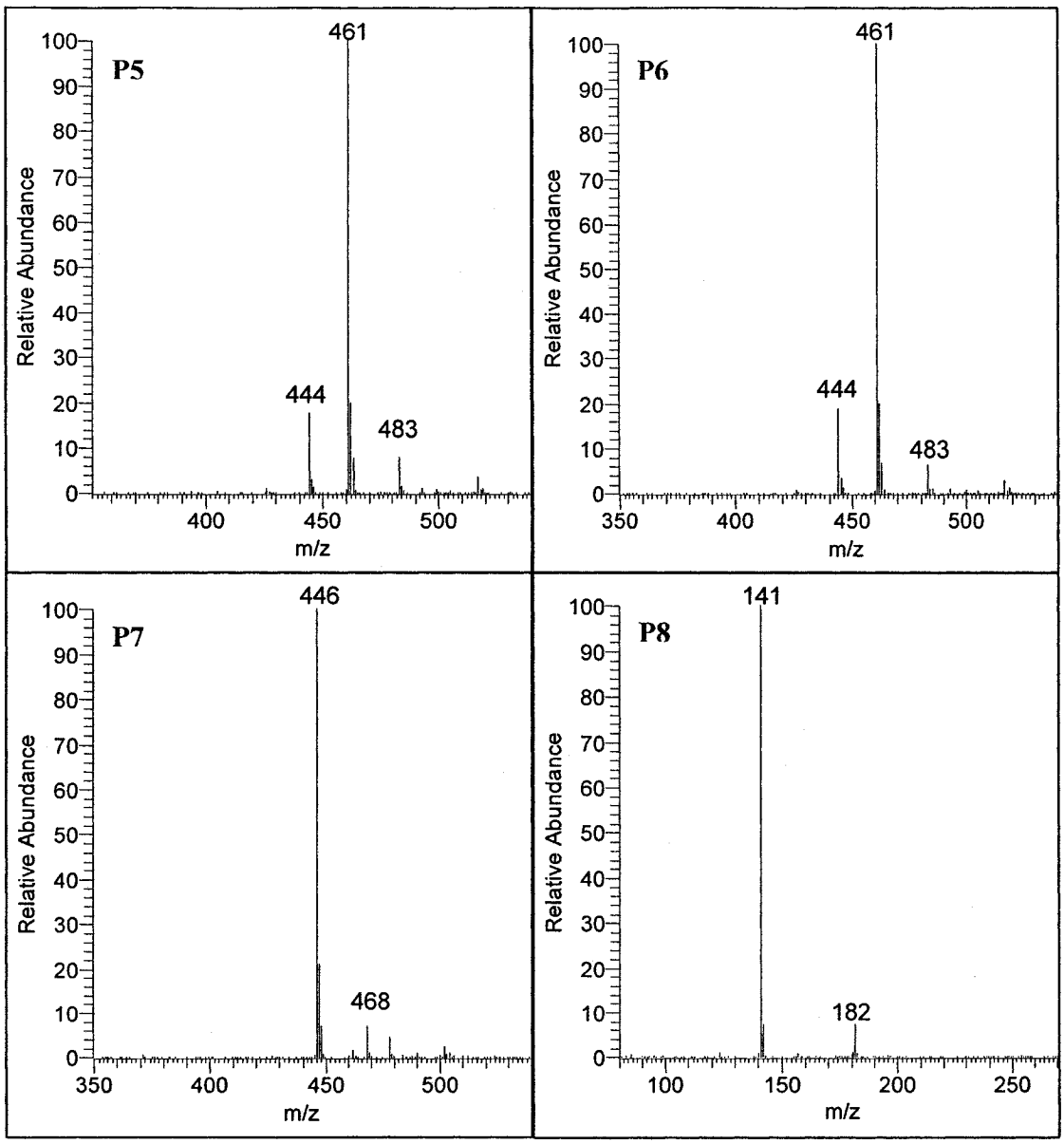


**Figure 5.6. ESI mass spectra of the additional GSNO thiolysis products formed in the presence of dimedone.** The experimental details are given in Figure 5.4 and the HPLC/ESI-MS method is described in Section 5.3.3.

**Table 5.1**- Changes in GSH and GSSG concentrations when ~ 75% GSNO was consumed

| Reactants[a] | Reaction time (h) | Δ[GSH][b] | Δ[GSNO][b] | Δ[GSSG] [b] | Δ[Dimedone] [b] |
|---|---|---|---|---|---|
| | | (mM) | (mM) | (mM) | (mM) |
| 1 mM GSNO + 1 mM GSH | 8 | - 0.68 | - 0.80 | 0.74 | - |
| 1 mM GSNO + 5 mM GSH | 4 | - 0.90 | - 0.74 | 0.84 | - |
| 1 mM GSNO + 5 mM GSH + 5 mM dimedone | 4 | - 1.3 | - 0.74 | 0.95 | - 0.30 |
| 1 mM GSNO + 10 mM GSH | 17 | - 1.4 | - 0.75 | 1.1 | - |

[a] The reactants dissolved in 50 mM sodium phosphate buffer (pH 7.4) (containing 0.1 mM DTPA) were stored in capped amber glass HPLC vials at RT and protected from light. The products were analyzed by HPLC as described in Section 5.3.3.

[b] Δ[GSH], Δ[GSNO], Δ[GSSG], and Δ[Dimedone] were calculated by comparing the final chromatographic peak areas at 210 nm to those from standard solutions.

Table 5.1 summarizes the changes in the concentrations of GSH and GSSG when ~75% of the GSNO was consumed. At this point in the reaction, the amount of GSSG formed is less than the amount of GSNO consumed, indicating that disulfide generation is the predominant reaction. Also, more GSH is consumed in the presence of dimedone than in its absence, suggesting that GSH-derived intermediates are trapped by dimedone since not all the additional GSH consumed appears as GSSG (Table 5.1). When these intermediates are removed by dimedone, GSNO decomposition *via* reaction with GSH is predominant.

Headspace GC/ESI-MS analysis revealed that 8.5 μM $N_2O$ was formed in the reaction of 1 mM GSNO with 10 mM GSH. The $N_2O$ yield was 1.7% based on the initial

GSNO concentration, but it has been observed in our group (*103*) that high [GSH] reduces HNO giving $NH_2OH$, and GSSG (eq. 5.2) (*30, 105*). The formation of $NH_2OH$ was not measured in this study but was reported by Wong *et al.* (*30*).

$$2\ GSH + HNO \rightarrow GSSG + NH_2OH \qquad (5.2)$$

## 5.5 Discussion

The decomposition of GSNO in the presence of added GSH is a complicated process as suggested by the two mechanisms proposed to date (Schemes 1.1 and 1.2) (*27, 30*). Also, the GSNO/GSH reactions have been found to be general for other RSNO/RSH couples (*28*).

One of the criticisms of previous studies of GSNO thiolysis is that the products were analyzed only after long incubation periods of 24–40 h (*31*). Our results show that the GSX end products begin to accumulate from the start of the reaction, and that their concentrations are constant after GSNO is depleted (Figure 5.3). Therefore, the GSX products observed in previous studies are not by-products of long incubation times, but result directly from GSNO thiolysis. The major GSX end-product is the disulfide, GSSG, and it accounts for over 90% of the GSH plus GSNO consumed (Table 5.1).

The thiolysis mechanisms proposed by both Wong *et al.* (*30*) (Scheme 1.2) and *Singh et al.* (Scheme 1.1) (*27*) include the initial formation of a *N*-hydroxysulfenamide intermediate, GSN(OH)SG, from nucleophilic attack by GSH, at the nitroso nitrogen. Wong *et al.* also proposed that nucleophilic attack occurs at the sulfur atom of GSNO,

generating GSSG and nitroxyl (HNO). They based this proposal on the detection of $GS(O)NH_2$ in solution (Reaction 5.3) and of $N_2O$ in the reaction headspace. However, it has been argued that $N_2O$ is not necessarily a marker for HNO since the reaction of NO with sulfhydryl groups also produces $N_2O$ (Reaction 5.4) (*106*).

$$RSH + HNO \rightarrow RS(O)NH_2 \qquad (5.3)$$

$$RSH + 2NO \rightarrow RSOH + N_2O \qquad (5.4)$$

$GS(O)NH_2$ formation in the reaction of HNO (from Angeli's salt) with GSH at pH 7.4 has been confirmed by mass spectrometric studies performed in our group (*105*) and by others (*102*). In the present study, $GS(O)NH_2$ was identified by HPLC/ESI-MS as a minor product of GSNO thiolysis by GSH (Figure 5.2) and the generation of $N_2O$ in the reaction headspace was confirmed by GC/ESI-MS. Together, these results provide further evidence to support the generation of HNO during GSNO thiolysis *via* attack at the nitroso sulfur (*30*). However, Scheme 1.1 (*30*) considers $GS(O)NH_2$ as an intermediate that reacted further over 24h with $H_2O$ and GSH to produce GS(O)SG, GS(O)OH and $NH_3$. Our results indicate that $GS(O)NH_2$ is an end product since its concentration does not decrease in the presence of excess GSH (data not shown). This is consistent with the observation in our group (*103*) that $GS(O)NH_2$ is stable over 24 h. A modification to Wong's mechanism is proposed in Scheme 5.1 to reflect the stability of $GS(O)NH_2$ in our reactions.

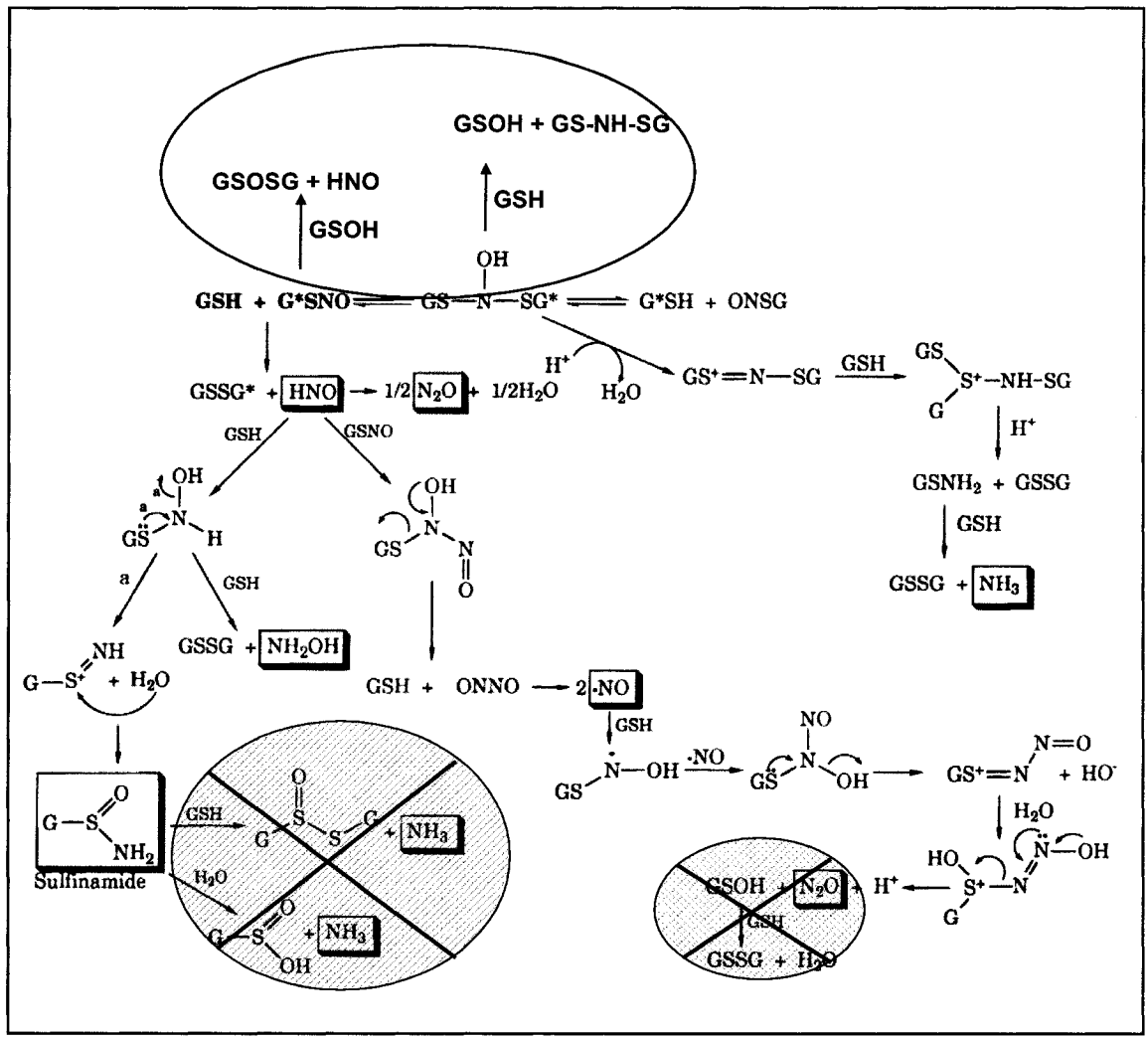


**Scheme 5.1. Modifications to reactions of GSNO at high GSH concentrations proposed by Wong *et al.* based on observations from the present study.**

In addition to $GS(O)NH_2$, less stable products such as GSN(OH)H and GSOH were proposed by Wong *et al.* (Scheme 1.1) to result from the initial attack of GSH on the nitroso sulfur. These likely have been trapped here as dimedone adducts (Figure 5.6), which futher supports nucleophilic attack at the nitroso sulfur as predicted in computational studies from our group (*19*). The fact that trapping GSN(OH)H and GSOH intermediates slows down the reaction indicates that these compounds also react with

GSNO and accelerate its decomposition in an autocatalytic mechanism. GSOH has been proposed to react with GSNO to produce GS(O)SG and HNO (Reaction 3.6) (*42*).

$$GSOH + GSNO \rightleftharpoons GS(O)SG + HNO \qquad (3.6)$$

In the mechanism proposed by both Sing *et al.* (*27*) and Wong *et al.* (*30*), GSOH is an intermediate product in GSNO decomposition that reacts with GSH to produce GSSG (Scheme 1.2, 5.1). In this mechanism, trapping GSOH would not decelerate GSNO decomposition as observed here (Figures 5.4, 5.5). Thus, an additional decomposition pathway likely exists in which GSNO is consumed by direct reaction with GSOH (eq. 3.6). Autocatalysis was not addressed in the GSNO thiolysis mechanisms (*27, 30*) proposed previously.

## 5.6 Conclusions

Our findings support previous proposals that the decomposition of GSNO in the presence of high GSH concentrations is a complex process involving nucleophilic attack at both the nitroso sulfur and nitrogen atoms. The thiolysis process generates HNO and other reactive intermediates resulting in an autocatalytic GSNO decomposition mechanism that accelerates thiolysis. However, once GSNO is consumed in 4–8 h there is no further reaction since the GSX products observed here after 8 h and those reported after 24–48 h are the same.

Our findings have implications for GSNO decomposition *in vivo* since high GSH concentrations are formed in cells. GSNO present intracellularly would be slowly

converted to GSSG by GSH-induced thiolysis, but this would not compete with copper-catalyzed decomposition, which is much faster. Only about 10% of the nitroso GSNO nitrogen would generate HNO, thus uncatalyzed GSNO thiolysis is unlikely a major biosynthetic pathway for HNO production.

In summary, the most significant finding from this work is that GSNO undergoes slow thiolysis to stable products in the presence of high concentrations of GSH at physiological pH *via* an autocatalytic mechanism. For example, Figure 5.5 reveals that the half-life of GSNO is ~ 2 h in the presence of 10 mM GSH, which is the level found in the human red blood cell. Thus, within the arterial-venous-transit time of a red blood cell, GSNO thiolysis would be negligible.

## 5.7 Acknowledgements

This work was supported by a grant from the Canadian Institutes for Health Research, and by grants from Merck Frosst Canada Inc.

# Chapter 6 - Factors affecting the fragmentation of glutathione, *S*-nitrosoglutathione and oxidized glutathione in a Z-spray ESI source

## 6.1 Abstract

The effects of the operating parameters of a Z-spray ESI source on the fragmentation of reduced glutathione (GSH), *S*-nitrosoglutathione (GSNO), and oxidized glutathione (GSSG) were investigated at pH 1.2 and pH 2.5. The major contributor to in-source fragmentation was the cone voltage, while increasing the capillary voltage and the source block temperature had little effect. The level of cone-voltage-induced fragmentation of the three compounds was pH-dependent, and occurred *via* loss of $H_2O$ and cleavage of the peptide bonds into *b* and *y* ions. Loss of $NH_3$ was observed only for GSH at pH 2.5. Homolytic cleavage of the S-NO bond preceded fragmentation of the glutathionyl moiety (GS), forming a $GS^{\bullet+}$ radical cation that yields fragment ions unique to GSNO. Strategies for the simultaneous analysis of GSX, as well as those to increase the sensitivity, selectivity, and specificity for the mass spectrometric quantitation of GSNO are discussed.

## 6.2 Introduction

Nitric oxide (NO) plays an important role in the cardiovascular system by regulating platelet aggregation and smooth muscle relaxation (*2*), and it also contributes to the regulation of the respiratory, digestive, and genitourinary systems (*2, 4*). It has been proposed that NO is transported from its point of synthesis to distant targets as *S*-nitrosothiols (RSNOs). Additionally, thiol *S*-nitrosation is believed to play a role in NO

signalling (*7, 107*). *S*-nitrosoglutathione (GSNO), *S*-nitrosocysteine (CysNO), *S*-nitroso-hemoglobin, and *S*-nitrosoalbumin have been detected *in vivo* (*8-11*), and NO-induced *S*-nitrosation of kinases, redox regulatory proteins, and extracellular matrix proteins has been reported (*108*).

Electrospray ionization mass spectrometry (ESI-MS) is used extensively for the analysis of biomolecule modification because ESI is a soft ionization method. HPLC/tandem mass spectrometry (HPLC/MS/MS) using ESI is the preferred technique for the measurement of GSH conjugates of chemically-reactive intermediates that result from biotransformation of xenobiotic compounds. Much work has been devoted to characterizing by MS/MS the fragmentation of the tripeptide GSH (γGlu-Cys-Gly) and its conjugates following collision-induced dissociation (CID) (*33, 109-115*). The product-ion spectra demonstrated that under MS/MS conditions GSH fragments *via* peptide bond cleavage to form *b* (*m/z* 130 and 233), *y* (*m/z* 76 and 179), and *z* ions (*m/z* 164) (Scheme 6.1). The CID-induced loss of species such as pyroglutamic acid (129 Da) facilitates the detection of GSH conjugates by HPLC/MS/MS in neutral-loss scanning mode.

GSNO, the *S*-nitrosated form of GSH, is a commonly used RSNO in the biomedical field (*34*) because of its high potency as a vasodilator (*35*), a muscle relaxant, and an inhibitor of platelet aggregation (*36, 37*). GSNO is also frequently used as a model compound to study the mechanistic details of *S*-nitrosation (*76, 99, 100*) and *S*-glutathiolation of cysteine residues (*32, 42*). ESI-MS analysis of GSNO in mixtures of glutathionyl species (GSX, X=H, NO, SG) is complicated by the lability of the *S*-NO bond, which is subject to homolytic cleavage in the ESI source (eq. 6.1). The fragments generated during the ionization process can undergo competing oxidation (eq. 6.2),

protonation (eq. 6.3), and dimerization reactions (eq. 6.4) in the gas phase to form ions that are isobaric with those of other GSX:

$$GSNO \rightarrow GS^{\bullet} + NO^{\bullet} \qquad (6.1)$$

$$GS^{\bullet} \rightarrow GS^{+} + 1\,e^{-} \qquad (6.2)$$

$$GS^{\bullet} + H^{+} \rightarrow [GS^{\bullet} + H]^{+} \qquad (6.3)$$

$$2\,GS^{\bullet} \rightarrow GSSG \qquad (6.4)$$

$$GSSG + H^{+} \rightarrow [GSSG + H]^{+} \qquad (6.5)$$

For example, the protonated $[GSSG + H]^{+}$ ion in equation 6.5 is isobaric with the $[M + H]^{+}$ ion of GSSG present in the sample solution prior to ionization in the ESI source. The goal of this work is to establish how the choice of instrumental parameters alters the ions observed during the mass spectrometric analysis of mixtures of GSH, GSNO, and GSSG. Conditions that minimize fragmentation of GSNO or that produce unique fragment ions are desirable in mechanistic studies of *S*-nitrosation and denitrosation reactions involving GSH since it is critical in studies of RSNO chemistry to distinguish between products formed in solution and in the mass spectrometer. Thus, we report here on a systematic investigation of the breakdown products of GSNO, GSH, and GSSG in the Z-spray ESI source of a Q-Tof 2 mass spectrometer (Waters) in positive-ion mode under different instrumental settings. Three parameters of the Z-spray source were varied: capillary voltage, source block temperature, and cone voltage. These parameters influence in-source fragmentation by varying the internal and kinetic energy of the ions (*116-118*). The source settings were varied within the ranges recommended by the manufacturer (capillary voltage, 2.5–4.5 kV; sampling cone, 15–150 V; source block

temperature, 80–150°C) (*119*). The effects of varying hydrogen and sodium ion concentrations on the observed dissociation patterns were also investigated to establish their influence on GSX stability in the Z-spray source.

## 6.3 Experimental

### 6.3.1 Materials

GSH, GSSG, and human [Glu$^1$]-fibrinopeptide B were purchased from Sigma; GSNO, purchased from Cayman Chemical (Ann Arbor, MI); $HCO_2H$, from Anachemia Chemicals (Montreal, Canada); NaCl, from Bioshop Canada (Ontario, Canada); HCl and acetonitrile (MeCN), from Fisher Scientific (Ontario, Canada). Argon was purchased from Praxair (Montreal, Canada).

### 6.3.2 Preparation of GSNO, GSH, and GSSG stock solutions

To investigate the effects of hydrogen and sodium ion concentrations on GSX fragmentation, 5 mM stock solutions of GSNO, GSH, and GSSG were prepared in 125 mM HCl, in 5 mM aqueous NaCl, and in water. The stock solutions were stored on ice in the dark for the duration of the experiments. Aliquots were diluted 1:1 with MeCN/1% $HCO_2H$ prior to injection into the mass spectrometer, so that ionization was carried out at 2.5 mM GSX in 50% MeCN/water/0.5% $HCO_2H$. The pH values of the diluted solutions, measured using an Accumet 50 pH meter with a Ag/AgCl combination electrode (Fisher Scientific, Ontario, Canada), were 1.2 for solutions containing HCl and 2.5 for those containing NaCl.

### 6.3.3 ESI mass spectral analysis

Spectra were collected on a Waters Micromass Q-Tof 2 mass spectrometer (Waters Corp., Milford, MA) equipped with a nano Z-spray ESI source operating in positive-ion mode, and mass calibrated with human [Glu$^1$]-fibrinopeptide B. The solutions were injected directly from a 50-μL Hamilton syringe at a flow rate of 1 μL/min using a Harvard syringe pump (Harvard Apparatus, Holliston, MA). The energy in the collision cell was set to 5 eV (which is less than the 10 eV setting recommended by the manufacturer) to minimize ion fragmentation (*119*). Ar was used as the collision gas.

**Table 6.1.** Combinations of Z-spray source cone and capillary voltages used at 5 source block temperatures[a]

| Source block temperature (°C) | Cone voltage (V) | Capillary voltage (V) | | | |
|---|---|---|---|---|---|
| 70 - 150°C | 20 | 2500 | 3000 | 3500 | 4000 |
| | 60 | 2500 | 3000 | 3500 | 4000 |
| | 100 | 2500 | 3000 | 3500 | 4000 |
| | 140 | 2500 | 3000 | 3500 | 4000 |

[a] The same voltage combinations were applied at 70°C, 90°C, 110°C, 130°C, and 150°C. Mass spectra were collected for 0.25 min using 2.5-s scans at each temperature and voltage combination to give a total of 80 (5 x 4 x 4) spectra. The collision energy in the collision cell was 5 eV.

The instrumental parameters are summarized in Table 6.1. At a given source temperature and cone voltage (e.g., 70°C, 20 V), the capillary voltage was increased from 2.5 to 4.0 kV in steps of 0.5 kV. Mass spectra were collected for 0.25 min using 2.5-s

scans. The cone voltage was then increased to 60 V and spectra were recorded again at the same capillary settings. This procedure was repeated for cone voltages up to 140 V. The temperature was increased to 90°C and the stepwise variation of cone and capillary voltages given in Table 6.1 was repeated.

## 6.4 Results

### 6.4.1 ESI mass spectra of GSH

The ESI mass spectrum of GSH obtained at pH 1.2 under the initial experimental parameters (capillary 2.5 kV, source block 70 °C, cone 20 V, Table 6.1) is dominated by the protonated molecular ion $[M + H]^+$ at *m/z* 308 and a weak protonated dimer $[2M + H]^+$ peak appears at *m/z* 615 (Figure 6.1A). No fragmentation of the $[M + H]^+$ ion was observed under increased capillary voltage or source block temperature (data not shown). Increasing the cone voltage resulted in fragmentation of the peptide bonds giving $b_2$ ($[M + H - Gly]^+$, *m/z* 233), $y_2$ ($[M + H - \gamma Glu]^+$, *m/z* 179), and $z_2$ ions (*m/z* 162) (See Scheme 6.1 and Figure 6.1B,C). Also, loss of water ($[M + H - H_2O]^+$, *m/z* = 290) is obvious at a cone voltage of 140 V (Figure 6.1C).

Figure 6.2 compares the cone-voltage-induced fragmentation of GSH at pH 2.5 in the absence (Figure 6.2A,C) and presence of 2.5 mM NaCl (Figure 6.2D-F). The fragmentation induced in both cases results in the appearance of the $b_2$, $y_2$, $z_2$, and $[M + H - H_2O]^+$ ions observed at pH 1.2 (Figure 6.1C) but at higher abundance relative to $[M + H]^+$, plus additional fragments at *m/z* 215 ($b_2 - H_2O$), *m/z* 245 $[M + H - H_2O - CO - NH_3]^+$, and *m/z* 291 $[M + H - NH_3]^+$ (Figure 6.2B,C). Sodiated ions are observed at *m/z* 330 $[M + Na]^+$ and *m/z* 637 $[2M + Na]^+$ in the presence of added $Na^+$ (Figure 6.2D). At

higher cone voltages no sodiated fragment ions are observed (Figure 6.2E,F) since loss of $Na^+$ giving rise to neutral organic molecules is the lowest energy channel for fragmentation of sodiated molecular ions. Thus, the relative abundance of sodiated ions (e.g., *m/z* 352 $[M - H + 2Na]^+$, *m/z* 374 $[M - 2H + 3Na]^+$) increases at the expense of the protonated ions although $[M + H]^+$ at *m/z* 308 remains the base peak.

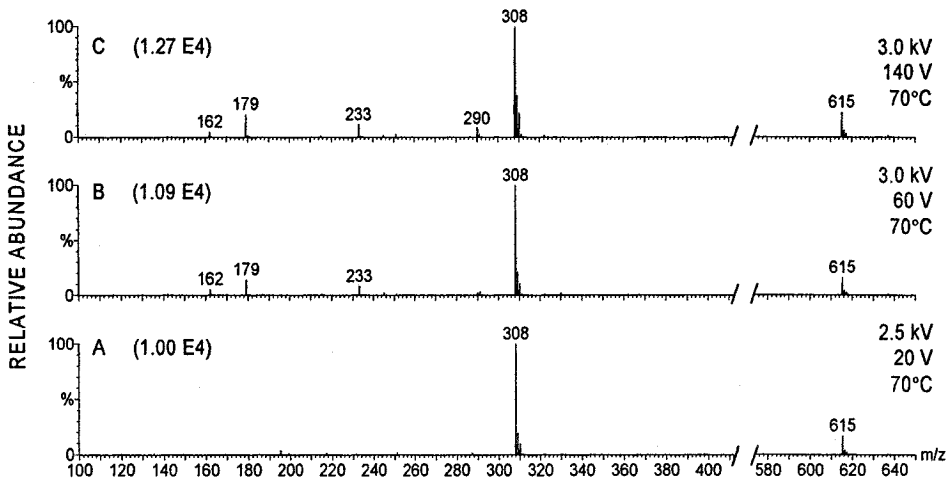


**Figure 6.1. ESI mass spectra of 2.5 mM GSH at pH 1.2 *vs* cone voltage at a source block temperature of 70°C, capillary voltage of 3.0 kV, and collision energy of 5 eV. (A)** 20 V, **(B)** 60 V, **(C)** 140 V. A solution of 5 mM GSH in 125 mM HCl was diluted 2-fold with acetonitrile/1% $HCO_2H$, and directly infused at 1 μL/min into the Z-spray source. The TICs in parentheses have been normalized to the TIC of spectrum (A) at 70 °C, 20 V cone V and 2.5 kV capillary V.

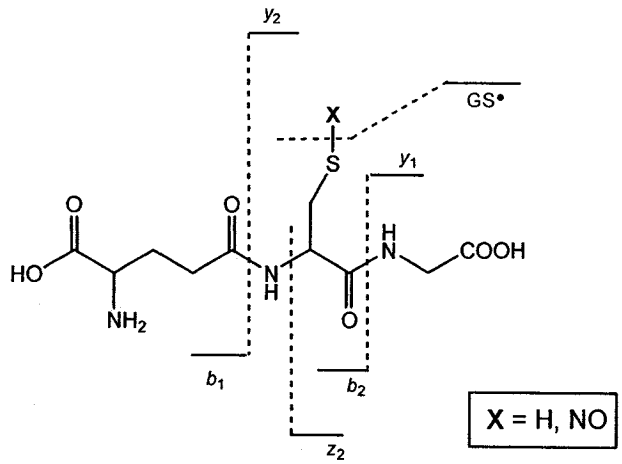


**Scheme 6.1. Fragmentation scheme for GSH and GSNO.** The sequence ions, *b*, *y* and *z*, result from in-source fragmentation. Note that following cleavage of *S*-NO, the sequence ions are 1-u lighter than those for GSH.

### 6.4.2 GSNO

Figure 6.3 reveals that GSNO undergoes homolysis in the Z-spray source at pH 1.2 under the mildest conditions necessary for efficient ionization (capillary 2.5 kV, source block 70°C, cone 20 V, collision energy 5 eV). The GSNO $[M + H]^+$ ion appears at *m/z* 337 and is accompanied by a peak at *m/z* 307 (Figure 6.3A), which is assigned to the protonated odd-electron ion $[GS^\bullet + H]^+$ that results from GSNO homolysis (eqs. 6.1, 6.3) in the source. Eliminating the collision gas in the collision cell, or decreasing the collision energy to 2 eV, attenuated the TIC but not fragmentation, confirming that GSNO dissociation occurs in the source. The protonated GSNO dimer $[2M + H]^+$ appears at *m/z* 673 and the disulfide ions $[GSSG + H]^+$ at *m/z* 613, which must arise from $GS^\bullet$ dimerization since no *m/z* 613 peak was detected in the spectrum of GSH (Figures 6.1,6.2). Also, the low abundance of the *m/z* 613 *vs m/z* 307 peak suggests that $GS^\bullet$ is

protonated (Reaction 6.3) faster than it dimerizes (Reaction 6.4) in the source. Increasing the capillary voltage from 2.5 kV to 4.0 kV did not alter the relative abundance of the $[GS^{\bullet} + H]^+$ and $[M + H]^+$ ions (Figures 6.3 A–C), but increasing the source block temperature from 70°C to 150°C (Figure 6.3A,D,E) increased the abundance of $[GS^{\bullet} + H]^+$ at the expense of $[M + H]^+$ consistent with the instability of GSNO at high temperatures.

Low-mass ions appeared in the spectrum at a cone voltage of 60 V (Figure 6.3F). The ions at *m/z* 130 and 232 are assigned to $b_1$ and $b_2$ ions arising from cleavage of $[GS^{\bullet} + H]^+$ at its peptide bonds, similar to that observed for GSH (Scheme 6.1). However, cone-voltage CID of $[GS^{\bullet} + H]^+$ resulted in the appearance of additional fragments at *m/z* 158, 205, and 243 that are attributed to radical-initiated fragmentation (see Discussion) since they do not correspond to sequence ions formed on peptide-bond cleavage.

The effects of cone voltage on the fragmentation of GSNO at pH 2.5 are demonstrated in Figure 6.4. As in the case of GSH, addition of NaCl and low pH suppresses fragmentation (Figure 6.3A,B,C *vs* Figure 6.4D,E,F or Figure 6.4A,B,C). In the presence of added $Na^+$, $[GS^{\bullet} + Na]^+$ and $[M + Na]^+$ ions appear at *m/z* 329 and 359, respectively, and grow in relative abundance as the cone voltage is increased (Figures 6.4D, E, F). Increased GSNO fragmentation promotes disulfide formation as evidenced by the increased abundance of the $[GSSG + H]^+$ and $[GSSG + Na]^+$ peaks at *m/z* 613 and 635, respectively (Figures 6.3F,G, 6.4B,C, and 6.4F). This is expected since $GS^{\bullet}$ dimerization is a bimolecular reaction (eqs. 6.4, 6.5) that also competes with formation of ions of the noncovalent dimer, which have low abundance at high cone voltage (peak at *m/z* 637,

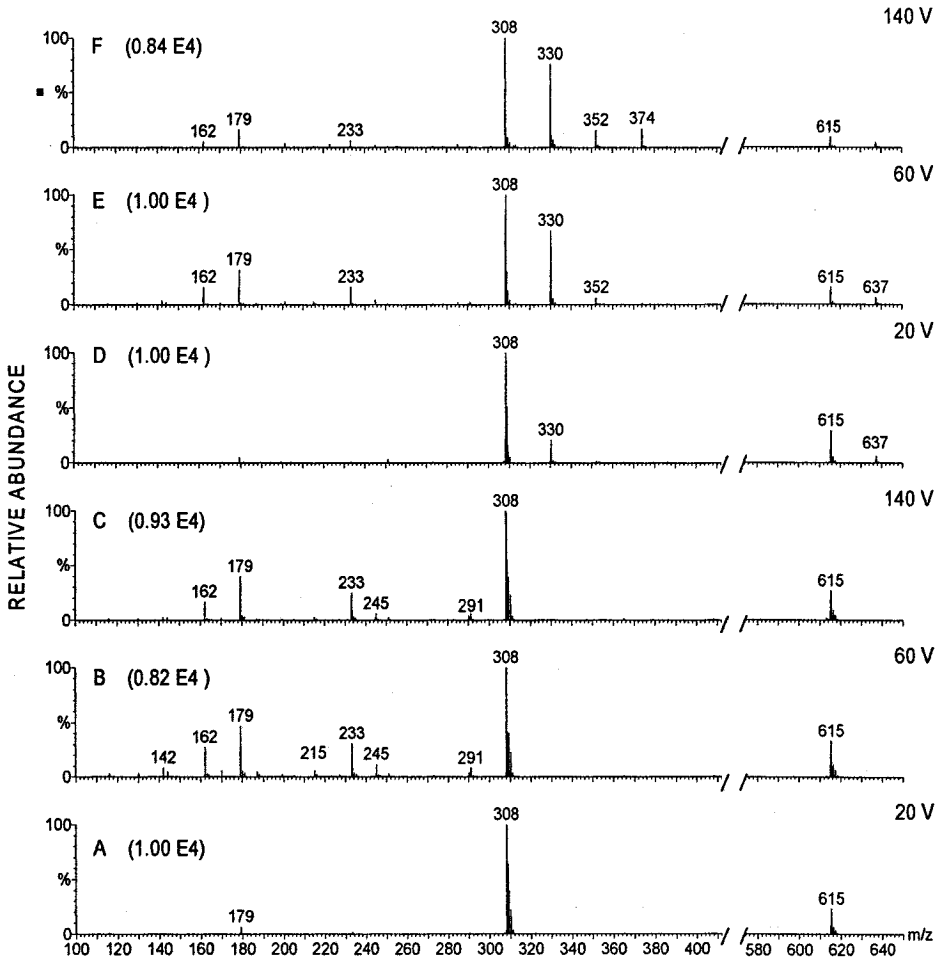


**Figure 6.2. ESI mass spectra of 2.5 mM GSH at pH 2.5 *vs* cone voltage at a source block temperature of 70°C, capillary voltage of 3.0 kV, and collision energy of 5 eV. (A, B, C)**, no $Na^+$. **(D, E, F)**, 2.5 mM $Na^+$. A solution of 5 mM GSH in water (A, B, C), or in 5 mM NaCl (aq) (D, E, F), was diluted 2-fold with acetonitrile/1% $HCO_2H$, and directly infused at 1 μL/min into the Z-spray source. The TICs in parentheses have been normalized to the TIC of spectrum (A) at 70 °C, 20 V cone V and 2.5 kV capillary V.

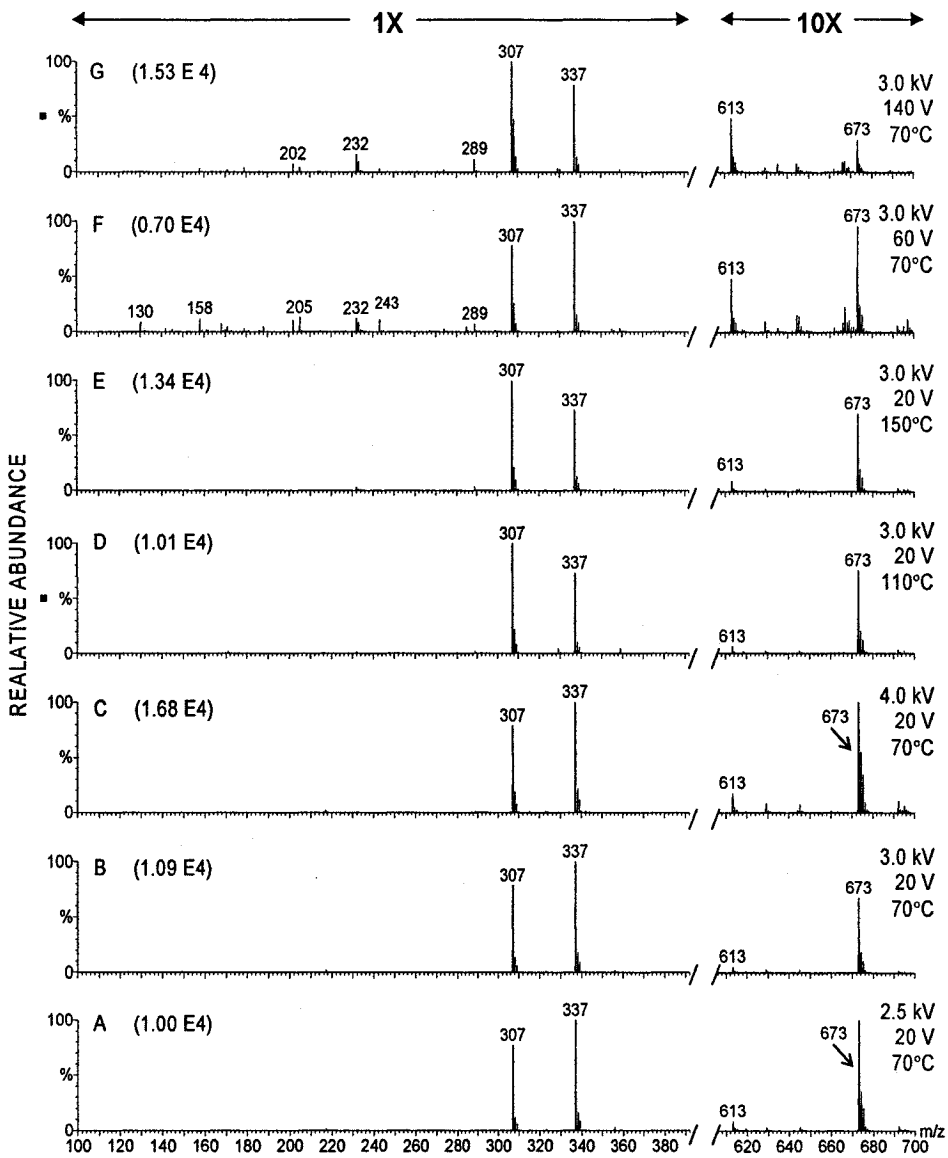


**Figure 6.3. ESI mass spectra of 2.5 mM GSNO at pH 1.2 *vs* capillary voltage (A, B, C), source block temperature (A, D, E), and cone voltage (A, F, G).** The collision energy was 5 eV. A solution of 5 mM GSNO in 125 mM HCl was diluted 2-fold with acetonitrile/1% $HCO_2H$, and directly infused at 1 μL/min into the Z-spray source. The higher mass range has been magnified 10X to show detail. The TICs in parentheses have been normalized to the TIC of spectrum (A) at 70 °C, 20 V cone V and 2.5 kV capillary V.

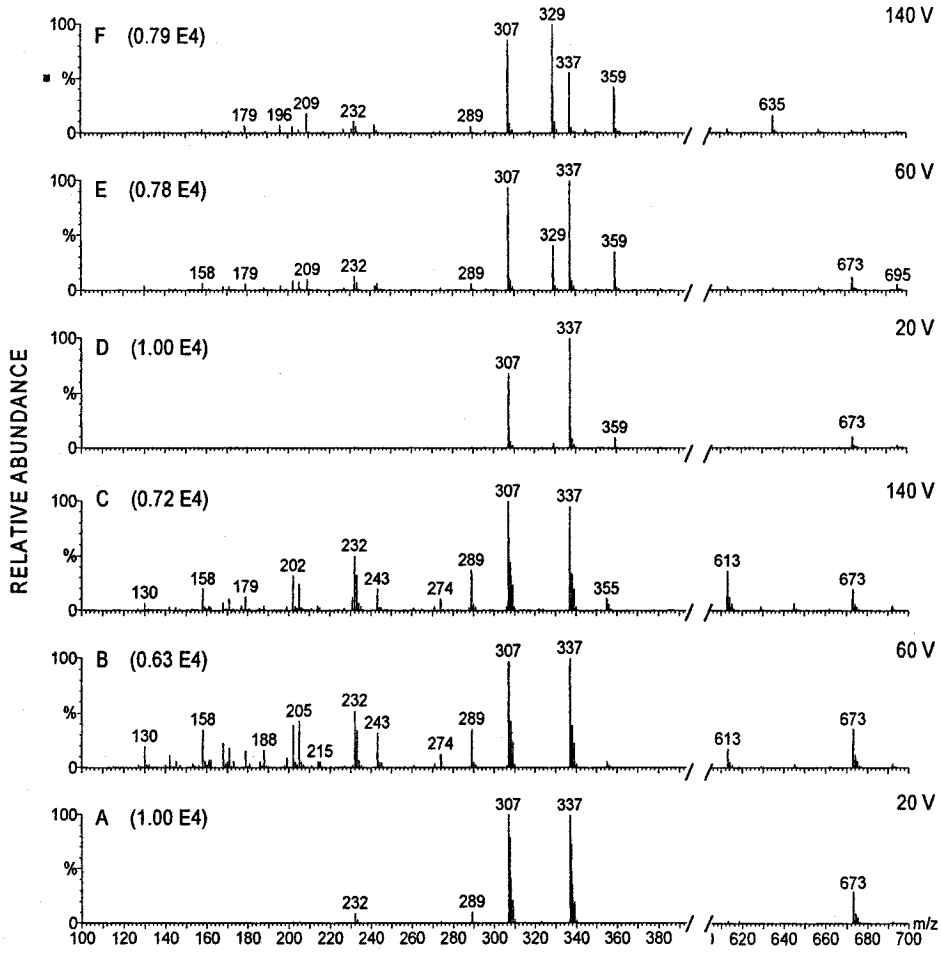


**Figure 6.4. ESI mass spectra of 2.5 mM GSNO at pH 2.5 *vs* cone voltage at a source block temperature of 70°C, capillary voltage of 3.0 kV, and collision energy of 5 eV. (A, B, C)**, no $Na^+$. (D, E, F), 2.5 mM $Na^+$. A solution of 5 mM GSNO in water (A, B, C), or in 5 mM NaCl (aq) (D, E, F), was diluted 2-fold with acetonitrile/1% $HCO_2H$, and directly infused at 1 μL/min into the Z-spray source. The TICs in parentheses have been normalized to the TIC of spectrum (A) at 70 °C, 20 V cone V and 2.5 kV capillary V.

Figure 6.4F). The peak at *m/z* 355 (Figure 6.4C) is probably a fragment of the [GSSG + H]$^+$ ion as discussed in Section 6.4.3. Since the most likely fragmentation channel for [GSSG + Na]$^+$ at *m/z* 635 is loss of Na$^+$ producing a neutral GSSG molecule, fragments of this sodiated ion are not observed.

### 6.4.3 GSSG

The mass spectrum of GSSG at pH 1.2 and low cone voltage (20 V) contains peaks at *m/z* 307 and 613 (Figure 6.5A) that are assigned to [M + 2H]$^{2+}$ and [M + H]$^+$, respectively. The *m/z* 307 peak exhibits isotope peaks with a Δm of 0.5 u (Figure 6.7D), confirming that it arises from the doubly charged [M + 2H]$^{2+}$ ion. Like the other GSX, the spectrum of GSSG is insensitive to changes in capillary voltage and source block temperature (data not shown), but the [M + 2H]$^{2+}$ and [M + H]$^+$ ions undergo fragmentation as a result of increased cone voltage (Figure 6.5A *vs* B,C). The spectra in panels B and C show the appearance of ions at *m/z* 308, *m/z* 231, and *m/z* 177, which are discussed below, as well as $b_5$ ([M + H – Gly]$^+$, *m/z* 538), $y_5$ ([M + H – γGlu]$^+$, *m/z* 484) and ([M + H – $H_2O$]$^+$, *m/z* 595) ions. Additional peaks assigned to fragments of the $b_5$ ([$b_5$ + H – $b_1$]$^+$, *m/z* 409), and $y_5$ ([$y_5$ + H – $b_1$']$^+$, *m/z* 355) sequence ions are also observed (Scheme 6.2).

Like GSH and GSNO, in-source fragmentation of GSSG is pH dependent. A comparison of Figures 6.5B,C and Figures 6.6B,C reveals that the relative abundance of the fragment ions is higher at the higher pH. Expansion of the *m/z* scale shows that a singly-charged ion at *m/z* 308 grows in abundance as the cone voltage is raised from 20 to 140 V at pH 1.2 (Figure 6.7D,F) due to more efficient cleavage of S-S, but not at pH 2.5 (Figure 6.7A,C). Rubino *et al.* (*120*) reported that the CID of disulfides (RSSR) produces sulfenium (RS$^+$) and [RSH + H]$^+$ ions due to heterolytic cleavage of the disulfide bond:

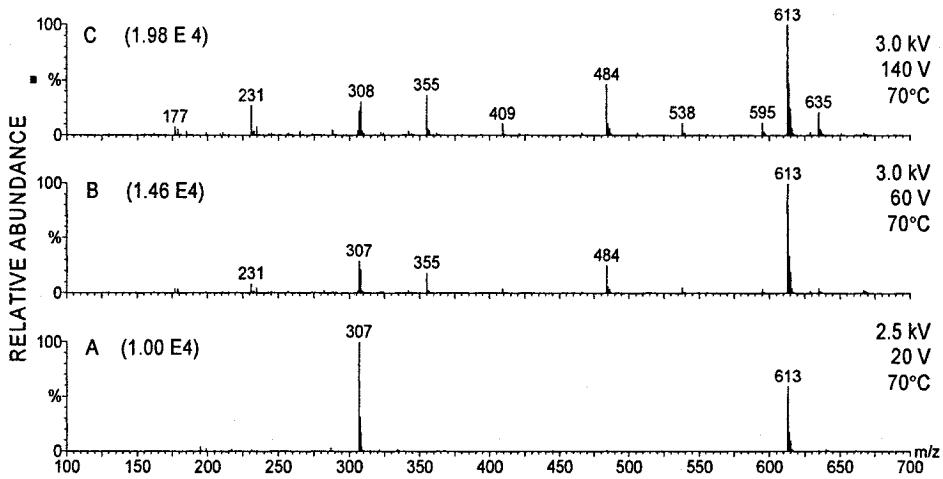


**Figure 6.5. ESI mass spectra of 2.5 mM GSSG at pH 1.2 *vs* cone voltage.** The collision energy was 5 eV. A solution of 5 mM GSSG in 125 mM HCl was diluted 2-fold with acetonitrile/1% $HCO_2H$, and directly infused at 1 μL/min into the Z-spray source. The TICs in parentheses have been normalized to the TIC of spectrum (A) at 70 °C, 20 V cone V and 2.5 kV capillary V.

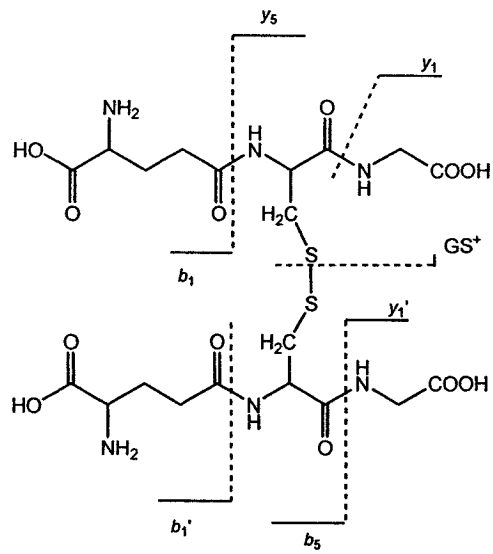


**Scheme 6.2 Fragmentation scheme for GSSG.** The sequence ions, *b*, *y* and *z*, result from in-source fragmentation.

$$RSSR \rightarrow RS^+ + RS^- \qquad (6.6)$$

$$RS^- + 2H^+ \rightarrow [RSH + H]^+ \qquad (6.7)$$

The peak at *m/z* 308 in Figure 6.5C is assigned to the $[GSH + H]^+$ formed on double protonation of $GS^-$ (eq. 6.7), and the peaks at *m/z* 231 and *m/z* 177 correspond to its $b_2$ and $y_2$ ions (Scheme 6.1), respectively. The weak peak at *m/z* 306, which appears at cone voltages of 60 V and higher (Figure 6.7B, C, E, F) is assigned to $GS^+$. The low abundance of the $GS^+$ ion may be a result of subsequent fragmentation by loss of Gly ($[GS^+ - 75]$; *m/z* 231) or Glu ($[GS^+ - 129]$; *m/z* 177) to give $b_2$ and $y_2$ ions, respectively (Figures 6.5C and 6.6B,C; Scheme 6.1). $GS^+$ could also arise from homolytic cleavage of GSSG and oxidation of $GS^\bullet$ in the ESI source (eq. 6.2). However, this is unlikely since $GS^\bullet$ formed on GSNO homolysis (eq. 6.1) is detected as $[GS^\bullet + H]^+$ at *m/z* 307 and not as $GS^+$ at *m/z* 306 (Figures 6.3, 6.4).

The ions observed during the mass spectrometric analysis of the GSX, and the corresponding assignments, are summarized in Table 6.2.

## 6.5 Discussion

The results of this study show that, in the Z-spray source of the Q-Tof 2, increasing the capillary voltage produces a slight increase in the total ion count, but it does not alter the relative abundance of the ions arising from GSX (Figures 6.1, 6.6). Higher source temperatures also do not affect the mass spectra of GSH or GSSG, but do increase the formation of the $[GS^\bullet + H]^+$ ion at *m/z* 307 that originates from the homolytic cleavage of GSNO (eq. 6.1,6.3). This was expected due to the reported thermal

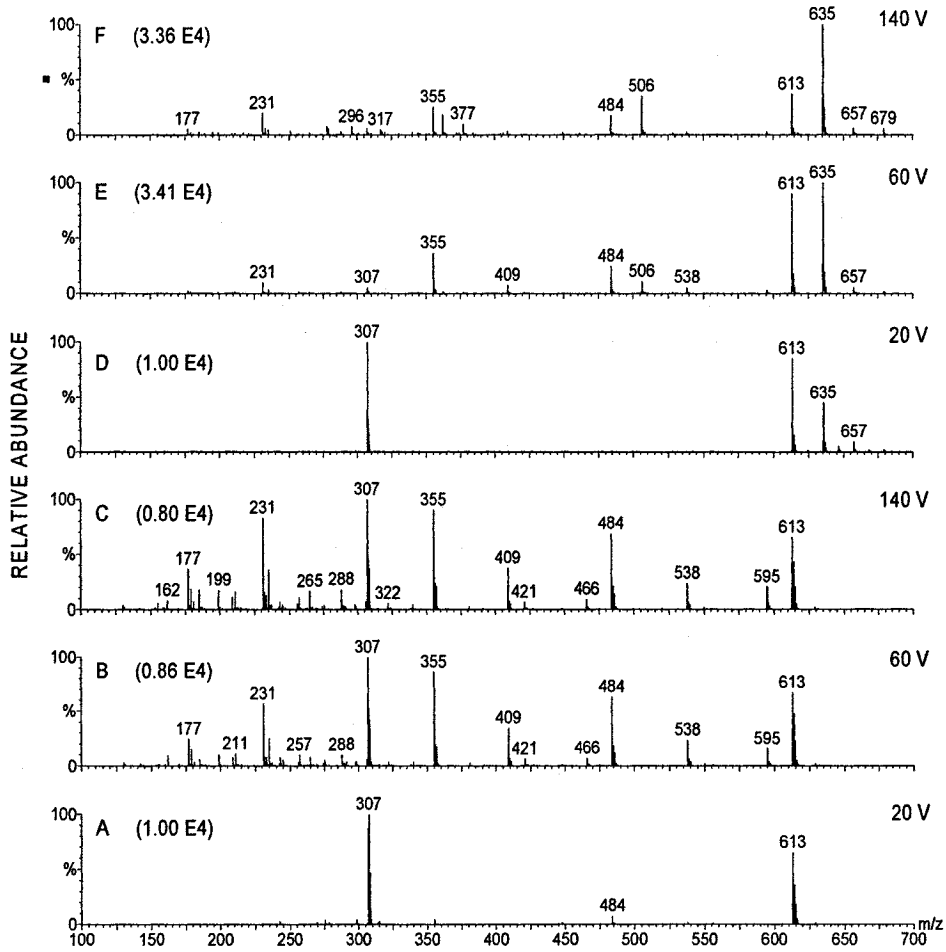


**Figure 6.6. ESI mass spectra of 2.5 mM GSSG at pH 2.5 *vs* cone voltage at a source block temperature of 70°C, capillary voltage of 3.0 kV, and collision energy of 5 eV. (A, B, C)**, no $Na^+$. **(D, E, F)**, 2.5 mM $Na^+$. A solution of 5 mM GSSG in water (A, B, C), or in 5 mM NaCl (aq) (D, E, F), was diluted 2-fold with acetonitrile/1% $HCO_2H$, and directly infused at 1 μL/min into the Z-spray source. The TIC in parentheses have been normalized to the TIC of spectrum (A) at 70 °C, 20 V cone V and 2.5 kV capillary V.

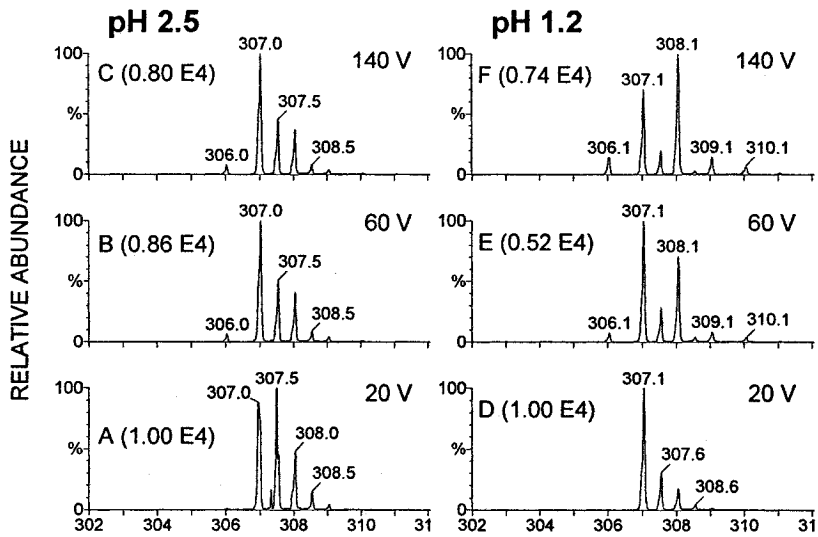


**Figure 6.7. Expanded ESI mass spectra of 2.5 mM GSSG *vs* cone voltage in the region of *m/z* 310 showing the effect of [$H^+$] on fragmentation. (A, B, C)** pH 2.5, no $Na^+$. **(D, E, F)** pH 1.2, no $Na^+$. Source block temperature at 70°C, capillary voltage at 3.0 kV, and collision energy of 5 eV. A solution of 5 mM GSSG in water (A, B, C), or in 125 mM HCl (D, E, F), was diluted 2-fold with acetonitrile/1% $HCO_2H$, and directly infused at 1 μL/min into the Z-spray source. The TIC in parentheses have been normalized to the TIC of spectrum (A) at 70 °C, 20 V cone V and 2.5 kV capillary V.

**Table 6.2.** Assignment of ions observed in the ESI mass spectra of GSX

| GSH | | GSNO | | GSSG | |
|---|---|---|---|---|---|
| m/z | assignment | m/z | assignment | m/z | assignment |
| 130 | $b_1$ | 130 | $b_1$ | 162 | |
| 142 | | 158 | $[GS^{\bullet} + H - H_2C{=}S - C_3H_5NO_3]^+$ | 177 | $[GS^+ + H - b_1]$ |
| 162 | $z_2$ | 162 | $z_2$ | 179 | $y_2$ from 308 |
| 179 | $y_2$ | 168 | | 209 | |
| 215 | $b_2 - H_2O$ | 171 | | 211 | |
| 233 | $b_2$ | 179 | $y_2$ - NO | 231 | $[GS^+ + H - y_1]$ |
| 245 | $[M + H - NH_3 - H_2O - CO]^+$ | 188 | | 233 | $b_2$ from 308 |
| 290 | $[M + H - H_2O]^+$ | 196 | | 235 | |
| 291 | $[M - NH_3 + H]^+$ | 202 | | 257 | |
| 308 | $[M + H]^+$ | 205 | $a_2$ | 265 | |
| 330 | $[M + Na]^+$ | 209 | | 288 | $GS^+ - H_2O$ |
| 352 | $[M- H + 2Na]^+$ | 215 | | 296 | |
| 374 | $[M - 2H + 3Na]^+$ | 232 | $b_2$ - NO | 306 | $GS^+$ |
| 615 | $[2M + H]^+$ | 233 | $b_2$ - NO + 1 | 307 | $[M + 2H]^{2+}$ |
| 637 | $[2M + Na]^+$ | 243 | $[GS^{\bullet} + H - H_2C{=}S - H_2O]^+$ | 308 | $[GSH + H]^+$ |
| | | 274 | $[GS^{\bullet} + H - HS^{\bullet}]^+$ | 322 | |
| | | 289 | $[GS^{\bullet} + H - H_2O]^+$ | 355 | $[y_5 + H - b_1']^+$ |
| | | 307 | $[GS^{\bullet} + H]^+$ | 362 | |
| | | 329 | $[M + H - H_2O]^+$ | 377 | $[y_5 + Na - b_1']^+$ |
| | | 337 | $[M + H]^+$ | 409 | $[b_5 + H - b_1]^+$ or $[y_5 + H - y_1']^+$ |
| | | 355 | $[y_5 + H - b_1']^+$ from 613 | 421 | $y_5 - NH_3 - H_2O - CO$ |
| | | 359 | $[M + Na]^+$ | 466 | $y_5 - H_2O$ |
| | | 613 | $[GSSG + H]^+$ | 484 | $y_5$ |
| | | 635 | $[GSSG + Na]^+$ | 506 | $(M - Glu + Na)^+$ |
| | | 673 | $[2M + H]^+$ | 538 | $b_5$ |
| | | 695 | $[2M + Na]^+$ | 595 | $[M + H - H_2O]^+$ |
| | | | | 613 | $[M + H]^+$ |
| | | | | 635 | $[M + Na]^+$ |
| | | | | 657 | $[M - H + 2Na]^+$ |
| | | | | 679 | $[M - 2H + 3Na]^+$ |

decomposition of GSNO in solution (*15*) and in ESI sources (*121*), and all the GSNO spectra recorded here exhibit a $[GS^{\bullet} + H]^+$ peak at *m/z* 307 (Figures 6.3, 6.4).

Increased cone voltage results in the acceleration of ions between the sample and extraction cones. This region is at a relatively high pressure of 1.6 torr, and ion

fragmentation between the sample and extraction cones is known to occur for instruments using atmospheric pressure ionization sources coupled to quadrupole mass analyzers (*122*). Fragmentation of the GS moiety of GSX at cone voltages ≥ 60 V occurs mainly *via* loss of $H_2O$, and cleavage of the γGlu-Cys and Cys-Gly peptide bonds to form *b* and *y* ions, respectively, that undergo further fragmentation. The *b* and *y* ions from GSH and GSSG (Schemes 6.1 and 6.2) are consistent with those observed by other investigators at pH 2–3 (*33, 109-115*). However, decreasing the solution pH from 2.5 to 1.2 depressed in-source fragmentation (Figure 6.2B *vs* 6.1C; 6.4B *vs* 6.3F; 6.6B *vs* 6.5C), suggesting that more rapid protonation at high $[H^+]$ may decrease the transit time in the source and thus decrease fragmentation in this region of the instrument.

A recent study examined cone-voltage CID pathways of Glu-containing tripeptides in the ESI source of a VG Platform mass spectrometer (Micromass) (*123*). Fragmentation of the $[M + H]^+$ ion of α-linked H-Glu-Gly-Phe-OH, dissolved in 50% MeCN/1% $HCO_2H$,was found to be characterized by loss of $H_2O$, whereas fragmentation of the γ-linked H-Glu(Gly-Gly-OH)-OH ion was characterized by loss of $NH_3$. Our GSH spectra at pH 2.5 (50% MeCN/0.5% $HCO_2H$) show ions at *m/z* 291 ($[M + H - NH_3]^+$) and *m/z* 245 ($[M + H - 63]^+$) (Figure 6.2B, C). The latter ion was also reported for protonated tripeptides with the γ-Glu-linkage, and are thought to arise from sequential loss of $NH_3$, $H_2O$, and CO (Table 6.1) (*123*). However, no ions are observed at *m/z* 245 and *m/z* 291 in the pH 1.2 spectra (Figure 6.1), but there is a peak at *m/z* 290 (Figure 6.1C) corresponding to $[M + H - H_2O]^+$. Thus, at higher pH, loss of $NH_3$ from $[GSH + H]^+$ is more favorable, but loss of $H_2O$ is preferred at lower pH. Also, only fragmentation by loss of $H_2O$ is observed in the spectra of GSNO (*m/z* 289; Figures 6.3,6.4) and GSSG

(*m/z* 595; Figures 6.5,6.6) at both pHs. Clearly, these results reveal that the loss of $H_2O$ *vs* $NH_3$ from Glu-containing tripeptides and their derivatives may not be diagnostic of peptides containing *α vs γ* linkage.

Studies on the conformation of GSH in solution around neutral pH have revealed interactions between the thiol and the *C*-terminal carboxylate ($pK_a = 2.1$), and the thiolate and *α*-ammonium groups. The *N*-carboxylate of Glu does not interact with the thiol (*40*). The preferred loss of $H_2O$ *vs* $NH_3$ from $[GSH + H]^+$ at pH 1.2 may be due to stabilization of $-NH_3^+$ by interaction with the thiol, which is weakened at pH 2.5 by competition with the *C*-terminal carboxylate for the thiol, thus resulting in loss of $NH_3$ at the higher pH (Figure 6.1C *vs* 6.2C). There are no reported studies on the conformation of GSNO and GSSG in solution. However, the absence of $[M - NH_3]$ fragment ions in their ESI mass spectra (Table 6.2) suggests that interactions between the α-ammonium and carboxyls groups promote release of $H_2O$ rather than $NH_3$ (Table 6.2).

The presence of equimolar $Na^+$ in the GSX solutions resulted in the appearance of monosodiated ions $[M + Na]^+$ (Figures 6.2D, 6.4D, 6.6D *vs* Figures 6.2A, 6.4A, 6.6A) at a cone voltage of 20 V, and of di- and tri-sodiated ions $[M - H + 2Na]^+$ and $[M - 2H + 3Na]^+$ at a cone voltage of 140 V. The $Na^+$-binding sites could be the carboxyl and the amino groups of the γGlu residue, and the carboxyl group of the Gly residue. At higher cone voltages, more abundant sodiated GSX peaks are observed (Figures 6.2F, 6.4F and 6.6F *vs* Figures 6.2C, 6.4C and 6.6C), suggesting that extraction of the sodiated ions is more efficient under these conditions.

Tsikas *et al.* (*124*) demonstrated the application of ESI-MS in the analysis of low-mass RSNOs including GSNO and CysNO, and observed $[M + H]^+$, $[2M + H]^+$ and [M +

H – NO]$^+$ ions using an API III+ (PE-Sciex) mass spectrometer. We observed (*121*) that increasing the temperature of the heated capillary transfer tube in an SSQ 7000 mass spectrometer (ThermoFinnigan) decreased the stability of the S-NO bond in RSNOs. Other researchers have reported that *S*-nitrosated proteins readily lose NO on increasing the capillary temperature of a TSQ 700 (Finnigan-MAT) mass spectrometer, or by increasing the nozzle-skimmer potential in the ESI source of a Mariner TOF (Applied Biosystems) mass spectrometer (*125, 126*). MALDI-MS analysis of an *S*-nitrosated peptide on a Voyager DE-RP MALDI-TOF mass spectrometer (Applied Biosystems) also resulted in formation of [M$^+$ H – NO]$^+$ ions independently of the type of laser or matrix used, suggesting that the denitrosation occurred in the desorption plume rather than in the laser beam (*125*).

Cone-voltage CID of [GS$^\bullet$ + H]$^+$ results in the appearance of additional fragments that are assigned to radical-initiated fragmentation. Wee *et al.* (*127*) studied the CID of radical cations of the tripeptides GXR (X = one of the 20 naturally occurring amino acids). They reported that when a thiyl radical is generated in GCR after abstraction of a side-chain H$^\bullet$, the peptide fragments by loss of HS$^\bullet$ (–33 Da) from the Cys side chain, and by loss of $H_2C$=S, producing an α-centered radical cation. The peaks at *m/z* 274 and 243 in Figure 6.4B,C can be assigned to loss of HS$^\bullet$ and ($H_2C$=S + $H_2O$) from GS$^\bullet$, respectively. Hao and Gross (*128*) also observed loss of HS$^\bullet$ and $H_2C$=S from thiyl radicals in peptides from denitrosated *S*-nitrosohemoglobin, with additional ions originating from fragmentation of the bonds on either side of the α-carbon of radical-containing residue side chains. They proposed a fragmentation pathway involving initial H-abstraction by the Cys β-carbon from a side chain and subsequent fragmentation on

either side of the α-carbon to form *a/x* and *c/z* ions. Loss of $H_2C{=}S$ (46 Da) followed by cleavage of the Cys $^{\alpha}$C-N bond (103 Da) with loss of $C_3H_5NO_3$ could give rise to the $(M + H - 149)^+$ ion at *m/z* 158. The ion at *m/z* 205 is assigned to an $a_2$ ion, formed on dissociation of the Cys $^{\alpha}$C-C, while the ion at *m/z* 162 is assigned to dissociation of the Cys $^{\alpha}$C-N bond to form a $z_2$ ion.

The $[GS^{\bullet} + H]^+$ ion appears relatively stable in the mass spectra of GSNO, as shown by the relative intensity of the *m/z* 307 peak as the cone voltage is increased from 20 V to 140 V (Figure 6.4). Figure 6.4D indicates that the $[GSNO + H]^+$ ion at *m/z* 337 is formed in higher abundance in the ion source relative to the $[GS^{\bullet} + H]^+$ ion. At higher cone voltages, increased fragmentation of the *m/z* 307 and *m/z* 337 (to *m/z* 307) ions results in an apparent increase in the relative abundance of their sodiated forms, $[GS^{\bullet} + Na]^+$ and $[GSNO + Na]^+$ at *m/z* 329 and *m/z* 359, respectively (Figures 6.4 D-F). In addition, the *m/z* 359 ion also fragments to *m/z* 329 *via* loss of NO with increasing cone voltage. Thus, loss of NO becomes competitive with loss of $Na^+$ at higher cone voltages (Figures 6.4D-F). Note that $Na^+$ ions at *m/z* 23 are not seen here since the *m/z* range of the Q-Tof is 50-4000 u.

## 6.6 Conclusions

Fragmentation of GSX species in a Z-spray source occurs at a sample cone voltage of 60 V and above. Fragmentation of the glutathionyl moiety of GSX occurs mainly *via* loss of $H_2O$ and cleavage of the γ-Glu-Cys and Cys-Gly peptide bonds to form *b* and *y* sequence ions that undergo further fragmentation. The extent of GSX fragmentation is pH dependent, with increased fragmentation occurring at pH 2.5

compared to pH 1.2. The higher pH directs fragmentation of GSH towards loss of $NH_3$ rather than $H_2O$, as previously reported for γGlu tripeptides (*123*), However, release of $NH_3$ *vs* $H_2O$ cannot be correlated with γ- *vs* α-Glu linked peptides, since $NH_3$ release from GSNO and GSSG was not observed. Most likely, the fragmentation channels depend on molecular conformation and intramolecular interactions.

Increasing the source block temperature to 150 °C causes increased homolytic cleavage of the S-NO bond of GSNO, but does not induce fragmentation of GSH or GSSG. Fragmentation of the $[GS^{\bullet} + H]^+$ radical cation formed by in-source denitrosation of GSNO yields ions at *m/z* 158, 162, 205, 243, and 274 that are unique to GSNO. Increased cone voltage also results in in-source generation of $[GSH + H]^+$ and $[GSSG + H]^+$ from GSSG and from GSNO, respectively, and these fragment ions are isobaric with $[M + H]^+$ ions from GSH and GSSG.

To distinguish species present in solution from those formed during MS analysis, in-source fragmentation of GSX, especially GSNO, can be minimized by conducting the analysis at low pH using low cone voltage and source-block-temperature settings. For example, the in-source generation of $[GSH + H]^+$ from GSSG, or $[GSSG + H]^+$ from GSNO can be suppressed by operating the Z-spray ESI source at a cone voltage of ≤ 20 V, capillary voltage of 3 kV, source temperature of 70–80 °C, and a collision energy of 5 V in the collision cell. If the nature of the sample requires that mass spectra be acquired at high pH and a cone voltage >20 V, the addition of $Na^+$ ions will simplify the spectra by decreasing fragmentation of the glutathionyl moiety, but will not prevent in-source formation of GSSG from $GS^{\bullet}$.

Since in-source fragmentation of GSNO occurs under the gentlest conditions consistent with ionization, a strategy for detecting GSNO using a Z-spray source would be to look for the simultaneous presence of $[GSNO + H]^+$ at *m/z* 337 and $[GS^\bullet + H]^+$ at *m/z* 307, or the corresponding sodiated ions. Furthermore, CID of the *m/z* 307 odd-electron ion produces unique radical-induced fragments, such as *m/z* 158 and *m/z* 243, that can be used in MRM experiments (307 → 158, 307 → 243) for the mass spectrometric quantitation of GSNO.

## 6.7 Supplementary Figures to Chapter 6

**Figure S6.1. ESI mass spectra of 2.5 mM GSH at pH 1.2 *vs* capillary voltage (A, B, C), source block temperature (A, D, E), and cone voltage (A, F, G).** The collision energy was 5 eV. A solution of 5 mM GSH in 125 mM HCl was diluted 2-fold with acetonitrile/1% $HCO_2H$, and directly infused at 1 μL/min into the Z-spray source. The TICs in parentheses have been normalized to the TIC of spectrum (A) at 70 °C, 20 V cone V and 2.5 kV capillary V.

**Figure S6.2. ESI mass spectra of 2.5 mM GSSG at pH 1.2 *vs* capillary voltage (A, B, C), source block temperature (A, D, E), and cone voltage (A, F, G).** The collision energy was 5 eV. A solution of 5 mM GSSG in 125 mM HCl was diluted 2-fold with acetonitrile/1% $HCO_2H$, and directly infused at 1 μL/min into the Z-spray source. The TIC in parentheses have been normalized to the TIC of spectrum (A) at 70 °C, 20 V cone V and 2.5 kV capillary V.

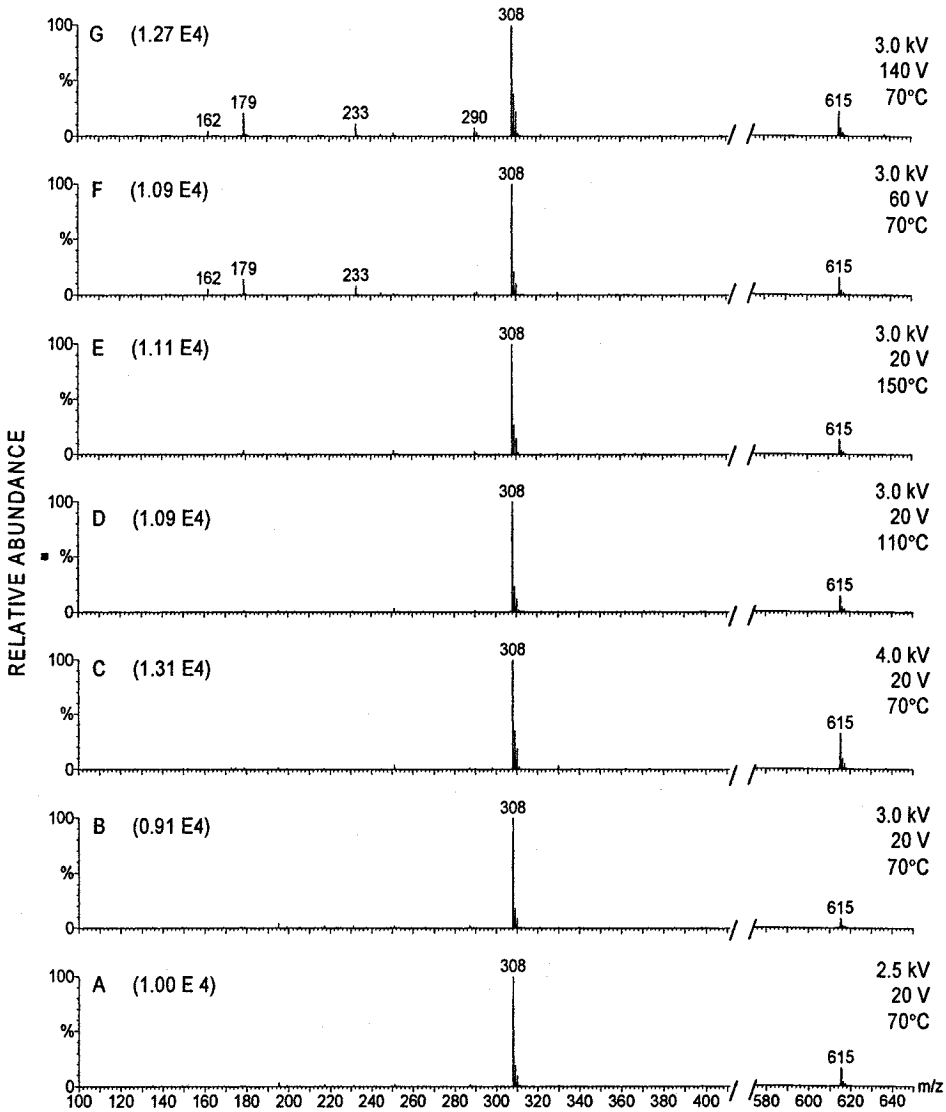
RELATIVE ABUNDANCE
G (1.27 E4)
3.0 kV
140 V
70°C
F (1.09 E4)
3.0 kV
60 V
70°C
E (1.11 E4)
3.0 kV
20 V
150°C
D (1.09 E4)
3.0 kV
20 V
110°C
C (1.31 E4)
4.0 kV
20 V
70°C
B (0.91 E4)
3.0 kV
20 V
70°C
A (1.00 E 4)
2.5 kV
20 V
70°C
308
615
162
179
233
290
m/z

**Figure S6.1**

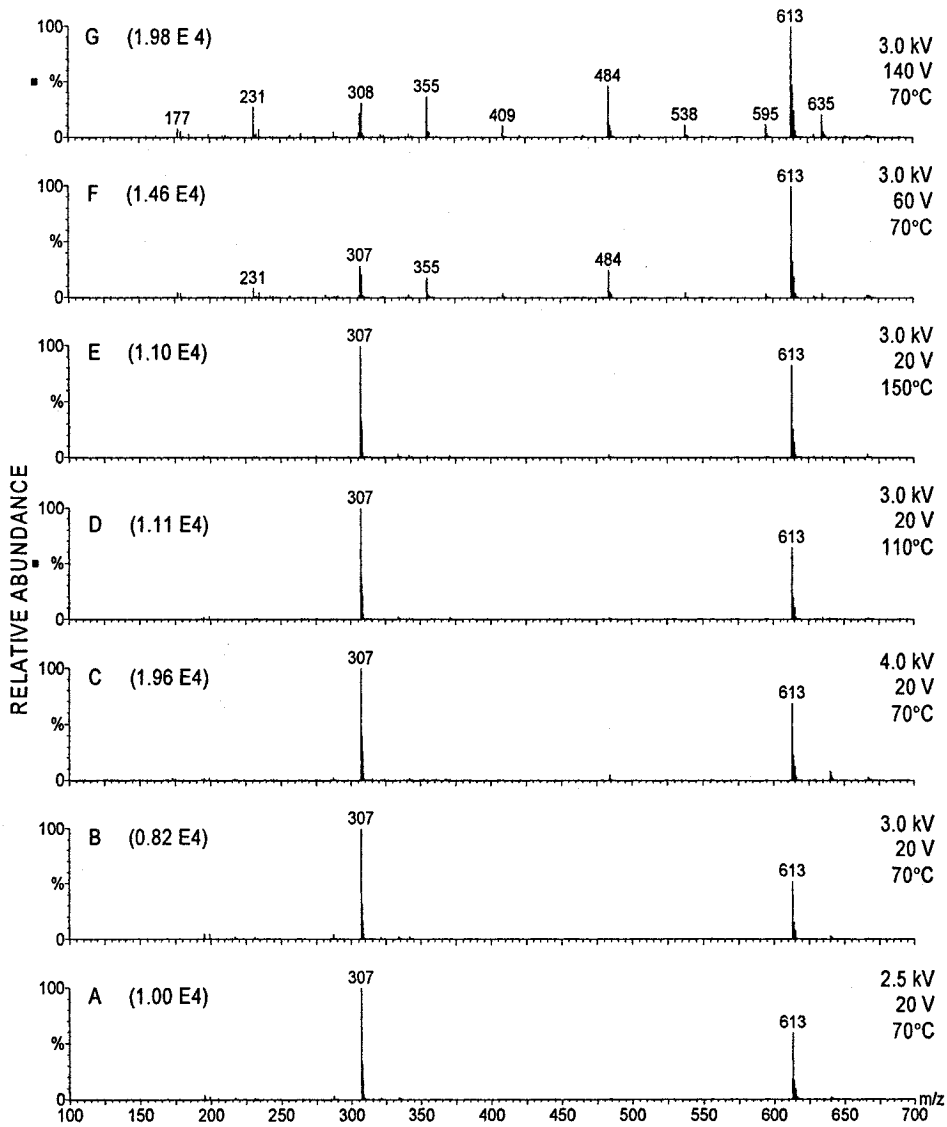
RELATIVE ABUNDANCE
G (1.98 E 4)
3.0 kV
140 V
70°C
F (1.46 E4)
3.0 kV
60 V
70°C
E (1.10 E4)
3.0 kV
20 V
150°C
D (1.11 E4)
3.0 kV
20 V
110°C
C (1.96 E4)
4.0 kV
20 V
70°C
B (0.82 E4)
3.0 kV
20 V
70°C
A (1.00 E4)
2.5 kV
20 V
70°C
m/z

**Figure S6.2**

# Chapter 7 - Advances towards the development an HPLC/ESI-MS method for direct measurement of intact GSNO at neutral pH

## 7.1 Abstract

Direct measurement using mobile phases at pH 7.0 of underivatized *S*-nitrosoglutathione (GSNO) has been achieved by high-performance liquid chromatography (HPLC) employing UV spectrophotometric (HPLC/UV) and electrospray mass spectrometric (HPLC/ESI- MS) detection. The method is robust and exhibits good linearity in the range of 0.2–100 μM GSNO when using UV detection, with a limit of detection (LOD) of 0.2 μM GSNO. Attempts to improve sensitivity by using ESI-MS detection in an ion trap mass spectrometer resulted in the same LOD and linearity in the range of 0.2–10 μM GSNO. The present method obviates the problems associated with the use of acidic mobile phases in currently used methodology. The potential for improved LOD for GSNO detection using mass spectrometric approaches is discussed.

## 7.2 Introduction

The role of nitric oxide in mammalian physiology has been the focus of intense research since it was discovered that NO is synthesized *in vivo* by nitric oxide synthases and that it is the so-called endothelium-derived relaxing factor (EDRF) (*97*). It is now accepted that, in addition to its role in vasodilation, NO is involved in physiological functions that include platelet adhesion and aggregation, inhibition of vascular smooth cell proliferation, leukocyte addition, and endothelial cell apoptosis (*2*).

Due to their proposed role in the stabilization, transport, and storage of NO *in vivo* (*11*), the detection and quantification of *S*-nitrosothiols (RSNOs) in biological fluids is a topic that has received much attention recently (*53, 55, 60, 129-133*). Many examples of RSNO detection in biological samples have been reported (*132, 133*), but much debate has centered around the RSNO levels measured in different laboratories, which vary by orders of magnitude (*59, 134, 135*).

The major reason for the divergent RSNO levels found in biological samples is thought to be the method of analysis (*59, 134*). The analytical methodology currently in use employs one of several indirect strategies that include measurement of nitrite from the decomposed RSNOs using spectrophotometry, fluorescence, or gas chromatography-mass spectrometry (GC-MS), and measurement of NO using chemiluminescence or NO-specific electrodes after cleavage of the S-NO bond (*133*). Some reversed-phase HPLC methods have been used to measure GSNO, a biologically relevant RSNO, employing $C_{18}$ analytical columns and mobile phases in the pH range of 2 to 4 (*56-58*).

It is argued that sample manipulation during the preanalysis phase has contributed to errors such as analyte loss during derivatization and RSNO formation *in situ* from nitrite and endogenous thiols (*135*). Recently, it has been shown that GSNO can be formed at low pH as an artifact when the analytical matrix is rich in GSH and nitrite, or peroxynitrite (*59, 60*). Thus, there is a need in the biomedical field for sensitive and specific analytical methods for the analysis of underivatized RSNOs that minimize loss and artifactual RSNO formation.

The formation of RSNO during HPLC analysis can be avoided by performing the analysis in mobile phases at neutral pH. To date only one such method has been reported

for GSNO, and it employs ion-pairing chromatography (*60*). The authors suggest that mass spectrometric detection could be used to increase the sensitivity of the method. While mass spectrometry can detect very low concentrations of analytes, the ion-pairing agent used (tetrabutylammoniumhydrogen sulfate, TBAHS) is non-volatile, and will likely suppress ionization in the mass spectrometer. The direct analysis of GSNO by in-line LC/MS using mobile phases at neutral pH has not yet been reported. This report summarizes the advances we have made towards the development of such a method with the goal of adapting it to the measurement of GSNO in biological fluids.

## 7.3 Experimental

### 7.3.1 Materials

HPLC amber glass vials were purchased from National Scientific (Rockwood, TN), diethylenetriaminepentaacetic acid (DTPA) from Koch-Light Laboratories (Colnbrook Bucks, England). All other reagents were purchased from Sigma-Aldrich (Milwaukee, WI)

### 7.3.2 Synthesis of stock GSNO

Stock GSNO solutions were prepared *in situ* by reacting equal volumes of 10 mM GSH in 125 mM HCl (aq) with 10 mM $NaNO_2$ in 2 mM DTPA (aq), for 10 min at room temperature in the dark (*14, 63*). Following 10-fold dilution with 20 mM sodium phosphate buffer (pH 7.0), the GSNO concentration was verified spectrophotometrically by measuring the absorption at 335 nm ($\varepsilon = 900\ M^{-1}\ cm^{-1}$) (*67*) on an Agilent 8453 UV diode-array spectrophotometer with an integration time of 0.1 s to minimize photodegradation during measurement. A fresh GSNO stock solution was prepared on the

same day as the experiment and kept on ice. GSNO standards were prepared by diluting the stock GSNO with 20 mM sodium phosphate buffer (pH 7.0) containing 0.1 mM DTPA.

### 7.3.3 HPLC/UV analysis

An Agilent 1090 HPLC with diode-array UV-vis detector was used for chromatographic analysis. The isocratic method used an Atlantis dC18 analytical column (150x3.0-mm, 5-μm particles, Waters) thermostated at 35 °C, and equilibrated with the mobile phase, 20 mM sodium phosphate buffer (pH 7.0). GSNO was eluted at a flow rate of 1 mL/min, and detected at 210, 220, 230, and 335 nm using a 1.0-cm pathlength. The injection volume was 10 μL for 1 mM GSNO solutions, and 100 μL for lower GSNO concentrations.

### 7.3.4 HPLC/ESI-MS

An Agilent 1100 HPLC equipped with a Spectra System UV6000LP UV detector (Thermo Separation Products) was interfaced to a ThermoFinnigan LCQ Deca ion trap mass spectrometer. The HPLC method was as described in Section 7.3.3 except that the injection volume was 100 μL, and the mobile phase was 20 mM ammonium acetate buffer (pH 7.0). To improve ionization, the eluent flow was mixed post-column 1:1 with acetonitrile containing 1% acetic acid, and split post column to 365 μL/min for introduction into the ESI source, operating in positive-ion mode, of the mass spectrometer. High purity nitrogen (>99.0%) was used as the sheath and auxiliary gas at settings of 80 and 20 units, respectively. The electrospray voltage was set at 5.0 kV, the heated capillary at 200 °C or 300 °C, and the capillary voltage at 44 V. Single-ion

monitoring (SIM) experiments were conducted by selecting the GSNO $[M + H]^+$ peak at *m/z* 337 and its denitrosated ion $[M - NO + H]^+$ at *m/z* 307. Tandem mass spectrometry (MS/MS) experiments for multiple reaction monitoring (MRM) were conducted on the ion trap with the heated capillary at 300 °C and a collision energy of 20%.

### 7.3.5 Method robustness

The sensitivity of the HPLC method to small variations in temperature and mobile-phase pH was evaluated by performing the analysis at HPLC column temperatures of 33 and 37 °C, and mobile-phase pH values of 6.8 and 7.2.

## 7.4 Results

### 7.4.1 HPLC/UV analysis

GSNO elution from the HPLC column was monitored at 210 nm. At pH 7.0, GSNO had a retention time of 3.6 min in 100% aqueous mobile phase (Figure 7.2). However, addition of even 2% acetonitrile resulted in GSNO eluting with the solvent front (data not shown). Thus, the highly hydrophilic GSNO molecule with two carboxylates and one ammonium group (Figure 7.1) interacts weakly with the Atlantis $dC_{18}$ column.

### 7.4.2 Linearity, LOD, and LOQ

Excellent linearity ($R^2 = 0.9999$) was observed in the GSNO concentration range of 0.1–100 μM at all the wavelengths monitored. Figure 7.3 shows the response curves at 210 nm, which is the most intense band, and at 335 nm ($\varepsilon = 900\ M^{-1}\ cm^{-1}$), which is more selective for GSNO due to absorption by the *S*-NO bond. Although the response at

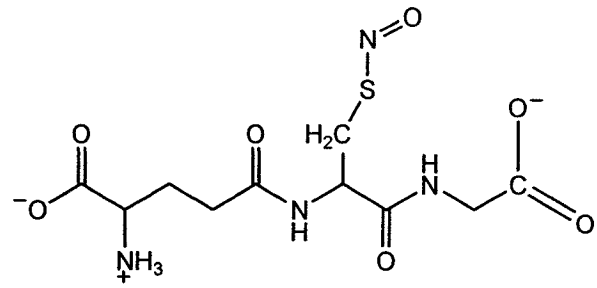

**Figure 7.1. Ionized form of *S*-nitrosoglutathione at pH 7.0.**

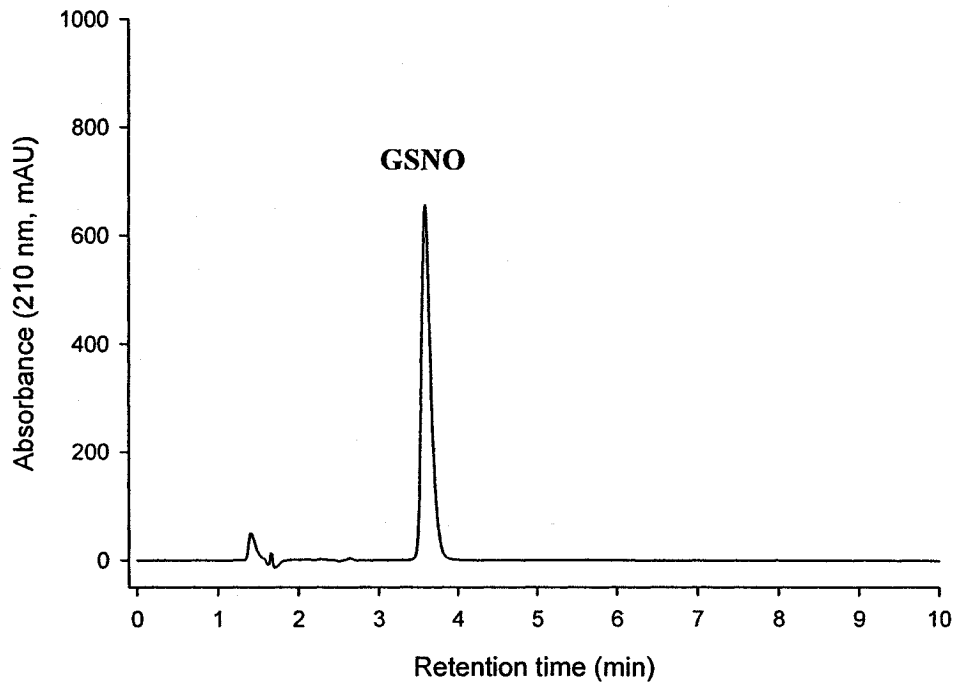


**Figure 7.2. HPLC/UV chromatogram of GSNO at pH 7.0.** A 100-μL aliquot of 0.1 mM GSNO in 20 mM sodium phosphate buffer (pH 7.0) containing 0.1 mM DTPA, was prepared in an amber glass HPLC vial in the dark was loaded within 60 min onto an Atlantis dC18 analytical column (150x3.0-mm, 5-$\mu$m particle size). GSNO was eluted at 35 °C with the same buffer at 1 mL/min and detected at 210 nm (Section 7.3.3) in a 1.0-cm flowcell.

**Table 7.1.** Limits of detection (LOD) and quantitation (LOQ) in GSNO analysis by HPLC with UV and MS detection using an ion trap mass spectrometer[a]

| Detection method | Wavelength (nm) | LOD[b] (μM) | LOQ[c] (μM) |
|---|---|---|---|
| UV-vis | 210 | 0.1 | 0.4 |
| | 220 | 0.2 | 0.6 |
| | 230 | 0.2 | 0.6 |
| | 240 | 0.7 | 2.3 |
| | 335 | 1.0 | 3.3 |
| ESI-MS SIM mode[d] (capillary 200 °C) | - | 0.2 | 0.7 |
| ESI-MS SIM mode[d] (capillary 300 °C) | - | 2.0 | 6.7 |
| ESI-MS MRM mode[e] (capillary 300 °C) | - | 0.5 | 1.7 |

[a] HPLC/MS details are given in the legend for Figure 5.3

[b] LOD = 3X S/N

[c] LOQ = 10X S/N

[d] SIM mode: the ions with *m/z* 307 and *m/z* 337 were selected in the ion trap.

[e] MRM mode: TIC chromatograms of the ions with *m/z* 232 and 289 were extracted from the full scan (*m/z* 100–400) MS/MS of the $(M-NO+H)^+$ ion at *m/z* 307.

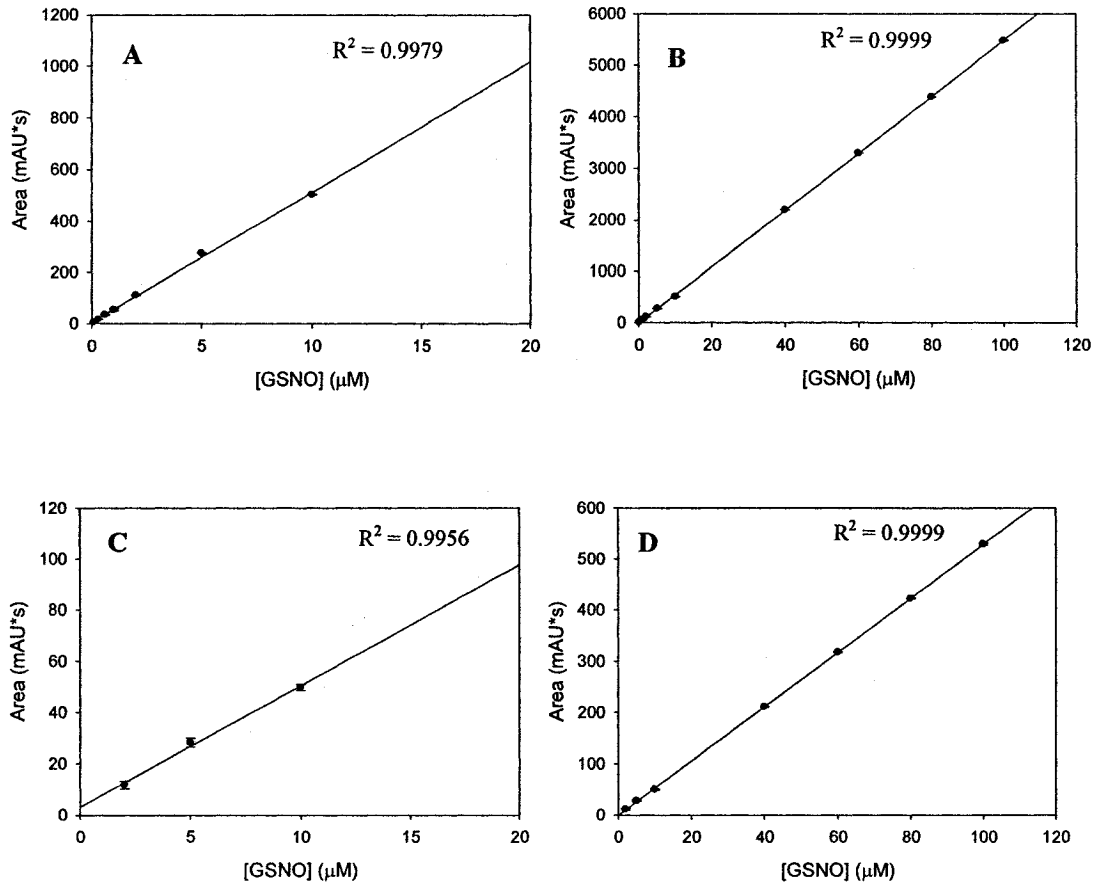


**Figure 7.3. HPLC/UV calibration curves for GSNO standards at pH 7.0.** Plots of **(A,B)** 210-nm and **(C,D)** 335-nm absorbance *vs* GSNO concentration. The experimental conditions are given in the legend of Figure 7.2. Data points represent n=3.

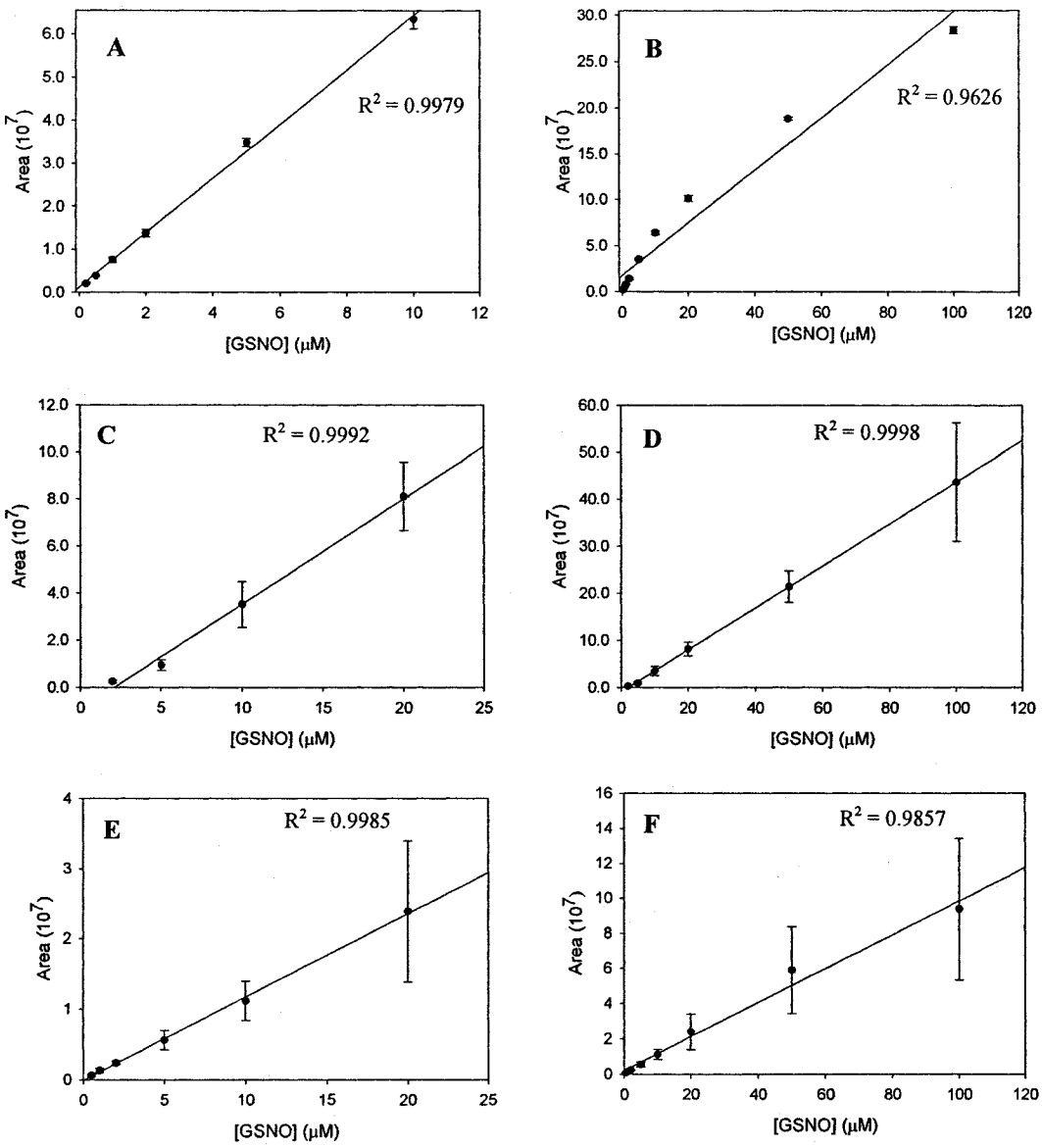


**Figure 7.4. HPLC/ESI-MS calibration curves for GSNO standards at pH 7.0. (A, B)** TIC *vs* [GSNO] in SIM mode at 200 °C; **(C, D)** TIC *vs* [GSNO] in SIM mode at 300 °C; **(E, F)** TIC *vs* [GSNO] in MRM mode at 300 °C. Aliquots (100-μL) of GSNO in 20 mM sodium phosphate buffer (pH 7.0) containing 0.1 mM DTPA were loaded onto an Atlantis dC18 analytical column (150x3.0-mm, particle size: 5-μm) at 35°C. GSNO was eluted with 20 mM ammonium acetate buffer (pH 7.0) at 1 mL/min. The eluent was mixed post column with (1:1) acetonitrile containing 1% acetic acid, and split to 365 μL/min for introduction to the ESI source. MS detection was performed using a LCQ Deca ion trap mass spectrometer operated in positive-ion mode, spray 5.0 kV, heated capillary 44 V. Data points represent n=3.

210 nm is 10 times that at 335 nm, both graphs yield excellent correlation coefficients ($R^2$) of 0.9999. Similar $R^2$ values were obtained at 220 nm and 230 nm (data not shown). LOD and LOQ values, which are the GSNO concentrations that give signal-to-noise ratios (S/N) of 3 and 10, respectively, with UV detection, are summarized in Table 7.1 for each wavelength examined. The assay is most sensitive with UV detection at 210 nm.

**Table 7.2.** Effect of minor operational changes on GSNO analysis by HPLC/UV at 210 nm[a].

| HPLC Column T | Buffer pH | Retention time (min) | Peak width (min) | Peak height (mAU) |
|---|---|---|---|---|
| 33 °C | pH 7.0 | 3.8 | 0.13 | 619 |
| 35 °C | pH 7.0 | 3.6 | 0.13 | 655 |
| 37 °C | pH 7.0 | 3.6 | 0.13 | 638 |
| 35 °C | pH 6.8 | 3.7 | 0.13 | 632 |
| 35 °C | pH 7.0 | 3.6 | 0.13 | 655 |
| 35 °C | pH 7.2 | 3.6 | 0.12 | 681 |

[a] 100-μL aliquots of GSNO in 20 mM sodium phosphate buffer (pH 7.0) containing 0.1 mM DTPA were loaded onto an Atlantis dC18 analytical column (150x3.0-mm, particle size: 5-μm) at the temperatures indicated. GSNO was eluted with the 20 mM sodium phosphate buffer with the pH values indicated at 1 mL/min and detected at 210 nm (Section 7.3.3) in a 1.0-cm flowcell

### 7.4.3 Effects of small changes in temperature and pH

The HPLC column temperature and mobile-phase pH were varied over a narrow range to determine how strictly these parameters need to be controlled during the analysis. Table 7.2 shows that the method is robust, since small variations in these

parameters do not cause significant changes in GSNO retention time or in the peak width and height of GSNO absorbance at 210 nm.

### 7.4.4 HPLC/ESI-MS analysis

The HPLC/UV method can be adapted for HPLC/MS by changing to volatile buffer salts compatible with MS analysis. Ammonium acetate, a common salt used in buffers at neutral pH because of its good chromatographic properties and MS compatibility (*136, 137*) was selected. Substituting 20 mM sodium phosphate (pH 7.0) buffer by 20 mM ammonium acetate (pH 7.0) buffer caused no change in GSNO retention time (data not shown).

GSNO undergoes thermally induced cleavage of its *S*-NO bond in ESI sources equipped with a heated capillary (*121*). An evaluation of the effects of the heated capillary temperature (T) revealed that at 200 °C thermally induced denitrosation of GSNO was minimal, and an adequate ionization current was still maintained. In contrast, at $T \geq 300$ °C GSNO denitrosation was almost complete, and at $T < 200$ °C, a stable ionization current could not be maintained (data not shown).

Single-ion monitoring (SIM), where a detector is focused on a single *m/z* value, improves the sensitivity of MS measurements because a higher number of ions are detected than when the *m/z* range is scanned. In the case of GSNO, the molecular ion $(M+H)^+$ undergoes homolytic denitrosation in an ESI source (see Section 6.4.2). Therefore, it was necessary to monitor the intensity of both the $(M+H)^+$ (*m/z* 337) and $(M-NO+H)^+$ (*m/z* 307) ions. Two capillary temperatures T, 200 °C and 300 °C, were selected to evaluate the effect of T on the linearity and sensitivity of detection in SIM mode. Figure 7.4A shows that there is good linearity in the range of 0.2–10 μM GSNO,

but the plot is nonlinear at concentrations > 10 μM when T = 200 °C (Figure 7.4B). The LOD and LOQ under these conditions were 0.2 μM and 0.7 μM, respectively (Table 7.1). Increasing T to 300 °C resulted in increased thermal denitrosation of GSNO, as expected, but extended the linearity to 100 μM (Figure 7.4 C, D). However, the increased baseline noise in the TIC chromatograms at T = 300 °C (data not shown) increased the LOD from 0.2 μM to 2 μM GSNO and the LOQ from 0.6 μM to 6 μM GSNO.

Multiple reaction monitoring (MRM) can be used to improve the S/N levels in MS measurements by focusing only on ions that undergo a specific fragmentation pathway. Since ion trap mass spectrometers cannot perform true MRM, TIC chromatograms of the ions with *m/z* 232 $(M - NO - Gly + H)^+$ and 289 $(M - NO - H_2O + H)^+$ were extracted from the full scan (*m/z* 100–400) MS/MS of the $(M - NO + H)^+$ ion at *m/z* 307. The response curves for the MRM experiments (Figure 7.4E,F) show the same improvement in linearity at the upper concentration range, and decreased precision above 20 μM GSNO a seen in Figure 7.4C,D. The LOD for this set of conditions was 0.5 μM GSNO (Table 7.1).

## 7.5 Discussion

The glutathione molecule (Figure 7.1) is highly hydrophilic at pH 7 due to its three charged groups. Thus, the first challenge to overcome in this study was to identify conditions under which intact GSNO was retained on a reversed-phase chromatographic column at neutral pH using MS-compatible mobile phases. Evaluation of different HPLC columns led (Table 7.3) to the identification of a stationary phase suitable for the analysis of peptides using highly aqueous mobile phases without the need for MS-incompatible additives such as TFA and other ion-pairing reagents.

**Table 7.3.** Analytical columns evaluated for the measurement of GSNO in neutral pH mobile phases.

| Column trade name | Manufacturer | Dimensions[a] |
|---|---|---|
| Nucleosil 120A C18 | Varian | 250x4.6 mm |
| Prism RP C18 | ThermoFisher | 250x3.0 mm |
| Extend C18 | Agilent Technologies | 250x3.0 mm |
| Atlantis HILIC | Waters | 250x3.0 mm |
| Atlantis dC18 | Waters | 250x3.0 mm |
| Atlantis dC18 | Waters | 150x3.0 mm |

[a]: stationary phase particle size was 5 μm for all columns

The HPLC method with UV detection exhibits robustness and excellent linearity in the range of 0.1–100 μM GSNO, with an LOD of 0.2 μM (Table 7.1). The Saville assay that uses Griess-type reagents also has an LOD of 0.2 μM with detection at 540 nm (*133*). However, the best LOD was achieved here with detection at 210 nm (Table 7.1), where the potential for interference from co-eluting components in a biological matrix is high. Also, the current LOD is over two orders of magnitude greater than that achieved with chemiluminescence detection (LOD 1 nM) (*133*) or by fluorimetric methods (LOD 20 nM) (*133*). Nevertheless, this method has the advantage that there is little sample processing and no need for derivatization or decomposition of the GSNO molecule prior to analysis.

Mass spectrometry is the detection method of choice in many bioanalytical measurements because of its high sensitivity and specificity. Several validated methods exist for the measurement of GSH and its conjugates using HPLC/MS (*110, 111, 115,*

*138*). Thus, it was expected that the use of MS detection would lower the LOD obtained using UV-vis detection, but the results show that the linear range is narrower and that the LOD is higher under the conditions of this study. Attempts to improve the method by generating the denitrosated ion of GSNO $(M - NO + H)^+$, increasing the heated capillary temperature, and employing MRM did not result in significant improvements.

The poor performance of the HPLC/ESI-MS method described here may be due to a number of factors. These include poor ionization in the ESI source due to the high water content of the mobile phase, the relatively high flow of the eluent (365 μL/min) into the source, or the high mobile-phase buffer concentration (20 mM). Decreasing the amount of eluent entering the source, or the buffer concentration, could yield improved ionization and sensitivity. Increased sensitivity could also be achieved by using a smaller stationary-phase particle size since this would result in narrower, more concentrated analyte bands eluting from the analytical column. The use of a triple quadrupole mass spectrometer should increase the sensitivity of GSNO detection since these instruments are known to be more sensitive than ion traps in SIM and MRM modes.

## 7.6 Conclusions

The results from this study show that the analysis of intact GSNO at neutral pH can be achieved on a reversed-phase HPLC system with either UV or ESI-MS detection without the use of ion-pairing reagents to retain GSNO on the column. Although the detection limits are not better than those previously published, good linearity and robustness were demonstrated with UV detection. Since the method is adaptable for use with ESI-MS detection, the potential for greatly improved sensitivity exists with access to a triple quadrupole mass spectrometer. Such a method should find use in biomedical

research involving GSNO measurements since around pH 7.0 there is no interfering formation of GSNO from GSH and nitrite that are frequently present in the sample matrix.

# Chapter 8 - Conclusions and suggestions for future work

## 8.1 GSX fragmentation in Z-spray ESI source (Chapter 2)

Evaluation of the effects of electrospray capillary voltage, source-block temperature, and cone voltage settings of the Z-spray ESI source of the Q-Tof 2 mass spectrometer showed that the cone voltage setting is the operating parameter that most influences the in-source fragmentation of GSX (X = H, NO, SG) species. Increased GSX fragmentation was observed at cone voltages of 60 V and above. The electrospray capillary voltage had only minor effects on the three GSX used in the study, but increasing the source-block temperature resulted in increased homolytic cleavage of the *S*-NO bond of GSNO. It was found that in-source cleavage of the *S*-NO bond could be prevented by minimizing any of the parameters tested.

In-source fragmentation of the glutathionyl (GS) moiety occurred mainly *via* loss of $H_2O$ and cleavage of the γ-Glu-Cys and Cys-Gly peptide bonds to form *b* and *y* sequence ions, as well as cleavage of the *S*-NO bond in GSNO. The formation of $GS^{\bullet}$ upon homolysis of the *S*-NO bond resulted in the appearance of additional ions that were attributed to radical-induced fragmentation. Increasing the solution pH from 1.2 to 2.5 resulted in increased fragmentation with preferential loss of $NH_3$ instead of $H_2O$ from GSH.

## 8.2 RSNO hydrolysis (Chapters 3, 4 and 5)

The rate of acid-catalyzed hydrolysis of RSNOs in high acid (~4 M $H_2SO_4$) was found to be structure dependent. Dimethyl substitution on the carbon attached to the nitroso sulfur increased the RSNO hydrolysis rate 12–38 fold due to the increased proton affinity of the sulfur atom. *N*-Acetylation of CysNO had no significant effect on its hydrolysis rate. The activation energies for the primary and tertiary RSNOs investigated were the same, within experimental error.

At pH 2, GSNO decomposition was shown to be initiated by *S*-NO hydrolysis *via* nucleophilic attack at the nitroso nitrogen, initially forming $HNO_2$. Decomposition was inhibited on addition of GSH or traps for $HNO_2$ and $N_2O_3$, and on deaeration. A chain-reaction mechanism with $N_2O_3$, formed *in situ*, as the chain carrier was proposed based on previous studies of RSNO decomposition in organic solvents (*16*). Identification of the main products of GSNO hydrolysis, $GSO_3H$, GSOSG, and $GSO_2SG$, support the proposed mechanism.

Base-catalyzed denitrosation of GSNO was investigated to determine if the reaction proceeds *via* nucleophilic attack by $OH^-$ at both the nitrogen and sulfur atoms of the *S*-NO bond. Decomposition was found to result mainly from attack at the nitroso nitrogen and to proceed *via* two competing decomposition pathways with product profiles that depend on $[OH^-]_o$ and $[GSNO]_o$. The predominant pathway at $[OH^-]_o/[GSNO]_o \leq 25$ is the attack by $OH^-$ at the nitroso nitrogen producing GSSG (from the autooxidation of $GS^-$) and $NO_2^-$. The second pathway produces GSSH and a sulfur-free glutathionyl derivative as the final GSX products, suggesting that it proceeds *via* a nitrosated disulfide intermediate formed on reaction of $GS^-$ and GSNO. This pathway was proposed based on

the nature of the reaction products and on similar observations in the literature. Attack by $OH^-$ at the nitroso sulfur may also occur, as evidenced by the detection of $N_2O$ in the reaction headspace, but < 10% nitroso *N* was detected as $N_2O$. The fate of the 30–50% nitroso *N* that was not detected as $NO_2^-$ or $N_2O$ was not established, but it could have been converted to $NH_2OH$ on reaction of $GS(O)NH_2$ with GSH (*30*).

## 8.3 GSNO thiolysis (Chapter 6)

The mechanism of GSNO decomposition in the presence of high thiol concentrations is more complicated than previously proposed (*27, 30*). Autocatalytic reactions must be included based on inhibition of thiolysis by dimedone. Product analysis confirms previous findings that GSSG is the major GSX product, but GSOH and GSN(OH)H are also formed, supporting the mechanism proposed by Wong *et al.* (*30*). Additionally, HNO may be generated based on the formation of the sulfinamide, $GS(O)NH_2$, as well as the detection of $N_2O$ indicating nucleophilic attack at the nitroso sulfur atom. Since only a small amount of $GS(O)NH_2$ was detected, HNO generation is likely a minor decomposition pathway at pH 7.4. Overall, uncatalyzed GSNO thiolysis is too slow to represent a biologically significant GSNO decomposition pathway *in vivo*.

## 8.4 Suggestions for future work

(1) The GSNO fragments formed from radical-induced dissociation of $GS^\bullet$ could be used as diagnostic ions in the detection by mass spectrometry of GSNO in samples containing other GSX. Investigations into the formation of $RS^\bullet$-derived fragments from other RSNOs could lead to the identification of diagnostic ions for RSNOs in general.

(2) The decomposition of other RSNOs at pH 2, especially those of potential pharmaceutical interest, should be investigated to determine if the reactions reported here for GSNO are general to other RSNOs. Excess $HNO_2$ should be added to the RSNO solutions under anaerobic conditions as further verification of the decomposition mechanism proposed in Chapter 4.

(3) The base-catalyzed decomposition reactions reported here were performed under aerobic conditions. Thus, the effect of oxygen on rates and decomposition products should be investigated. Munro and Williams (*34*) reported that the measured $NO_2^-$ accounted for only 50% of the expected nitrogen product in base-catalyzed decomposition of 1 mM GSNO in 60–200 mM NaOH. The GSX and nitrogen products formed under these conditions should be analyzed to determine if the reactions proposed in Chapter 5 occur at higher $OH^-$ concentrations.

(4) The main nitrogen-containing GSNO decomposition product reported by Wong *et al.* (*30*) and Singh *et al.* (*27*) in the presence of high GSH (1–10 mM) concentrations was $NH_3$. Wong *et al.* proposed that $NH_3$ was formed from the reaction of the sulfinamide, $GS(O)NH_2$, with GSH or with $H_2O$, but our data show that the sulfinamide is stable in the presence of 10 mM GSH in aqueous solutions at neutral pH. A full investigation into the time course of the formation of nitrogen-containing products would shed light into the source of $NH_3$ in these reactions.

(6) The sensitivity of HPLC/ESI-MS detection of GSNO using mobile phases around neutral pH should be improved. The S/N could be increased by using narrower bore analytical columns (i.e. 50x1.0 mm) which result in more concentrated chromatographic bands, and carrying out the analysis on a triple quadrupole mass

spectrometer. In addition, the method should be elaborated for detection of GSNO in biological samples.

## References.


1. McCleverty, J.A. (2004) *Chem. Rev.*, **104**, 403-418.
2. Walford, G. and Loscalzo, J. (2003) *J. Thromb. Haemost.*, **1**, 2112-2118.
3. Williams, D.L.H. (2003) *Org. Biomol. Chem.*, **1**, 441-449.
4. Al-Sa'doni, H.H. and Ferro, A. (2004) *Curr. Med. Chem.*, **11**, 2679-2690.
5. Fukuto, J.M., Bartberger, M.D., Dutton, A.S., Paolocci, N., Wink, D.A., and Houk, K.N. (2005) *Chem. Res. Toxicol.*, **18**, 790-801.
6. Lancaster, J.R. (1994) *Proc. Natl. Acad. Sci. U. S. A.*, **91**, 8137-8141.
7. Blaise, G.A., Gauvin, D., Gangal, M., and Authier, S. (2005) *Toxicology*, **208**, 177-192.
8. Stamler, J.S., Singel, D., and Loscalzo, J. (1992) *Science*, **258**, 1898-1902.
9. Girard, P. and Potier, P. (1993) *FEBS Lett.*, **320**,(1): 7-8.
10. Jia, L., Bonaventura, C., Bonaventura, J., and Stamler, J.S. (1996) *Nature*, **380**,(21 March): 221-226.
11. Stamler, J.S., Jaraki, O., Osborne, J., Simon, D.I., Keaney, J., Vita, J., Singel, D., and Valeri, C.R. (1992) *Proc. Natl. Acad. Sci. U. S. A.*, **89**, 7674-7677.
12. Krezel, A. and Bal, W. (2004) *Chem. Res. Toxicol.*, **17**, 392-403.
13. Beloso, P.H. and Williams, D.L.H. (1997) *Chem. Commun.*, **1**,(1): 89.
14. Williams, D.L.H., *Nitrosation reactions and the chemistry of nitric oxide*. 2004: Elsevier.
15. Williams, D.L.H. (1999) *Acc. Chem. Res.*, **32**, 869-876.
16. Grossi, L. and Montevecchi, P.C. (2002) *Chem. Eur. J.*, **8**,(2): 380-387.

17. Grossi, L., Montevecchi, P.C., and Strazzari, S. (2001) *Eur. J. Org. Chem.,* 131-135.

18. Coupe, P.J. and Williams, D.L.H. (2001) *J. Chem. Soc., Perkin Trans. 2,* 1595-1599.

19. Timerghazin, Q.K., Peslherbe, G.H., and English, A.M. (2007) *Org. Lett.,* **9**,(16): 3049-3052.

20. Stamler, J.S. and Toone, E.J. (2002) *Curr. Opin. Chem. Biol.,* **6**, 779-785.

21. Catani, M.V., Bernassola, F., Rossi, A., and Melino, G. (1998) *Biochem. Biophys. Res. Commun.,* **249**,(1): 275-278.

22. Konorev, E.A., Kalyanaraman, B., and Hogg, N. (2000) *Free Radic. Biol. Med.,* **28**,(11): 1671-1678.

23. Lander, H.M., Hajjar, D.P., Hempstead, B.L., Mizra, U.A., Chait, B.T., Campbell, S., and Quilliam, L.A. (1997) *J. Biol. Chem.,* **272**,(Feb. 14): 4323-4326.

24. Ferranti, P., Malorni, A., Mamone, G., Sannolo, N., and Marino, G. (1997) *FEBS Lett.,* **400**, 19-24.

25. Bartberger, M.D., Mannion, J.D., Powell, S.C., Stamler, J.S., Houk, K.N., and Toone, E.J. (2001) *J. Am. Chem. Soc.,* **123**, 8868-8869.

26. Komiyama, T. and Fujimori, K. (1997) *Bioorg. Med. Chem. Lett.,* 7,(2): 175-180.

27. Singh, S.P., Wishnok, J.S., Keshive, M., Deen, W.M., and Tannenbaum, S.R. (1996) *Proc. Natl. Acad. Sci. U. S. A.,* **93**, 14428-14433.

28. Dicks, A.P., Li, E., Munro, A.P., Swift, H.R., and Williams, D.L.H. (1998) *Can. J. Chem.,* **76**, 789-794.

29. Barnett, D.J., Rios, A., and Williams, D.L.H. (1995) *J. Chem. Soc., Perkin Trans. 2,* 1279-1282.

30. Wong, P.S.-Y., Hyun, J., Fukuto, J.M., Shirota, F.N., DeMaster, E.G., Shoeman, D.W., and Nagasawa, H.T. (1998) *Biochemistry,* **37**, 5362-5371.

31. Tsikas, D., Sandmann, J., Rossa, S., Gutzki, F.-M., and Frolich, J.C. (1999) *Anal. Biochem.,* **270**, 231-241.

32. Li, J., Huang, F.L., and Huang, K.-P. (2001) *J. Biol. Chem.,* **276**,(5): 3098-3105.

33. Pastore, A., Federici, G., Bertini, E., and Piemonte, F. (2003) *Clin. Chim. Acta,* **333**, 19-39.

34. Munro, A.P. and Williams, D.L.H. (1999) *J. Chem. Soc., Perkin Trans. 2,* 1989-1993.

35. Ignarro, L.J., Lippton, H., Edwards, J.C., Baricos, W.H., Hyman, A.L., Kadowitz, P.J., and Greuter, C.A. (1981) *J. Pharmacol. Exp. Ther.,* **218**,(3): 739-749.

36. Radomski, M.W., Rees, D.D., Dutra, A., and Moncada, S. (1992) *Br. J. Pharmacol.,* **107**,(3): 745-749.

37. DeBelder, A.J., Macallister, R., Radomski, M.W., Moncada, S., and Vallance, P.J.T. (1994) *Cardiovasc. Res.,* **28**, 691-694.

38. Konorev, E.A., Tarpey, M.M., Joseph, J., Baker, J.E., and Kalyanaraman, B. (1995) *J. Pharmacol. Exp. Ther.,* **274**, 200-206.

39. Butler, A.R. (1990) *Chem. Br.,* **26**, 419-421.

40. Krezel, A. and Bal, W. (2003) *Org. Biomol. Chem.,* **1**, 3885-3890.

41. Noble, D.R. and Williams, D.L.H. (2000) *Nitric Oxide,* **4**,(4): 392-398.

42. Tao, L. and English, A.M. (2004) *Biochemistry,* **43**, 4028-4038.

43. Percival, M.D., Ouellet, M., Campagnolo, C., Claveau, D., and Li, C. (1999) *Biochemistry,* **38**, 13574-13583.

44. Allison, W.S. (1976) *Acc. Chem. Res.,* **9**, 293-299.

45. Al-Kaabi, S.S., Williams, D.L.H., Bonnet, R., and Ooi, S.L. (1982) *J. Chem. Soc., Perkin Trans. 2,* 227-230.

46. Tummavuori, J. and Lumme, P. (1968) *Acta Chem. Scand.,* **22**, 2003.

47. Burg, A., Cohen, H., and Meyerstein, D. (2000) *J. Biochem. Inorg. Chem.,* **5**, 213-217.

48. Holmes, A.J. and Williams, D.L.H. (2000) *J. Chem. Soc., Perkin Trans. 2,* 1639-1644.

49. de Oliveira, M.G., Shishido, S.M., Seabra, A.B., and Morgon, N.H. (2002) *J. Phys. Chem. A,* **106**, 8963-8970.

50. Noble, D.R., Swift, H.R., and Williams, D.L.H. (1999) *Chem. Commun.,* 2317-2318.

51. Smith, J.N. and Dasgupta, T.P. (2000) *Nitric Oxide,* **4**,(1): 57-66.

52. Singh, R.J., Hogg, N., Joseph, J., and Kalyanaraman, B. (1996) *J. Biol. Chem.,* **271**,(31): 18596-18603.

53. Goldman, R.K., Vlessis, A.A., and Trunkey, D.D. (1998) *Anal. Biochem.,* **259**, 98-103.

54. Jourd'heuil, D., Hallen, K., Feelisch, M., and Grisham, M.B. (2000) *Free Radic. Biol. Med.,* **28**,(3): 409-417.

55. Tsikas, D., Sandmann, J., Holzberg, D., Pantazis, P., Raida, M., and Frolich, J.C. (1999) *Anal. Biochem.,* **273**,(1): 32-40.

56. Meyers, P.R., Minor Jr, R.L., R., G.J., Bates, J.N., and Harrison, D.G. (1990) *Nature,* **345**,(10 may): 161-163.

57. Balazy, M., Kaminski, P.M., Mao, K., Tan, J., and Wolin, M.S. (1998) *J. Biol. Chem.,* **273**,(48): 32009-32015.

58. Welch, G.N., Upchusch Jr., G.R., and Loscalzo, J. (1996) *Methods Enzymol.,* **28**, 293.

59. Tsikas, D. (2003) *Nitric Oxide,* **9**, 53-55.

60. Tsikas, D., Denker, K., and Frolich, J.C. (2001) *J. Chromatogr. A,* **915**, 107-116.

61. Fukuto, J.M., Switzer, C.H., Miranda, K.M., and Wink, D.A. (2005) *Annu. Rev. Pharmacol. Toxicol.,* **45**, 335-355.

62. *The Merck Index.* 12th ed. 1996, Whitehouse Station, NJ: Merck & Co, Inc.

63. Hart, T.W. (1985) *Tetr. Lett.,* **26**,(16): 2013-2016.

64. *SigmaPlot v.9.1*, Systat Software Inc.: San Jose, CA.

65. Timerghazin, Q.K., *personal communication.* 2007.

66. Kim-Shapiro, D.B., Schechter, A.N., and Gladwin, M.T. (2006) *Arterioscler. Thromb. Vasc. Biol.,* **26**, 697-705.

67. Mohr, S., McCormick, T.S., and Lapetina, E.G. (1998) *Proc. Natl. Acad. Sci.,* **95**,(9): 5045-5050.

68. Ellison, G. and Williams, D.L.H. (1981) *J. Chem. Soc., Perkin Trans. 2,* 699.

69. Arnelle, D.R. and Stamler, J.S. (1995) *Arch. Biochem. Biophys.,* **318**,(2): 279-285.

70. Dicks, A.P., Swift, H.R., Williams, D.L.H., Butler, A.R., Al-Sa'doni, H.H., and Cox, B.G. (1996) *J. Chem. Soc., Perkin Trans. 2,* 481-487.

71. Panchali, R. and Williams, D.L.H. (1988) *J. Chem. Res., Synop.,* **4**, 122-123.

72. Davis, F.A., Jenkins, L.A., and Billmers, R.L. (1986) *J. Org. Chem.*, **51**, 1033-1040.

73. Cremlyn, R.J., *An introduction to organosulfur chemistry*. 1996, Chichester, West Sussex, England: John Wiley & Sons Ltd.

74. Benitez, L.V. and Allison, W.S. (1974) *J. Biol. Chem.*, **240**,(19): 6234-6243.

75. Moore, J.W. and Pearson, R.G., *Kinetics and mechanism*. 3rd ed. 1981, New York: Wiley-Interscience.

76. Tao, L. and English, A.M. (2003) *Biochemistry*, **42**, 3326-3334.

77. Grossi, L., Montevecchi, P.C., and Strazzari, S. (2001) *Eur. J. Org. Chem.*, (4): 741-748.

78. Zhao, Y.L., McCarren, P.R., Houk, K.N., Choi, B.Y., and Toone, E.J. (2005) *J. Am. Chem. Soc.*, **127**,(31): 10917-10924.

79. Scatena, R., Bottoni, P., Martorana, G.E., and Giardina, B. (2005) *Expert Opin. Investig. Drugs*, **14**,(7): 835-846.

80. Liu, L., Hausladen, A., Zeng, M., Que, L., Heitman, J., and Stamler, J.S. (2001) *Nature*, **410**, 490-494.

81. Hou, Y., Guo, Z., Li, J., and Wang, P.G. (1996) *Biochem. Biophys. Res. Commun.*, **228**,(1): 88-93.

82. Sliskovic, I., Raturi, A., and Mutus, B. (2005) *J. Biol. Chem.*, **280**,(10): 8733-8741.

83. Root, P., Sliskovic, I., and Mutus, B. (2004) *Biochem. J.*, **382**,(2): 575-580.

84. Zhang, Y. and Hogg, N. (2004) *Proc. Natl. Acad. Sci.*, **101**,(21): 7891-7896.

85. Shafirovich, V. and Lymar, S.V. (2002) *Proc. Natl. Acad. Sci.*, **99**,(11): 7340-7345.

86. Accorsi, A., Barbieri, A., Raffi, G.B., and Violante, F.S. (2001) *Int. Arch. Occup. Environ. Health,* **74**, 541-548.

87. Munro, A.P. and Williams, D.L.H. (2000) *J. Chem. Soc., Perkin Trans. 2,* 1794-1797.

88. Seel, F. and Wagner, M. (1985) *Naturforsc. Teil B.,* **40**, 1607.

89. Seel, F. and Wagner, M. (1988) *Anorg. Allg. Chem.,* **558**, 189.

90. Lide, D.R., *Handbook of Chemistry and Physics*. 79th ed, ed. D.R. Lide. 1998, Boca Raton, FL: CRC Press.

91. Houk, K.N., Hietbrink, B.N., Bartberger, M.D., McCarren, P.R., Choi, B.Y., Voyksner, R.D., Stamler, J.S., and Toone, E.J. (2003) *J. Am. Chem. Soc.,* **125**, 6972-6976.

92. Rao, G.S. and Gorin, G. (1959) *J. Org. Chem.,* **24**, 749.

93. Peterson, L.A., Wagener, T., Sies, H., and Stahl, W. (2007) *Chem. Res. Toxicol.,* **205**,(5): 721-723.

94. Bell, S.E., Shah, C.M., and Gordge, M.P. (2007) *Biochem. J.,* **403**,(2): 283-288.

95. Sadidi, M., Geddes, T.J., and Kuhn, D.M. (2005) *Antiox. Redox. Sig.,* 7,(7 & 8): 863-869.

96. Giustarini, D., Rossi, R., Milzani, A., Colombo, R., and Dalle-Donne, I. (2003) *Rec. Res. Dev. Biochem.,* **4**,(Pt. 2): 1001-1016.

97. Ignarro, L.J., Buga, G.M., Wood, K.S., Byrns, R.E., and Chaudhuri, G. (1987) *Proc. Natl. Acad. Sci. U. S. A.,* **84**, 9265-9267.

98. Spencer, N.Y., Zeng, H., Patel, R.P., and Hogg, N. (2000) *J. Biol. Chem.*, **275**,(47): 3562-3567.

99. Romeo, A.A., Capobianco, J.A., and English, A.M. (2002) *J. Biol. Chem.*, **277**,(27): 24135-24141.

100. Romeo, A.A., Capobianco, J.A., and English, A.M. (2003) *J. Am. Chem. Soc.*, **125**, 14370-14378.

101. Meister, A. and Anderson, M.E. (1983) *Annu. Rev. Biochem.*, **52**,(1): 711-760.

102. Donzelli, S., Espey, M.G., Thomas, D.D., Mancardi, D., Tocchetti, C.G., Ridnour, L.A., Paolocci, N., King, S.B., Miranda, K.M., Lazzarino, G., Fukuto, J.M., and Wink, D.A. (2006) *Free Radic. Biol. Med.*, **40**,(6): 1056-1066.

103. Shen, B. (In preparation).

104. Barnett, D.J., McAinly, J., and Williams, D.L.H. (1994) *J. Chem. Soc., Perkin Trans. 2,* 1131-1133.

105. Shen, B., Thesis in the Department of Chemistry and Biochemistry, 2007, Concordia University, Montreal, Canada.

106. DeMaster, E.G., Quast, B.J., Redfern, B., and Nagasawa, H.T. (1995) *Biochemistry,* **34**,(36): 11494-11499.

107. Gow, A.J. and Ischiropoulos, H. (2001) *J. Cell. Physiol.*, **187**, 277-282.

108. Kim, J.-E. and Tannenbaum, S.R. (2004) *J. Biol. Chem.*, **279**,(11): 9758-9764.

109. Murphy, C.M., Fenselau, C., and Gutierrez, P.L. (1992) *J. Am. Soc. Mass Spectrom.*, **3**, 815-822.

110. Norris, R.L., Eaglesman, g.k., Shaw, G.R., Smith, M.J., Chiswell, R.K., Seawright, A.A., and Moore, M.R. (2001) *J. Chromatogr. B. Biomed. Appl.*, **762**, 17-23.

111. Camera, E., Rinaldi, M., Briganti, S., Picardo, M., and Fanali, S. (2001) *J. Chromatogr. B. Biomed. Appl.*, **757**,(1): 69-78.

112. Piraud, M., Vianey-Saban, C., Petritis, K., Elfakir, C., Steghens, J.-P., Morla, A., and Bouchu, D. (2003) *Rapid Commun. Mass Spectrom.*, **17**, 1297-311.

113. Dieckhaus, C.M., Fernandez-Metzler, C.L., King, R., Krolikowski, P.H., and Baillie, T.A. (2005) *Chem. Res. Toxicol.*, **18**, 630-638.

114. Castro-Perez, J., Plumb, R., Liang, L., and Yang, E. (2005) *Rapid Commun. Mass Spectrom.*, **19**, 798-804.

115. Levsen, K., Schiebel, H.-M., Behnke, B., Dotzer, R., Dreher, W., Elend, M., and Thiele, H. (2005) *J. Chromatogr. A*, **1067**, 55-72.

116. Kebarle, P. (2000) *J. Mass Spectrom.*, **35**,(7): 804-817.

117. Gabelica, V., De Pauw, E., and Karas, M. (2004) *Int. J. Mass Spec.*, **231**,(2-3): 189-195.

118. Cole, R.B. (2000) *J. Mass Spectrom.*, **35**, 763-772.

119. *Q-Tof 2 User's Guide*. First ed: Micromass Corporation.

120. Rubino, F.M., Verduci, C., Giampiccolo, R., Pulvirenti, G.B., and Colombi, A. (2004) *J. Mass Spectrom.*, **39**, 1408-1416.

121. Romeo, A.A., Capobianco, J.A., and English, A.M. at *51st ASMS Conference*, 2003. Montreal, Quebec, Canada.

122. Harrison, A.G. (1999) *Rapid Commun. Mass Spectrom.*, **13**, 16663-1670.

123. Harrison, A.G. (2003) *J. Mass Spectrom.*, **38**, 174-187.

124. Tsikas, D., Raida, M., Sandmann, J., Rossa, S., Forssmann, W.-G., and Frolich, J.C. (2000) *J. Chromatogr. B. Biomed. Appl.*, **742**, 99-108.

125. Kaneko, R. and Wada, Y. (2003) *J. Mass Spectrom.*, **38**, 526-530.

126. Mirza, U.A., Chait, B.T., and Lander, H.M. (1995) *J. Biol. Chem.*, **270**,(29): 17185-17188.

127. Wee, S., O'Hair, R.A.J., and McFadyen, W.D. (2004) *Int. J. Mass Spec.*, **234**, 101-122.

128. Hao, G. and Gross, S.S. (2006) *J. Am. Soc. Mass Spectrom.*, **17**,(12): 1725-1730.

129. Yang, B.K., Vivas, E.X., Reiter, C.D., and Gladwin, M.T. (2003) *Free Radic. Res.*, **37**,(1): 1-10.

130. Wang, Y., Vivekananda, s., Men, L., and Zhang, Q. (2004) *J. Am. Soc. Mass Spectrom.*, **15**, 697-702.

131. Tsikas, D., Sandmann, J., Rossa, S., Gutzki, F.-M., and Frolich, J.C. (1999) *Anal. Biochem.*, **272**, 117-122.

132. MacArthur, P.H., Shiva, S., and Gladwin, M.T. (2007) *J. Chromatogr. B. Biomed. Appl.*, **851**,(1-2): 93-105.

133. Giustarini, D., Milzani, A., Dalle-Donne, I., and Rossi, R. (2007) *J. Chromatogr. B. Biomed. Appl.*, **851**,(1-2): 124-139.

134. Giustarini, D., Milzani, A., Colombo, R., Dalle-Donne, I., and Rossi, R. (2004) *Trends Pharmacol. Sci.*, **25**,(6): 311-31.

135. Tsikas, D. (2004) *Circ. Res.*, **94**,(12): e106.

136. Zhao, J.J., Yang, A.Y., and Rogers, D.J. (2002) *J. Mass Spectrom.*, **37**, 421-433.

137. Lim, C.K. and Peters, T.J. (1984) *J. Chromatogr.*, **316**, 397-406.

138. Camera, E. and Picardo, M. (2002) *J. Chromatogr. B. Biomed. Appl.*, **781**, 181-206.